POLITECNICO DI TORINO

DET - Dipartimento di Elettronica e Telecomunicazioni

Master degree in Electronic Engineering

TCAD analysis of GaN FinFET structures and their parametric sensitivity

Supervisors:

Prof. Simona Donati Guerrieri
Prof. Fabrizio Bonani

Candidate:

Eva Catoggio

April, 2019

Acknowledgements

A tutta la mia famiglia e in particolare alla mia mamma Lucia, per tutti i sacrifici fatti durante questi anni e per aver sempre creduto in me. A mia nonna Ninetta e a mia zia Maria per essere state le mie seconde mamme. A mia sorella Michela per aver creato dei piccoli istanti di felicita' nei periodi peggiori della nostra vita.

Ai miei "Quallari" per l'amore con cui mi aspettano ogni volta a casa, soprattutto a Lucia e Valentina perche' sono le mie amiche speciali da sempre, a Nicola per la saggezza dei suoi consigli, a Leo per le lamentele con cui esprime affetto, a Simona per la complicita' che si e' creata tra noi in poco tempo.

A tutti gli amici del Collegio Einaudi, in particolare a Gloria per essere stata una guida durante i miei studi e Claudia per essere stata la mia quotidianeita' e per gli attimi piu' spensierati vissuti insieme. Ai miei adorati "Cheesecakers" per i momenti stupendi che abbiamo condiviso, soprattutto a Elena per essere "l'amica che ho sempre voluto", Mattia per le risate e gli scherzi fatti insieme, Frida per essere un grande punto di riferimento per me, Enrico per essere il mio fratellone, Salvatore per i vecchi discorsoni in balcone, Angela per gli spritz confortanti nei momenti tristi.

A Miriam per esserci raccontate tutta la vita in cosi' poco tempo.

Ad Antonio perche' non mi ha mai fatta sentire sola.

Un grazie speciale

Vorrei ringraziare i miei professori Simona Donati e Fabrizio Bonani per avermi dato l'opportunita' di studiare e approfondire questo meraviglioso tema. Un grazie particolare a Simona Donati che mi ha aiutata in questi mesi con perseveranza e interesse. Infine non posso dimenticare di ringraziare Andrea Palmieri per la sua disponibilita' e per aver sempre cercato di risolvere ogni dubbio.

Abstract

Nitride-based semiconductors, such as gallium nitride (GaN) and aluminum nitride (AlN) and relative alloys, are promising materials thanks to their superior characteristics with respect to the more conventional ones: wide band gap, low intrinsic carrier density, high electron mobility, high critical field, high thermal stability and high saturation velocity. Despite these advantages, GaN-based materials suffer from the high costs of the growth technique due to the presence of non-intentional doping and the development of dislocation layers which result in worse electrical and optical properties and may compromise the resulting structure.

For technological applications, those materials are employed in their hexagonal structure characterized by a strong polarization in the <0001> direction, known as C-direction, whose effect is very important to understand the electronic properties of these materials. The total polarization field has two different components, the piezoelectric and the spontaneous one. The piezoelectric field is associated to an electrostatic charge produced in a strained material, while the spontaneous field corresponds to the same charge density in relaxed conditions. These polarization charges exist in the whole crystal, but the sum of the internal components is zero, therefore the remaining charge density is distributed along the two opposite faces of the material forming a dipole.

The electronic properties of gallium nitride and the effect of polarization charges are exploited in an AlGaN/GaN hetero-structure to obtain a two-dimensional electron gas (2DEG) at the interface between the two materials without the use of dopants. Recently, this 2DEG channel is not considered into a conventional planar device, but in a three-dimensional structure like the FinFET, that can be called more precisely Fin-HEMT.

Purpose of this thesis is to highlight advantages and disadvantages of using, in the same structure, an interesting material like GaN and a Fin-shaped channel instead of the conventional planar one.

With this aim, numerical simulations are performed on TCAD Synopsys Sentaurus in order to understand how the device works and what are the physical mechanisms responsible for a certain behaviour.

The simulations are carried on by modulating precise quantities that characterize the device. On one hand, the parameters under analysis can be the most conventional ones, like the thickness of the heterostructure, the spontaneous and piezoelectric charges and the presence of traps in the nitride semiconductor regions. On the other hand, the quantities to be modified in the Fin-shaped structure are the geometrical ones, for example the gate length, the fin width and the fin height.

The simulation results are then evaluated in order to characterize the effects of this non-mature technology, optimize the device and understand the possible advantages that it shows with respect to a conventional planar structure and if each positive feature can be exploited for a specific application. For example, digital applications require the shift of the threshold voltage towards positive values, while analogue applications need an improvement in the cut-off frequency, gains and output power density.

Contents

Abbreviations

Si	Silicon
SiC	Silicon Carbide
GaAs	Gallium Arsenide
GaN	Gallium Nitride
AlGaN	Alluminum Gallium Nitride
AlN	Alluminum Nitride
InN	Indium Nitride
Al2O3	Sapphire
CB	Conduction Band
VB	Valence Band
2DEG	Two dimentional electron gas
HEMT	High electron mobility transistor

Physical constants

Electron charge	$e = 1.60217733 \cdot 10^{-19} C$
Permittivity of vacuum	$\varepsilon_0 = 8.854187817 \cdot 10^{-12} F/m$
Boltzmann constant	$k_B = 1.380658 \cdot 10^{-23} J/K$

Chapter 1

Introduction

[1] For many years, the *First generation technology* based on silicon has been largely used for the realization of different electronic devices. To improve their technology and performances, silicon characteristics have been analysed and its positive aspects have been exploited: low cost, good mechanical robustness, high reliability, high thermal conductivity and the consequent low temperature rise of the device. In the last years, the rate of improvement has slowed due to the limits imposed by silicon intrinsic properties, such as the small band gap, the low electron mobility and the high intrinsic carrier density.

The technological solution for these limits has been the *Second generation technology* and the introduction of new materials, one of the most important is gallium arsenide (GaAs). It has been especially exploited for high-frequency applications thanks to its superior characteristics with respect to conventional silicon, as shown in table 1.1.
Gallium arsenide is characterized by an energy gap equal to 1.42 eV, a larger value than silicon's gap of 1.12 eV. This leads to a higher maximum working temperature and a higher breakdown voltage, defined as the maximum voltage that can be safely applied to a device, whose precise value is 0.4 MV/cm. Moreover, the direct band gap allows an efficient recombination of electrons and holes which is not verified in silicon because of its indirect gap. [3]
GaAs also has a much higher electron mobility of 8500 $cm^2/(V\cdot s)$, that corresponds to a lower transition time of the carriers, and a higher saturation velocity equal to $1.2 \cdot 10^7$ cm/s. These properties are necessary to achieve higher operating frequencies.
In addition, it is possible to produce gallium arsenide in the form of semi-insulating substrates with a very high resistivity and, as a consequence, its parasitic parameters have lower values than silicon. In conclusion, GaAs resists against radiations, therefore it is used for military and spatial applications. [4]
Nevertheless, as in the previous case, the intrinsic properties of this material have not allowed great improvements in the technology and a concrete progress in this field, therefore the need of a new solution has been realized.

The *Third generation technology* has represented the way to overcome those limits through the introduction of nitride-based materials, such as gallium nitride (GaN) and the relative alloys formed with aluminum nitride (AlN) and indium nitride (InN), whose characteristics are shown in table 1.1.
Looking at gallium nitride, it is evident that its band gap of 3.39 eV is much wider with respect to the previous materials. For this reason, it produces a definitely higher breakdown voltage of 3.3 MV/cm. In addition, the intrinsic carrier concentration has a value equal to $1.9 \cdot 10^{-10}$ cm^{-3}, which results very small thanks to the wide band gap and allows to operate at higher temperatures.
Due to the reduced ionized impurity scattering, the electron mobility is larger: in the bulk it is equal to 1000 $cm^2/(V \cdot s)$, while in a 2DEG channel the value is 2000 $cm^2/(V \cdot s)$. Moreover, the saturation velocity has a higher value equal to $2.5 \cdot 10^7$ cm/s and, together with the electron mobility, is responsible of a larger current density [5]. The combination of higher mobility and higher saturation velocity allows a higher operating frequency.
Another important property is the thermal conductivity, whose value of 1.3 W/(cm·K) results better than the one appreciated for gallium arsenide. As a consequence, the temperature rise is not so evident in this case.
The improvement in breakdown voltage, current density and thermal conductivity implies an output power density much higher than the one produced in GaAs devices. In figure 1.1, the output power density is represented with respect to the operating frequency in order to highlight the differences between the materials just compared.

The capability to handle high power levels implies the fabrication of smaller devices. In fact, for a given power density, it is possible to fabricate smaller devices with respect to GaAs materials and, even more so, with respect to silicon devices [6]. In figure 1.2, the size difference between silicon devices and GaN devices can be noticed. In conclusion, reducing the device size, the impedence becomes greater, because it is inversely proportional to the area, and the losses result lower [8].

In this wide panorama, the physical properties of the materials, from conventional silicon to nitride semiconductors, can be exploited for the realization of different electronic devices. One of the most recent and unconventional proposals is the FinFET, a three dimensional device characterized by a gate contact that wraps around a fin-shaped body. This structure represents a turning point with respect to conventional planar devices thanks to the provided advantages. First, the improvement in the gate electrostatic control of the channel leads to reduced short channel effects (SCE), higher threshold voltage values and better OFF state performances, for example lower subthreshold swing, higher ON/OFF current ratio, smaller leakage current and lower ON resistance. These aspects can be exploited in digital applications, while in the analog field other improvements can be mentioned. Valid examples are the transconductance linearity, the higher current density, output power density, maximum frequency and cutoff frequency.

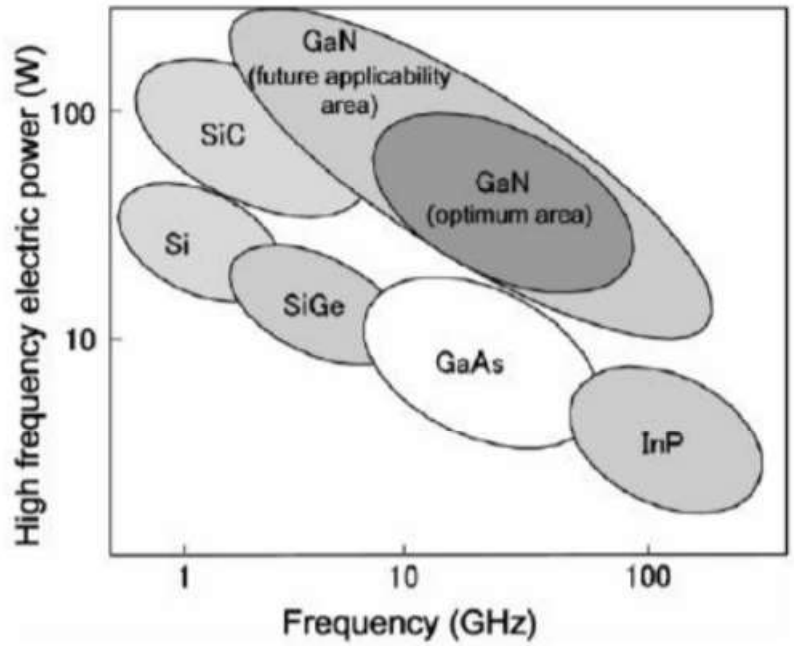

Figure 1.1: [7] Output power density as a function of the operating frequency for different materials

Figure 1.2: [8] Size comparison between silicon device and GaN device

There are few experimental implementations of this new structure, therefore it can be interesting to simulate it in order to characterize the device and try to optimize it. Purpose of this work is implement and simulate a GaN FinFET, in order to exploit the

Table 1.1: [2] Properties of conventional and nitride-based semiconductors at 300 K

	Si	**GaAs**	**GaN**	**AlN**	**InN**
Lattice constant [Å]	5.431	5.653	a = 3.189 c = 5.158	a = 3.111 c = 4.981	a = 3.544 c = 8.703
Band gap [eV]	1.12	1.42	3.39	6.2	1.89
Electron mobility $[cm^2/(V \cdot s)]$	1400	8500	1000 (Bulk) 2000 (2DEG)	300	3200
Intrinsic carrier density $[cm^{-3}]$	$1 \cdot 10^{10}$	$2.1 \cdot 10^{6}$	$1.9 \cdot 10^{-10}$	$9.4 \cdot 10^{-34}$	920
Thermal conductivity $[W/(cm \cdot^{\circ} C)]$	1.3	0.55	1.3	2.85	0.45
Breakdown field $[MV/cm]$	0.3	0.4	3.3	1.2 - 1.8	3
Electron saturation velocity $[x10^7 cm/s]$	1.03	1.2	2.5	1.7	4.5

excellent electronic properties of nitride semiconductors and, at the same time, verify the improvements of a three-dimensional structure with respect to a conventional planar one.

1.1 Thesis organization

The thesis is organized in five chapters that can be summarize as follows.

The first chapter briefly describes from a historical point of view the evolution of the electronic devices, going from silicon technologies to the most recent ones that include nitride-based semiconductors. A comparison between different materials and their electronic properties is shown in order to underline what are their performances in terms of operating frequency and output power.

In the second chapter the chemical, physical and electrical characteristics of nitride-based semiconductors are presented. First, the difference between nitride binary compounds and alloys is explained, then their crystal structure is analysed paying attention on the crystal system and the kind of symmetry. To follow, the band structure is studied in order to highlight the connection between the lattice constant and the band gap of a material. Moreover, the consequences derived from a certain band gap are reported. A brief explanation about the epitaxial growth of nitride semiconductors is added: a comparison between the possible substrates is inserted and some growing techniques are

analysed. In conclusion an insight about the polarization effect is presented: it can be understood the difference between spontaneous and piezoelectric polarization and their effect at heterointerfaces.

In the third chapter, a review on the conventional planar GaN HEMT is presented in order to highlight how the electronic properties of nitride semiconductors are exploited. In particular, the structure of the device and its operating principle are described, paying attention on the formation of the two-dimensional channel under and out of the gate.

In the fourth chapter, some possible FinFET structures are presented in order to understand the different technologies and their possible applications. Then, concepts of one recently proposed Fin-HEMT are described: the geometry of the structure is highlighted and the operating principle of the device is explained, along with its possible applications. First the calculation of the polarization charges is carried out, then the formation of the two-dimensional channel(2DEG) in absence of doping is explained.

The fifth chapter is focused on the numerical simulations on the TCAD Synopsys Sentaurus. The simulations codes are described paying attention on the geometry of the structure and the physical models necessary to describe it. The equilibrium and out-of-equilibrium analysis is performed and a comparison with respect to a conventional planar structure is done.

The sixth chapter analyses the parametric sensitivity of the device: a parameter of the FinFET device is varied of a certain quantity, then the modified structure is simulated and the obtained results are compared with the reference ones. The parameters taken into account are fin width, fin height, traps concentration, polarization charges and temperature.

The seventh chapter shows all the conclusions of this analysis.

Chapter 2

Nitride-based semiconductors

Nitride-based semiconductors can be divided in two categories: binary compounds and alloys. The first category includes those semiconductors composed of one nitride and one element of the III group, such as gallium, aluminum and indium. The main examples are GaN, AlN and InN. Alloys semiconductors are often mixtures of compounds semiconductors and their properties are intermediate with respect to the "original" components. In general there are ternary (al least two compounds and three elements) and quaternary (at least four compounds and elements) alloys and their characteristics are approximated, respectively, by a linear and bilinear combination of the initial components. Examples for nitride-based alloys are $Al_xGa_{1-x}N$, $In_xGa_{1-x}N$ and $In_xAl_{1-x}N$. In most cases a generic alloy property P is found, at first approximation, through the *Vegard's Law*, which implies the linear combination of the properties of each component as a function of the mole fraction x [9]. Equation (2.1) shows the expression of the *Vegard's Law* for ternary alloys: if a material $A_xB_{1-x}C$ is considered, $P^{(A)}$ and $P^{(B)}$ represent the alloy properties of the elements A and B, respectively. Instead, if a quaternary alloy $A_xB_{1-x}C_yD_{1-y}$ is taken into account, equation (2.2) can be applied and $P^{(A)}$, $P^{(B)}$, $P^{(C)}$ and $P^{(D)}$ are the alloy properties of the elements A, B, C and D, respectively.

$$P = xP^{(A)} + (1-x)P^{(B)} \Longrightarrow Ternary\ alloy \tag{2.1}$$

$$P = xP^{(A)} + (1-x)P^{(A)} + yP^{(C)} + (1-y)P^{(D)} \Longrightarrow Quaternary\ alloy \tag{2.2}$$

Purpose of this chapter is to review the crystal structure and the electronic properties of nitride semiconductors. In particular, the band structure and the substrates for the materials growing are presented and, in conclusion, origin and effects of the polarization effect are explained.

2.1 Crystal structure

A crystal is a solid material whose components, such as atoms, molecules or ions, are organized in a geometrically regular structure that ideally extends indefinitely in the three directions, forming a crystal lattice or Bravais lattice. The crystal structure is defined by two important concepts: the lattice and the basis. The first one represents a set of points ordered in the space into a periodic structure, while the second one is a building block of atoms to be fixed in each lattice point in order to define the physical characteristics of the crystal. Any lattice point **R'** can be calculated from any other lattice point **R** through the translation shown in equation (2.3): m_1, m_2 and m_3 are integers, while a_1, a_2 and a_3 are primitive vectors if the volume of the cell considered is the smallest possible and it is called, in this case, primitive unit cell.

$$\mathbf{R'} = \mathbf{R} + m_1 a_1 \cdot m_2 a_2 \cdot m_2 a_2 \tag{2.3}$$

Because of the periodicity of the structure, it is important to define its symmetry. "Natural" crystals have a crystalline symmetry defined by nature, while artificial crystals are realized through new growth techniques which modify their symmetry [10]. There are seven crystal systems to define this characteristic: triclinic, monoclinic, orthorhombic, tetragonal, hexagonal and cubic. Each one can have until 4 lattice classes, which are defined by the different relationships between the primitive vectors a_1, a_2 and a_3 and the angles between them α, β and γ [11] .

Nitride semiconductors are typically grown on a *wurtzite* structure, which belongs to the hexagonal crystal system whose primitive vectors a_1, a_2 and a_3 are called respectively a, b and c. The 3D representation of the wurtzite structure and the arrangement of atoms along the c-axis are shown in figure 2.1 [12] .

In order to identify the values of primitive vectors and the relative angles of this structure, a distinction between binary compounds and alloys is necessary. For the first category, these relationships are expressed in equations (2.4) and (2.5): the values of the lattice constants a and b are shown in table 1.1 for GaN, InN and AlN. As regards the nitride alloys category, the relationships between angles is the same, while the lattice constants of a generic material $A_xB_{1-x}N$ are calculated from the binary constituents AN and BN through the Vegard's law for ternary alloys, for example: $a_{alloy} = xa^{(A)} + (1-x)a^{(B)}$ [12].

$$a = b \qquad c = a \cdot \sqrt{\frac{8}{3}} \tag{2.4}$$

$$\alpha = \beta = 90^\circ \qquad \gamma = 120^\circ \tag{2.5}$$

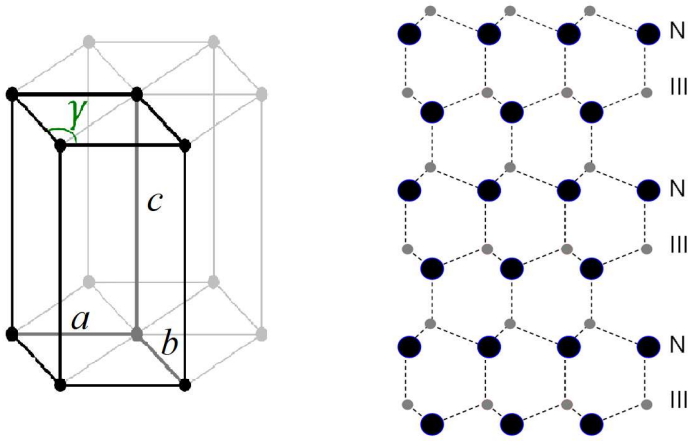

(a) Hexagonal unit cell

(b) Arrangement of atoms of a III-nitride binary compound

Figure 2.1: Wurtzite crystal along the c-axis

The crystal structure and type of symmetry play an important role in the electronic properties of materials. In particular, the band diagram of nitride semiconductors and their band gap are strictly related to the lattice constant of the crystal structure. Moreover, as regards the symmetry, it influences the polarization effect of these materials [12]
.
These aspects will be analysed in the following sections.

2.2 Band structure

The crystal lattice has a strong influence on the band structure of a semiconductor, which is a description of the electron energy levels as a function of the position. Its two-dimensional representation is called band diagram and consists of drawing a E-k plot, where k goes from zero to a maximum value along the (100) direction, (111) direction and so on, within the Brillouin zone.
It is possible to distinguish two different band structures depending on the type of band gap: direct or indirect. A semiconductor has a direct gap when the top of the valence band and the bottom of the conduction band coincide in the Γ-point, while the gap is indirect when this condition in not verified in the same point. This concept can be easily understood through the figure 2.2 where the curves I, II, III of the valence band are called heavy holes, light holes and split-off.

In the specific case of nitride semiconductors, figure 2.3 shows the band diagrams for wurtzite GaN, AlN and InN and the most significant energy values. As it can be noticed, these semiconductors, but also their relative alloys, have a direct band gap whose values are in a range between $\sim$ 1.0 eV and 6.0 eV. The precise energy gap values can be found

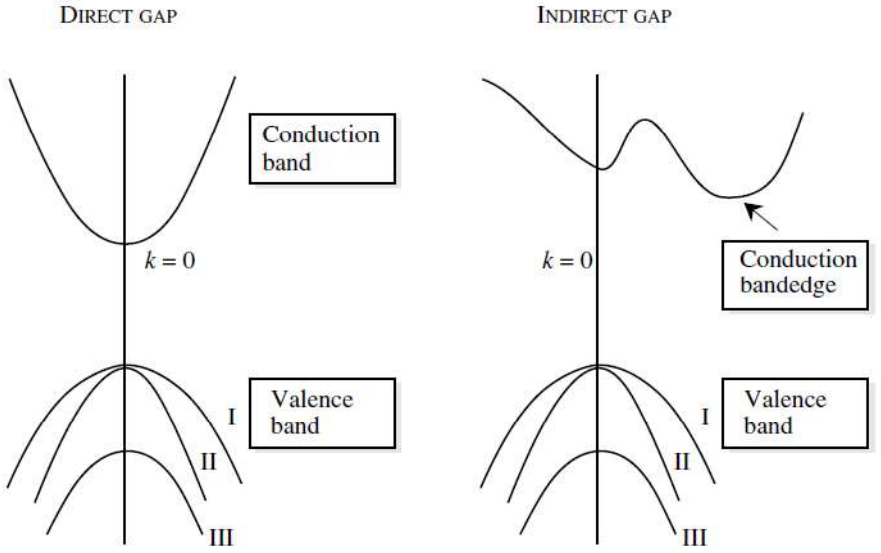

Figure 2.2: Band diagrams of a direct and indirect semiconductor

in table 1.1 for nitride binary compounds and through the Vegard's Law (2.1) for all the alloys [10].

The influence that the crystal structure has on the band diagram can be clearly seen in the relationship between the energy gap and the lattice constant of the semiconductor. As it is shown in figure 2.4, the smaller the lattice constant, the larger the energy gap. Therefore, small values of the lattice constant in nitride semiconductors are responsible of wider energy gaps with respect to conventional materials, as it can be seen in table 1.1 [9].

This advantage has many consequences on the electronic properties of these materials. First of all, the intrinsic carrier density n_i depends on the energy gap E_g as expressed in equation (2.6), therefore a larger E_g produces a lower value of n_i. Moreover, it can be noticed that the intrinsic concentration of carriers increases with the temperature, therefore a wider energy gap allows to operate at higher temperatures than a lower gap [9].

The band gap is also related to the breakdown voltage, the maximum voltage that can be safely applied to a device. In this case, the energy gap is related to the minimum energy necessary to accelerate electrons between scattering events in order to create electron-hole pairs. These pairs are then accelerated to create other pairs, that above a critical field produce an avalanche of particles and, therefore, the "breakdown" of the device. In conclusion, the more is the energy, the more is the critical field.
Another consequence of the wider band gap is the presence of a higher saturation veloc-

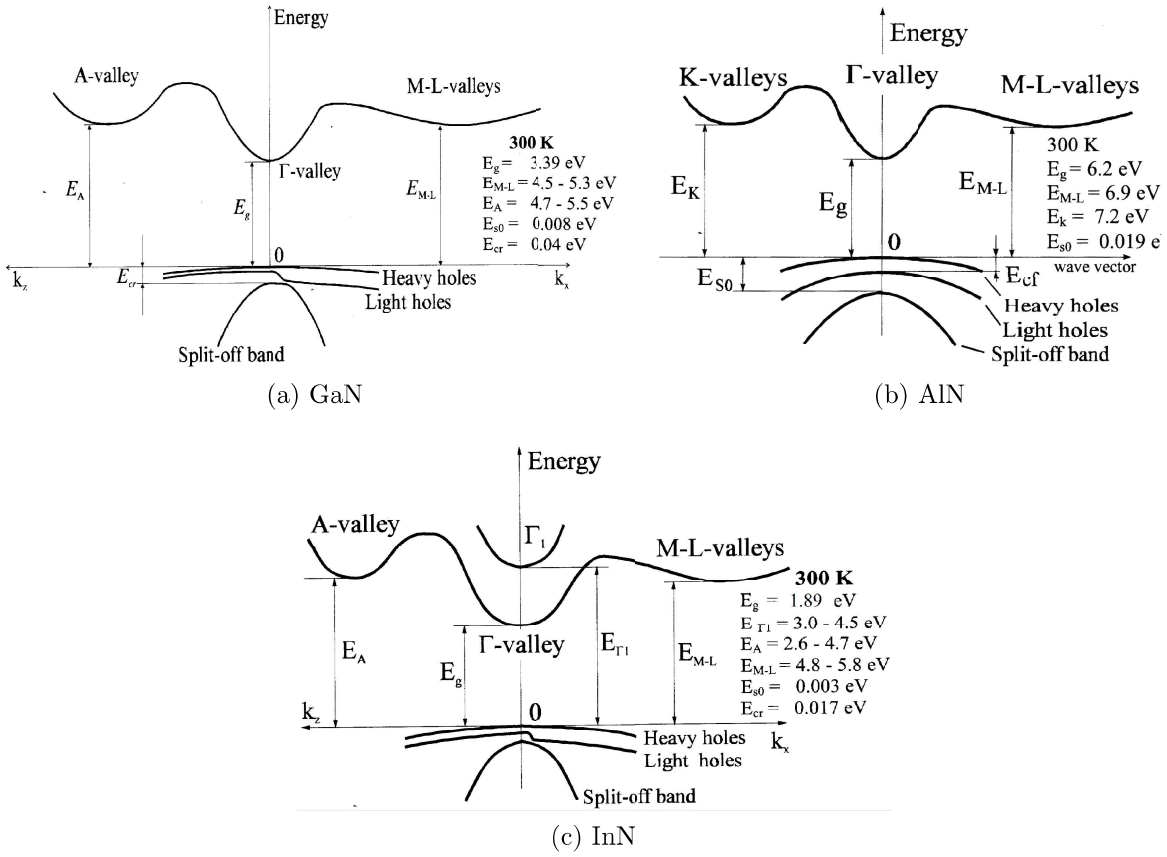

Figure 2.3: Band structures of wurtzite crystals

ity, whose behaviour depends on the higher breakdown voltage [9] .

The values of intrinsic concentration, the breakdown field and the saturation velocity can be found in table 1.1 for GaN, AlN and InN, while the alloys parameters can be calculated using the Vegard's Law.

$$n_i = (N_c N_v)^{\frac{1}{2}} \cdot e^{-\frac{E_g}{2k_B T}} \tag{2.6}$$

2.3 Substrates

The epitaxial growth of crystal structures is considered one of the main problems for nitride semiconductors. The term epitaxy refers to the deposition of a crystalline material, called epitaxial layer, on a crystalline substrate, that gives to the overlayer, a well-defined orientation and defines its structural properties. There are two types of epitaxy: when the deposited material has the same composition of the substrate crystal, the process is called *homoepitaxy*, while when they have different composition the term is modified

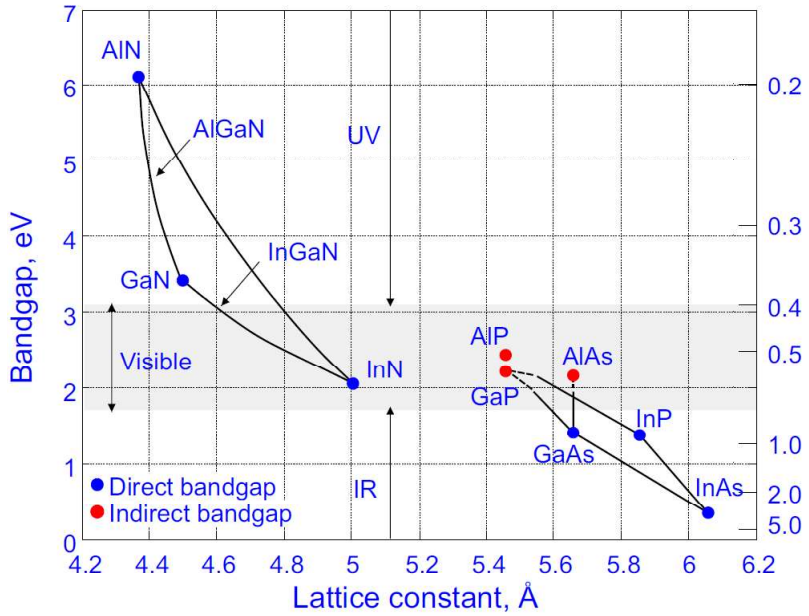

Figure 2.4: [9] Behaviour of the energy gap of different semiconductors with respect to the lattice constant

into *heteroepitaxy* [13].

The fabrication of GaN and other nitride semiconductors on a material of the same type is not yet possible because, even if it would lead to many advantages, the practical realization results too complicate. Therefore, the only solution is the heteroepitaxy that exploits substrates of different materials and chooses them with respect to their characteristics [13]. For example, the lattice constant and the thermal expansion coefficient of the deposited material should be similar to the substrate ones. This avoids the formation of dislocations that degradates the crystal properties: the mobility of the carriers is reduced, noise and gate leakages are increased. Moreover, the price of the substrate and the quality of its crystalline structure are also important [1].

Paying attention only on gallium nitride, the most common substrates used for its fabrication are *Sapphire* and *silicon Carbide*, which are analysed in the following lines.

Sapphire

Sapphire is the first material used as substrate for the GaN growing for several reasons: the hexagonal crystal structure as GaN materials, good stability at the required temperatures, low cost. Nevertheless, it shows some negative aspects, such as the large lattice and thermal mismatches equal respectively to 16% and 39%. This leads to the formation of dislocations that reduce the mobility of carriers.

A first solution to this problem is the deposition of an AlN layer between the GaN and the substrate which produces an increasing of the mobility and a reduction of free electrons in GaN. An alternative found recently consists of using a GaN buffer instead of an AlN one [7].

Silicon Carbide

Silicon Carbide is the other material used as substrate and shows some advantages with respect to Sapphire. The lattice and thermal mismatches are respectively equal to 3.4% and 25%, therefore they are much lower than the previous ones. Moreover, SiC has a very good electrical and thermal conductivity: the first one allows to reduce the dimensions of a device, the second one implies the dissipation of high heat quantities. However, the cost of this material turns out to be very high with respect to Sapphire [7].

2.3.1 Growth techniques

[7] There are different fabrication techniques for the epitaxial growth of nitride semiconductors and the most important ones are summarized as follows:

- HVPE (Hydride Vapor Phase Epitaxy)
- MBE (Molecular Beam Epitaxy)
- MOCVD (Metal Organic Chemical Vapor Deposition)

In the following lines, each technique is briefly explained, taking into account the GaN material as example.

HVPE

The HVPE method is the first epitaxial technique developed in 1960 and often employed for the fabrication of III-N semiconductors. At elevated temperature (850 $°C$), the hydrogen chloride (HCl) reacts with a III-group metal, such as gallium, to produce a gaseous metal chloride, like GaCl. Then, it reacts with ammonia in order to produce the III-nitride material. Equation (2.7) shows an example of this reaction for the fabrication of GaN.

$$GaCl(g) + NH_3(g) \longrightarrow GaN(s) + HCl(g) + H_2(g) \tag{2.7}$$

The growth velocity in this process has excellent results (30-130 $\mu m/h$), nevertheless the produced layers do not have good crystal quality and for this reason this method has been replaced by other techniques.

MBE

The Molecular Beam Epitaxy is a more recent technique born in 1970, that introduces the possibility to operate in high vacuum with a pressure around 10^{-10} torr. This allows to obtain high purity materials because collisions between molecules or atoms of the elements incident on the substrate, are avoided. Moreover, vacuum and low pressure lead to the possibility of monitoring the growing of the materials in real time.
The temperature range goes from a minimum of 600 $°C$ to a maximum of 800 $°C$, therefore these values are lower than the previous ones and imply a low growing velocity (3 nm/h). The monitoring and the low deposition rate allow the layers to grow epitaxially.

Despite of many advantages introduced by this technique, the optical and electrical qualities of the fabricated materials are not the best ones, therefore a new solution has to be found.

MOCVD

The MOCVD method is the most recent technique for the fabrication of materials, in particular III-N semiconductors. It is based on a chemical reaction called *chemical vapour deposition* and not on a physical deposition as the MBE. The operating conditions take place not in vacuum, but from a gas phase with pressure in the range 10-760 torr.
From a thermodynamic point of view, the required temperatures are around 1000 $°C$ and this implies a higher non-intentional doping in the material. But, as already mentioned, the electrical and optical properties of the fabricated layer are better than the previous ones.

2.4 Polarization effect

The crystal symmetry plays a fundamental role in electronic properties of materials, in particular the inversion symmetry is very important to define some physical phenomena of semiconductors.

In crystallography, a point group, defined as a group of geometric symmetries with at least one point fixed, has an *inversion symmetry* if one of its symmetry elements is an inversion center. It means that there is no difference between the generic points (x,y,z) and (-x,-y,-z). Crystals with inversion symmetry cannot have some properties, such as the piezoelectric polarization, an effect due to an applied strain that produces an electrostatic potential across the opposite faces of the material.
The space groups that do not exhibit inversion symmetry can be divided in two subclasses: polar and non-polar materials. A crystal is polar when it shows a spontaneous polarizations without the presence of a mechanical stress, while it is non-polar if it does not show this behaviour. An example of polar-type structure can be the wurtzite, which

is typically used for the growing of nitride-based semiconductors, as already explained previously [14].

The spontaneous and the piezoelectric polarizations of nitride semiconductors in their wurzite structure are explained in detail in the following lines.

2.4.1 Spontaneous polarization

In an unstrained wurtzite material, such as AlN, GaN, InN and alloys, the relative movement of cations and anions with respect to their ideal position produces a *spontaneous polarization*, which results aligned along the <0001> direction, known also as the C-direction. The spontaneous polarization vector is expressed in equation (2.8): the x and y components are null, while P_{SP_z} assumes a certain value with respect to the material. In table 2.1, the z-components for AlN, GaN and InN are shown, while the correspondent values for the relative alloys can be calculated using the Vegard's Law (2.1), as always [10].

$$\overline{P_{SP}} = \begin{pmatrix} P_{SP_x} \\ P_{SP_y} \\ P_{SP_z} \end{pmatrix} = \begin{pmatrix} 0 \\ 0 \\ P_{SP_z} \end{pmatrix} \tag{2.8}$$

The polarization charges due to this phenomenon exist in the whole crystal, but the sum of the internal components is null, therefore the remaining *polarization sheet charge density* $\pm Q_{\pi_{SP}}$ is distributed along the two opposite faces of the material, as it can be seen in figure 2.5, forming a dipole. Gallium nitride is an example of a nitride semiconductor characterized by this behaviour: if it is considered along the C-axis, the Ga-face on the top of the material shows a negative polarization sheet charge, while the N-face on the bottom is characterized by a positive one, as it can be seen in figure 2.6 [10].

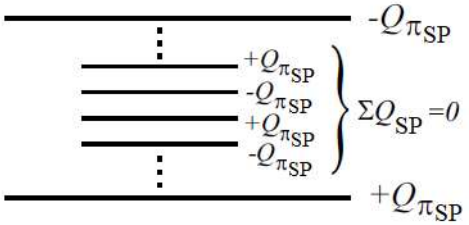

Figure 2.5: Sheet charge density associated to spontaneous polarization in a polar material

It can be noticed that the spontaneous sheet charge density is characterized by a positive and a negative contribution, called respectively $+Q_{\pi_{SP}}$ and $-Q_{\pi_{SP}}$. Their absolute value can be easily obtained using the expression (2.9).

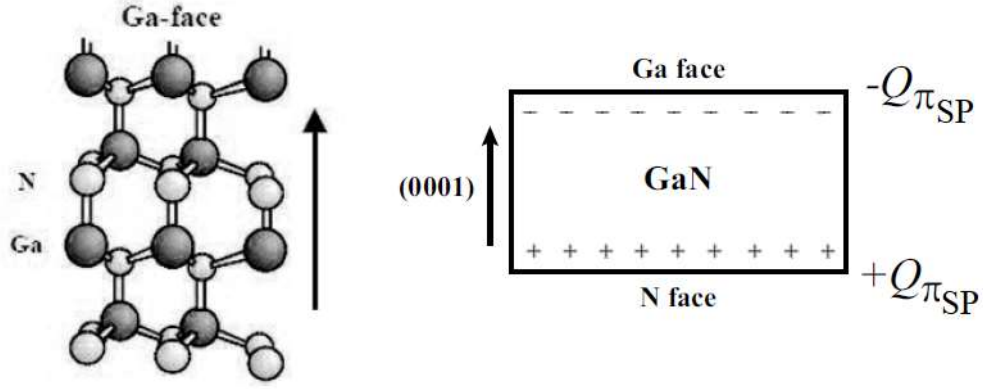

Figure 2.6: Wurtzite GaN crystal structure and representation of the polarization sheet charge

$$Q_{\pi_{SP}} = |P_{SP_z}| \tag{2.9}$$

2.4.2 Piezoelectric polarization

The second phenomenon that leads to the polarization of the material is the *piezoelectric effect*. A mechanical strain applied to the semiconductor produces a relative shift of anion and cation sub-lattices and a net polarization charge can be obtained [10].

The piezoelectric polarization vector $\overline{P_{PE}}$ is shown in equation (2.10): it depends on the local strain tensor $\overline{\varepsilon}$ and the strain-charge piezoelectric coefficients or tensors e_{ij} [18].

$$\begin{pmatrix} P_{PE_x} \\ P_{PE_y} \\ P_{PE_z} \end{pmatrix} = \begin{pmatrix} e_{11} & e_{12} & e_{13} & e_{14} & e_{15} & e_{16} \\ e_{21} & e_{22} & e_{23} & e_{24} & e_{25} & e_{26} \\ e_{31} & e_{32} & e_{33} & e_{34} & e_{35} & e_{36} \end{pmatrix} \begin{pmatrix} \varepsilon_{xx} \\ \varepsilon_{yy} \\ \varepsilon_{zz} \\ \varepsilon_{yz} \\ \varepsilon_{xz} \\ \varepsilon_{xy} \end{pmatrix} \tag{2.10}$$

The crystal system and, in particular the kind of symmetry, are necessary to define the components of the strain and the piezoelectric tensors. In the case of nitride semiconductors with a wurtzite structure the previous expression is simplified as shown in equation (2.11).

Table 2.1: [10] Spontaneous and piezoelectric polarization values for some wurtzite crystal semiconductors (c-axis growth)

	GaN	**AlN**	**InN**
a [Å]	3.189	3.111	3.544
$P_{SP_z}[C/m^2]$	-0.029	-0.081	-0.032
$e_{31}[C/m^2]$	-0.35	-0.5	-0.48
$e_{33}[C/m^2]$	1.27	1.79	1.06
c_{13} [Pa]	$1.06 \cdot 10^{11}$	$1.08 \cdot 10^{11}$	$9.2 \cdot 10^{10}$
c_{33} [Pa]	$3.98 \cdot 10^{11}$	$3.73 \cdot 10^{11}$	$2.24 \cdot 10^{11}$

$$\begin{pmatrix} P_{PE_x} \\ P_{PE_y} \\ P_{PE_z} \end{pmatrix} = \begin{pmatrix} 0 & 0 & 0 & 0 & e_{15} & 0 \\ 0 & 0 & 0 & e_{15} & 0 & 0 \\ e_{31} & e_{31} & e_{33} & 0 & 0 & 0 \end{pmatrix} \begin{pmatrix} \varepsilon_{xx} \\ \varepsilon_{yy} \\ \varepsilon_{zz} \\ 0 \\ 0 \\ 0 \end{pmatrix} = \begin{pmatrix} 0 \\ 0 \\ e_{31}\varepsilon_{xx} + e_{31}\varepsilon_{yy} + e_{33}\varepsilon_{zz} \end{pmatrix} \quad (2.11)$$

The only component different from zero is P_{PE_z}, whose expression depends on two piezoelectric coefficients and two strain tensors. The piezoelectric coefficients e_{31} and e_{33} assume a certain value that depends on the nitride semiconductor, as it can be seen appreciated in table 2.1. The relative alloys of GaN, AlN, InN depend on the mole fraction, therefore their piezoelectric tensors are calculated through the *Vegard's Law.*
As regards the strain tensors, they can be expressed as shown in equations (2.12), where a is the substrate lattice constant, a_0 is the overlay lattice constant, c_{13} and c_{33} are the elastic constants. These parameters depend on the type of semiconductor: in table 2.1, the values assumed by GaN, AlN and InN for a_0, c_{13} and c_{33} are inserted, while for the relative alloys, the *Vegard's Law* can be used to calculate them, as written above.

$$\begin{aligned} \varepsilon_{xx} &= \varepsilon_{yy} = (1 - relax) \cdot \frac{a - a_0}{a_0} \\ \varepsilon_{zz} &= \frac{-2 \cdot c_{13}}{c_{33}} \cdot \varepsilon_{xx} = \frac{-2 \cdot c_{13}}{c_{33}} \cdot (1 - relax) \cdot \frac{a - a_0}{a_0} \end{aligned} \quad (2.12)$$

Substituting the equations (2.12) into P_{PE_z}, the final expression for the z-component of the piezoelectric vector is found, as shown in equation (2.13).

$$P_{PE_z} = 2 \cdot (1 - relax) \cdot \frac{a - a_0}{a_0} \cdot \left(e_{31} - \frac{c_{13}}{c_{33}} e_{33} \right) \tag{2.13}$$

The behaviour of the piezoelectric charge density does not show differences with respect to the previous case: inside the semiconductor the polarization charges neutralize each other, but on both the opposite surfaces a sheet charge density $\pm Q_{\pi_{PE}}$ is created. As in the previous case, it can be noticed that there is a positive and a negative component for the polarization sheet charge, but its absolute value is found through the formula (2.14).

$$Q_{\pi_{PE}} = |P_{PE_z}| \tag{2.14}$$

2.4.3 Total polarization

The total polarization vector $\overline{P}$ is written in equation (2.15) as the sum of spontaneous and piezoelectric polarizations.

$$\overline{P} = \overline{P_{SP}} + \overline{P_{PE}} = \begin{pmatrix} P_{SP_x} \\ P_{SP_y} \\ P_{SP_z} \end{pmatrix} + \begin{pmatrix} P_{PE_x} \\ P_{PE_y} \\ P_{PE_z} \end{pmatrix} = \begin{pmatrix} 0 \\ 0 \\ P_{SP_z} \end{pmatrix} + \begin{pmatrix} 0 \\ 0 \\ P_{PE_z} \end{pmatrix} = \begin{pmatrix} 0 \\ 0 \\ P_{PE_z} + P_{SP_z} \end{pmatrix} \tag{2.15}$$

The gradient of the total polarization vector allows the calculation of the polarization-induced charge density through the formula in equation (2.16).

$$\rho_\pi = -\nabla \overline{P} \tag{2.16}$$

The total polarization sheet charge density is distributed along the two opposite faces, as always, and its absolute value is calculated through formula (2.17). It produces a built-in electric field expressed in equation (2.18), where Q_π is the absolute value of the sheet charge density and ϵ the permittivity. From the electric field, it is possible to calculate the voltage across the material, whose expression is shown in equation (2.19), where ε is the electric field and d the thickness of the material [10].

$$Q_\pi = |P_z| = |P_{SP_z} + P_{PE_z}| \tag{2.17}$$

$$\varepsilon = \frac{Q_\pi}{\epsilon} \tag{2.18}$$

$$V = \varepsilon \cdot d \tag{2.19}$$

The polarization-induced electric field causes a slope of the energy bands of the semiconductor, as shown in figure 2.7. Depending on the thickness of the material

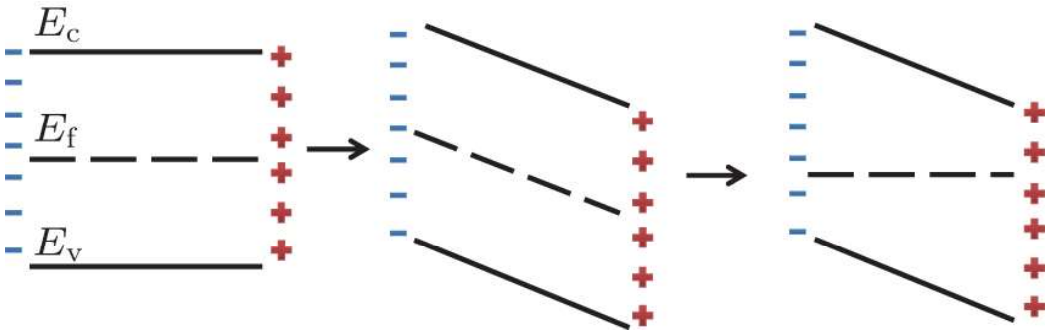

Figure 2.7: Behaviour of a nitride semiconductor under the effect of the polarization-induced electric field

under analysis, this slope produces different consequences and, to understand them, an undoped GaN material on a substrate is considered. Due to the non-availability of GaN substrates, as already explained, it is grown heteroepitaxially on sapphire, silicon or silicon carbide, which are highly defective and able to trapping mobile charges.
When the thickness of the material d is very small, the only presence of the polarization sheet charges $\pm Q_\pi$ on the two opposite faces can be seen, as shown in figure 2.8a. If the value of d increases, the valence band moves closer to the Fermi level E_f until a critical thickness d_{cr} is reached (figure 2.8b). This parameter is obtained through equation (2.20), where E_g is the energy gap of the material, q is the electron charge and ε is the electric field [10].

$$d_{cr} = \frac{E_g}{q\varepsilon} \tag{2.20}$$

Once $d > d_{cr}$, electrons are stimulated into the conduction band, move under the effect of the polarization-induced electric field and accumulate at the interface with the substrate (N-face). Therefore, an equal concentration of holes is created at the surface of the material (Ga-face), forming a screening dipole $\pm Q_{scr}$ (figure 2.8c).

It can be interesting the analysis of the same structure in slightly different conditions. The existence of a surface donor state is taken into account: the screening dipole is due to ionized surface donors as it is shown in figure 2.9. When the GaN material is thick enough (figure 2.9b), E_{DD} reaches E_f and surface donors become ionized [10].

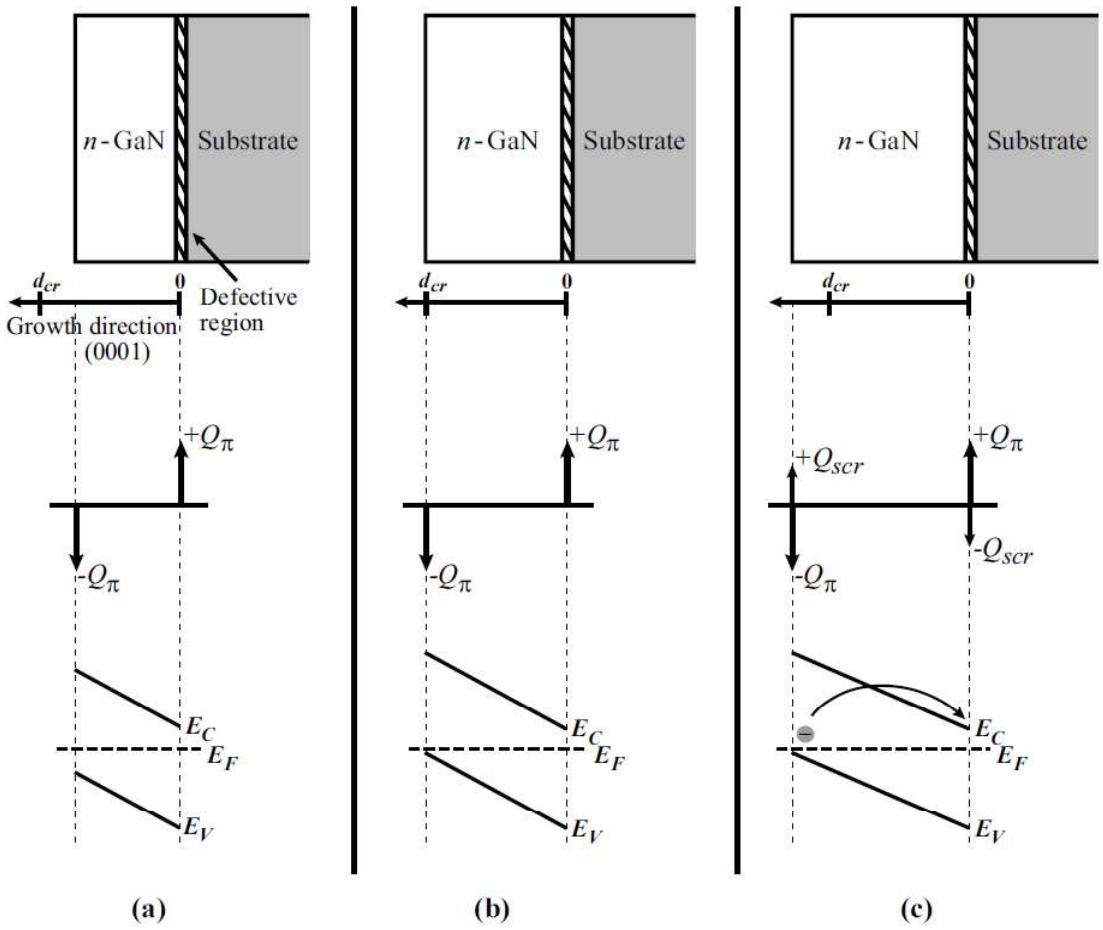

Figure 2.8: Charge distribution and band diagram of an undoped GaN material (a) $d < d_{cr}$, (b) $d = d_{cr}$ and (c) $d > d_{cr}$

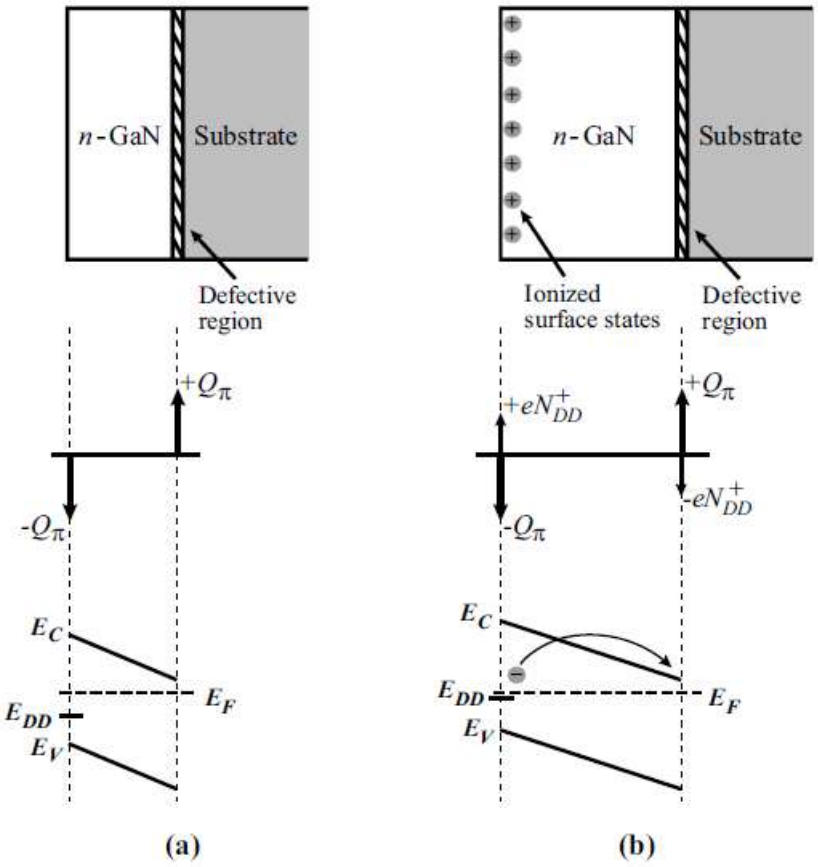

Figure 2.9: Charge distribution and band diagram of an undoped GaN material with surface donor states (a) $d < d_{cr}$ and and (c) $d > d_{cr}$

Chapter 3

Conventional HEMT device

The *Third generation technology* is characterized by the introduction of nitride-based semiconductors into an electronic device. In fact, the excellent electronic properties of these materials, widely analysed in the previous chapter, can be exploited in order to understand their positive and negative effects. For many years, the most common structure based on III-N semiconductors has been the HEMT device (High electron mobility transistor): it has been widely studied in order to evaluate its performances in different application fields and many technological solutions have been introduced to obtain improvements with respect to other devices.

In this chapter, a brief description of a conventional GaN HEMT is presented in order to highlight the main characteristics of this planar device. First, the geometry of the structure is described, paying attention on materials and contacts. Then, an explanation about the operating principle is presented in order to understand how the formation of the channel is achieved and what is the role of gate contact and passivation layer in this device.

3.1 Device structure

The structure of the HEMT is shown in figure 3.1. Going from the bottom to the top of the device, it is possible to see an oxide layer, a GaN buffer layer and an $Al_xGa_{1-x}N$ barrier. On the top of this barrier between the source/drain contact and the gate, a passivation layer of Si_3N_4 can be seen. The gate contact is only deposited on the top of the $Al_xGa_{1-x}N$ barrier, while the source and the drain contacts are, respectively, on the left and right hand sides of the structure. The device is totally undoped, therefore the source and drain electrodes are recessed.

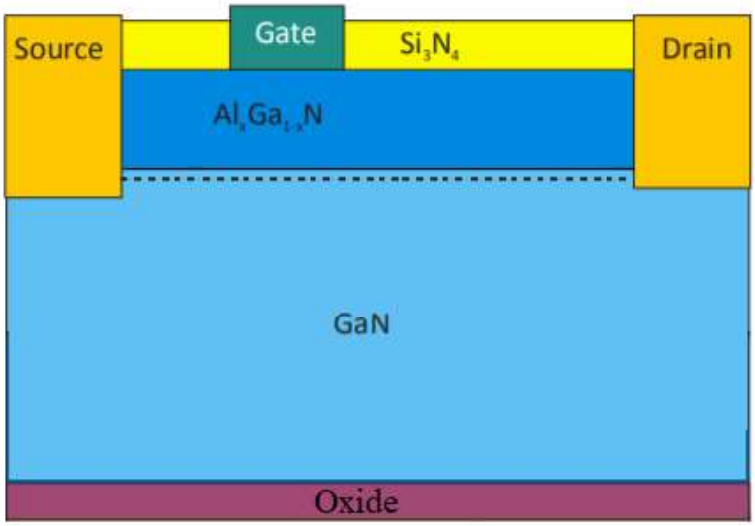

Figure 3.1: Device structure of the GaN HEMT

3.2 Operating principle of the HEMT device

The device under analysis is composed of two nitride semiconductors, AlGaN and GaN, which are considered in their wurtzite crystal structure. Wurtzite crystals do not exhibit inversion symmetry, therefore they are characterized by piezoelectric polarization, as already explained in the previous chapter. Moreover, they also show spontaneous polarization because they belong to the category of polar materials. The spontaneous and piezoelectric polarization effects are interesting to analyse not only in a freestanding material, as already done in the previous chapter, but especially if a heterostructure is considered. In fact, the polarization charges can substitute dopants in these structures because they are responsible of the formation of the two-dimensional channel, as it will be explained.

The operating principle of the device is based on the formation of the two-dimensional channel at the interface AlGaN/GaN in two different regions: under the gate contact and under the passivation layers, which can be found on the left and right hand sides of the device. In the following lines, a general explanation about the polarization effect at heterointerfaces is presented, then a more accurate analysis is carried out on the formation of the channel under the gate and the passivation layer.

3.2.1 Formation of the 2DEG channel

The starting point of the analysis is a generic heterostructure composed of two materials, in this case two nitride semiconductors called A and B. Each material is characterized of a charge sheet density on the opposite faces and if the polarization values assumed by

A and B are different, a net polar charge can be seen at the interface as shown in figure 3.2 [10].

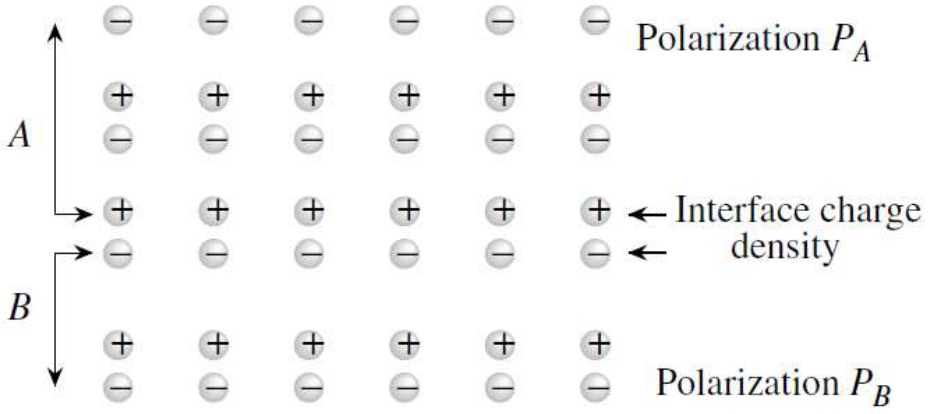

Figure 3.2: Interface charge density at the interface between two materials

The interface charge can be used to substitute dopants in heterostructures, therefore the $Al_xGa_{1-x}N/GaN$ heterostructure of the HEMT device is considered in order to explain this phenomenon. The polarization vectors represented in figure 3.3a only have the z-component along the C-direction, as already explained in the previous chapter. The relaxed GaN is characterized by a spontaneous component $P_{SP_z}(GaN)$ whose value is given by table 2.1 and shown in equation (3.1) [10].

$$P_z(GaN) = P_{SP_z}(GaN) = -0.029 \;\; C/m^2 \tag{3.1}$$

On the other hand, the strained $Al_xGa_{1-x}N$ layer is characterized by spontaneous and piezoelectric polarizations, which are obtained through the *Vegard's Law* applied between GaN and AlN, using the coefficients of table 2.1. The spontaneous contribution can be found in equation (3.2), while the piezoelectric one $P_{PE_z}(Al_xGa_{1-x}N)$ can be calculated through equation (2.13), where a is the GaN lattice constant and a_0, e_{31}, e_{33}, c_{13}, c_{33} are obtained in the following equations.

$$P_{SP_z}(Al_xGa_{1-x}N) = x(-0.081) + (1-x)(-0.029) \;\; [C/m^2] \tag{3.2}$$

$$a_0(Al_xGa_{1-x}N) = x(3.111) + (1-x)(3.189) \;\; [\mathring{A}] \tag{3.3}$$

$$e_{31}(Al_xGa_{1-x}N) = x(-0.5) + (1-x)(-0.35) \;\; [C/m^2] \tag{3.4}$$

$$e_{33}(Al_xGa_{1-x}N) = x(1.79) + (1-x)(1.27) \;\; [C/m^2] \tag{3.5}$$

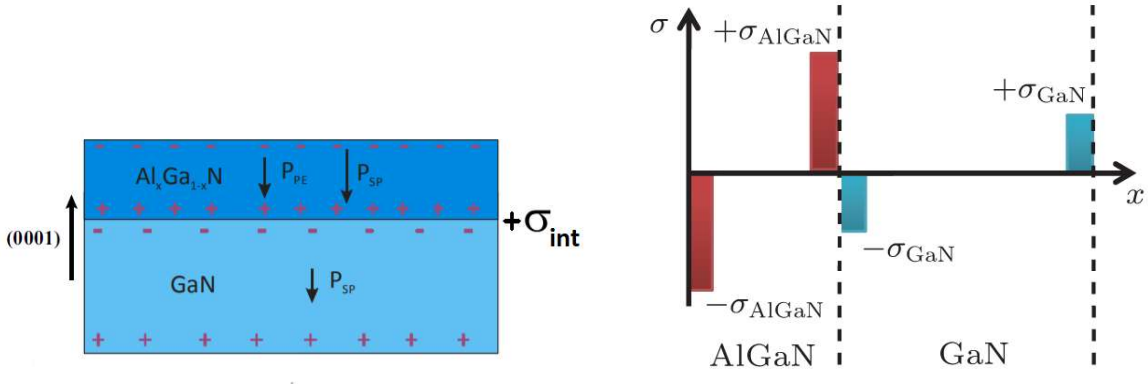

(a) Spontaneous and piezoelectric polarization (b) Charge density distribution

Figure 3.3: AlGaN/GaN heterostructure

$$c_{13}(Al_xGa_{1-x}N) = x(1.08 \cdot 10^{11}) + (1-x)(1.06 \cdot 10^{11}) \quad [Pa] \tag{3.6}$$

$$c_{33}(Al_xGa_{1-x}N) = x(3.73 \cdot 10^{11}) + (1-x)(3.98 \cdot 10^{11}) \quad [Pa] \tag{3.7}$$

This procedure leads to the calculation of the total polarization component, called $P_z(Al_xGa_{1-x}N)$, through the sum between $P_{SP_z}(Al_xGa_{1-x}N)$ and $P_{PE_z}(Al_xGa_{1-x}N)$.

The values $P_z(GaN)$ and $P_z(Al_xGa_{1-x}N)$ are used to calculate the absolute value of the polarization sheet charge density in each material, here called σ_{GaN} and $\sigma_{Al_xGa_{1-x}N}$, whose distribution is shown in figure 3.3b. Their expressions are found through formula (2.17) and indicated in equations (3.8) and (3.9).

$$\sigma_{GaN} = |P_z(GaN)| = |P_{SP_z}(GaN)| \tag{3.8}$$

$$\sigma_{Al_xGa_{1-x}N} = |P_z(Al_xGa_{1-x}N)| = |P_{SP_z}(Al_xGa_{1-x}N) + P_{PE_z}(Al_xGa_{1-x}N)| \tag{3.9}$$

Moreover, it can be interesting to find the net polarization sheet charge density σ_{int} at the interface of the heterostructure as shown in equation (3.10). The terms $P_z(top)$ and $P_z(bottom)$ correspond, respectively, to AlGaN and GaN polarization vectors along the z direction. Therefore the final formula shown in equation (3.11) can be obtained: the net interface sheet charge along the <0001> direction results positive.[15].

$$\sigma_{int} = P_z(bottom) - P_z(top) \tag{3.10}$$

$$\begin{aligned} \sigma_{int} &= P_z(GaN) - P_z(Al_xGa_{1-x}N) = \\ &= P_{SP_z}(GaN) - (P_{SP_z}(Al_xGa_{1-x}N) + P_{PE_z}(Al_xGa_{1-x}N)) \end{aligned} \tag{3.11}$$

Heterostructure under the gate

The AlGaN/GaN heterostructure is now considered under the Schottky contact of the gate at zero bias, as it can be appreciated in figure 3.4.

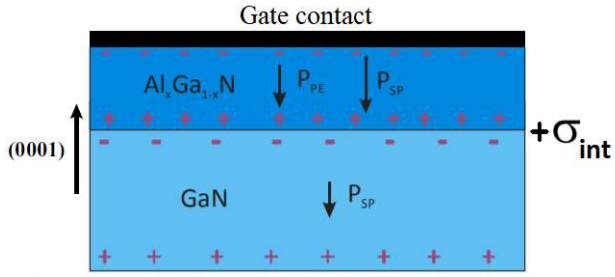

Figure 3.4: AlGaN/GaN heterostructure under the gate contact

The formation of the two-dimensional channel can be understood starting from the electric field due to the polarization charge of the AlGaN semiconductor. It depends on the thickness of this material, which is higher than the critical one, therefore electrons are stimulated into the conduction band, as explained in the previous chapter, and move under the force of the electric field (figure 2.8). Then, they contact the GaN and accumulate in the conduction band of the material, forming a 2DEG channel, which is shown in figure 3.5.

Notice that the AlGaN/GaN heterostructure under analysis is considered under a gate contact, therefore the formation of the channel is possible thanks to the Schottky barrier that pushes down the energy bands of the structure and let electron to go into the GaN side.

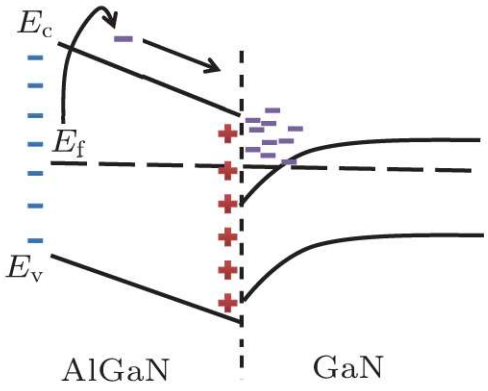

Figure 3.5: 2DEG in an AlGaN/GaN heterostructure under the gate

With the formation of the two-dimensional channel, the distribution of charges changes with respect to the previous representation 3.3b, as it can be noticed in figure 3.6a where

$+\sigma_{scr}$ is the screening charge and $-qn_s$ the 2DEG interface charge.

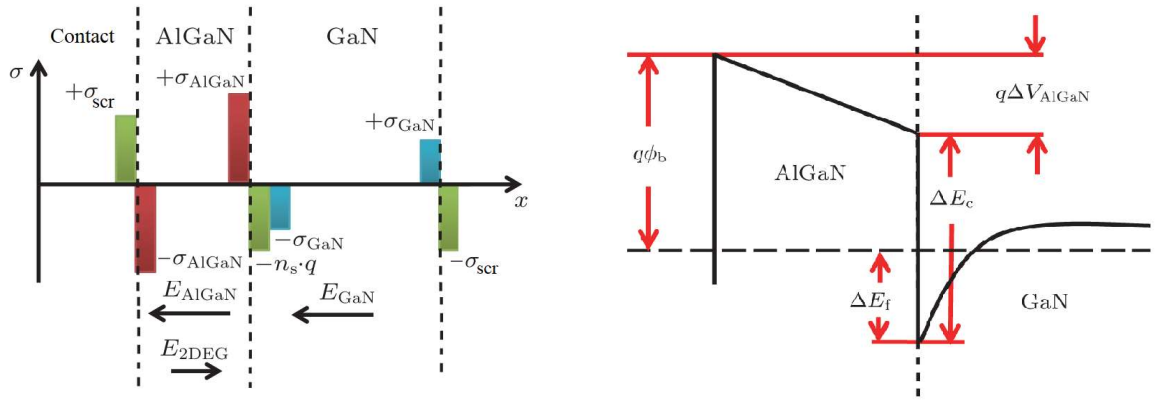

(a) Charge density distribution

(b) Conduction Band diagram

Figure 3.6: AlGaN/GaN heterostructure in presence of the 2DEG channel

In these conditions, the 2DEG density n_s can be calculated starting from the expression of the electric field in the AlGaN layer (see figure 3.6a), whose formula is shown in equation (3.12). It can be noticed the dependence on two parameters: the first one is ΔV_{AlGaN}, shown in the band diagram of figure 3.6b and defined as the potential drop on the conduction band of the AlGaN side, while the second one is the thickness of the layer, called d_{AlGaN}.

$$E_{AlGaN} = \frac{\Delta V_{AlGaN}}{d_{AlGaN}} \tag{3.12}$$

This expression can be written as a function of the 2DEG charge sheet density n_s:

$$\frac{\Delta V_{AlGaN}}{d_{AlGaN}} = \frac{\sigma_{AlGaN}}{\epsilon_{AlGaN}} - \frac{qn_s}{\epsilon_{AlGaN}} \tag{3.13}$$

where σ_{AlGaN} is the sheet charge density of the AlGaN side, ε_{AlGaN} is the AlGaN permittivity and q is the electron charge.

Taken into account the heterostructure band diagram (figure 3.6b), it can be noticed that the potential drop can be written as shown in equation (3.14), where $q\phi_B$ is the Schottky, ΔE_c the conduction band discontinuity between AlGaN and GaN, ΔE_f is the difference between the Fermi level and the minimum edge of E_c.

$$q\Delta V_{AlGaN} = q\phi_B - \Delta E_c + \Delta E_f \tag{3.14}$$

Substituting this expression in equation (3.13), the final charge sheet density can be appreciated in equation (3.15).

$$n_s = \frac{\sigma_{AlGaN}}{q} - \frac{\epsilon_{AlGaN}}{q^2 d_{AlGaN}}(q\phi_B - \Delta E_c + \Delta E_f) \tag{3.15}$$

Heterostructure under the passivation layer

In a second step, the AlGaN/GaN heterostructure is considered under the passivation layer at zero bias, as it can be appreciated in figure 3.7.

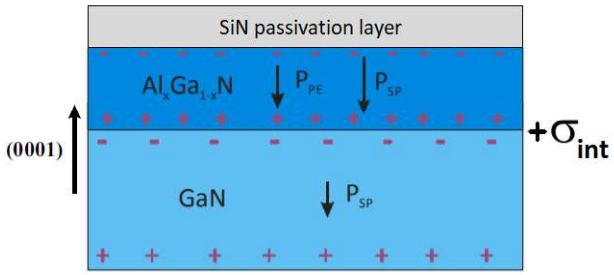

Figure 3.7: AlGaN/GaN heterostructure under the passivation layer

As in the previous case, the electric field due to the polarization charge of the AlGaN semiconductor is taken into account. It depends on the thickness of this material, therefore if it is higher than the critical one ($d > d_{cr}$), electrons are stimulated into the conduction band and move under the force of the electric field. Then, they contact the GaN, but its Fermi level may be higher than the AlGaN one, therefore very few electrons arrive into the GaN side and no 2DEG channel can be considered (see figure 3.8a) [16]. The passivation layer does not act as a Schottky contact because it is not able to push down the conduction band and enable the formation of the channel.

The solution for this problem is found assuming the existence of surface donor states on the AlGaN surface, as shown in figure 3.8b. If the AlGaN layer is thick enough ($d > d_{cr}$) and the donor state level reaches the Fermi level, surface donors become ionized and go into the conduction band. Then, under the force of the electric field, they move to the GaN side and accumulate at the interface with the AlGaN layer, forming a real 2DEG channel.

As in the heterostructure under the contact, with the formation of the two-dimensional channel, there is a different distribution of charges with respect to the first representation 3.3b. It can be noticed in figure 3.9a where $+\sigma_s$ is the ionized surface donor charge and $-qn_s$ the 2DEG interface charge.

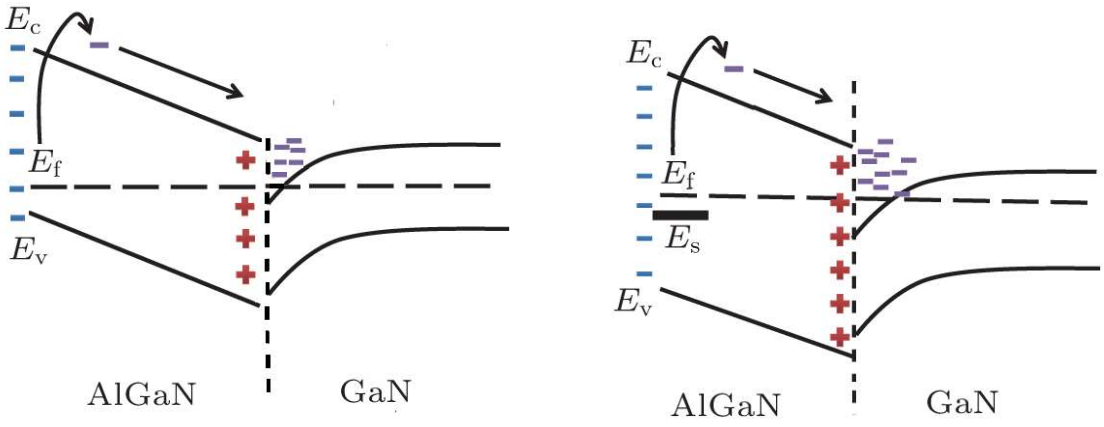

(a) Absence of surface donors (b) Presence of surface donors

Figure 3.8: AlGaN/GaN heterostructure

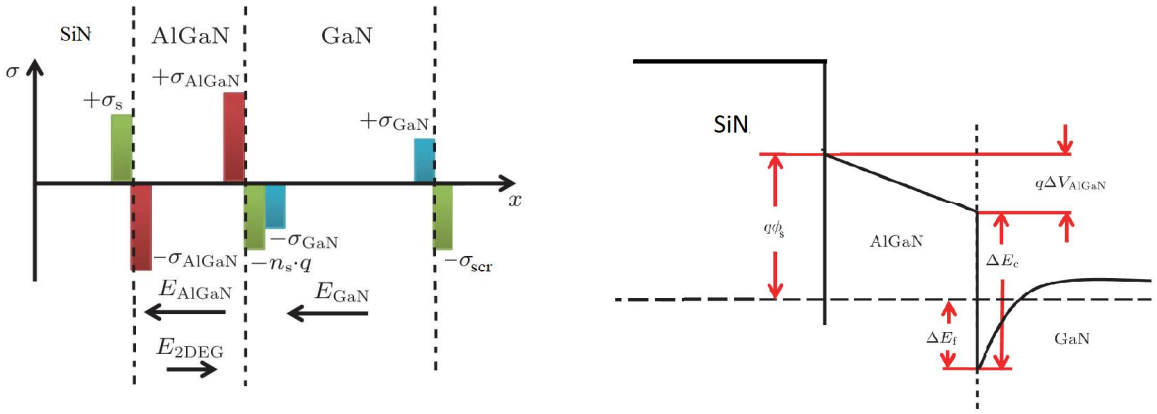

(a) Charge density distribution (b) Conduction Band diagram

Figure 3.9: AlGaN/GaN heterostructure in presence of the 2DEG channel

Now, the calculation of the 2DEG density n_s can be performed and the procedure is the same explained for the heterostructure under the gate. Therefore, the only final expression of the charge density is presented in equation (3.16), where $q\phi_s$ is the only different quantity that corresponds to the donors barrier height.

$$n_s = \frac{\sigma_{AlGaN}}{q} - \frac{\epsilon_{AlGaN}}{q^2 d_{AlGaN}}(q\phi_s - \Delta E_c + \Delta E_f) \tag{3.16}$$

Chapter 4

Fin-HEMT device

For many years, the electronic properties of nitride semiconductors have been exploited in conventional planar structures, like the HEMT devices, widely explained in the previous chapter. Many technological solutions have been studied in order to improve their performances in different application fields, but today they still present some limits. In the last years, a new structure has been proposed in order to overcome those limits and verify the advantages with respect to the conventional planar HEMT: the FinFET. It is characterized by a three dimensional structure, whose gate contact wraps around a fin-shaped body and represents a turning point with respect to other conventional devices, due to the great improvements provided for both analog and digital applications. The main advantage for digital applications is the strong gate electrostatic control of the channel, which leads to a reduction of the short channel effects (SCE), an increasing of the threshold voltage which is typically negative in conventional HEMTs, a lowering of the subthreshold swing, a higher ON/OFF ratio and finally a smaller ON resistace. On the other hand, analog applications exploit other improvements, such as the high transconductance linearity and higher values of current density, output power density, maximum and cutoff frequencies. Moreover, due to the stronger control of SCEs a melioration of the device output conductance can be achieved, with corresponding better efficiency of power stages and, hence, better thermal management.

There are different kind of FinFET devices proposed in the last years and in the following lines, a brief explanation about their structure and their improvements will be presented.

- The AlGaN/GaN FinFET with gate dielectric is characterized by a GaN buffer layer, an AlGaN barrier, an oxide layer and a gate contact that wrap around the fin body. The core of the device is composed of three channels: the first one is the two-dimensional channel at the AlGaN/GaN heterointerface, controlled by the top gate contact and the others are simply MOSFET channels created by the sidewall contacts. This configuration allows excellent ON state performances characterized

by a low ON resistance and a high drain current, but suffers from poor subthreshold characteristics due to the very low threshold voltage of the 2DEG channel [20].
An improvement of this structure can been achieved for a very low value of the fin width (20 nm) that leads not only to a shift of the threshold towards positive values, but also a reduction of OFF current and subthreshold swing. On the other hand, too narrow fin widths decrease the total amount of current and are not suited for analog/power applications [21].

- The heterojunction-free GaN nanochannel is only composed of a GaN buffer layer, which is heavily doped with silicon, due to the fact that there is no junction in the core of the device. The oxide layer and the gate contact wrap around the fin body. Some improvements can be appreciated in the ON behaviour, but it also shows excellent OFF-state performances in terms of leakage current, subthreshold slope, ON/OFF current ratio [20].

- The AlGaN/GaN recessed-gate FinFET is characterized by a more complicate structure: under the fin-shaped gate, the GaN buffer and the oxide layer are present, while in the non-gated region there are a GaN buffer layer, an AlGaN barrier and an oxide layer around the fin. In the gated region three sidewall MOS channels can be found and out of the gate, a 2DEG channel is formed at the heterointerface. The device performances are tested through modulations of the fin height and the fin width. The results show that the ON drain current remains unchanged with the geometric variations and the same effect is obtained in the OFF current [22].

- The GaN/AlGaN/GaN FinFET is characterized by a GaN buffer layer, an AlGaN barrier and a GaN cap. The oxide layer is not present and the gate wraps directly around the fin body forming a Schottky contact. The two-dimensional channel is formed at AlGaN/GaN heterointerface and it controlled not only by the top gate, but also by the side gates, responsible of the formation of depletion regions that can affect the channel. One of the advantages is the shift of the threshold towards positive values, but an interesting result can also be the lowering of the thermal resistance with respect to a planar device, which leads to higher drain currents [23].
  An improvement of the structure is realized for a gate length of 100 nm and the results show a positive threshold voltage, good subthreshold swing, reduced SCEs, high ON/OFF current [24].
  The same structure has been simulated in order to improve its RF performances. Due to the larger gate capacitance, it may turn out to have worse effects compared with its planar counterpart, but at the same time some improvements are obtained concerning the maximum and cutoff frequencies. This structure is the one directly extending planar HEMTs for analog/power applications. [25].

- The AlGaN/GaN heterostructure with double channel is characterized by a double heterostructure between AlGaN and GaN. The main advantages introduced are the increased drain current due to the double 2DEG channel, the broader transconductance and the better linearity [26].
- The Multi-Mesa-Channel AlGaN/GaN HEMT is characterized by a periodic trench composed of only AlGaN and GaN under a gate contact, that wraps around the body. The core of the device is always a 2DEG current density and the advantages produced are not very promising: a shallower threshold voltage, a smaller subthreshold slope and a decreased ON resistance with respect to a planar device.

From now on, the analysis is only focused on one of these structures, in particular the GaN/AlGaN/GaN FinFET described in [25], which gives the possibility to investigate the analog/RF performances of the device and compare them with a conventional planar structure. The device is characterized by a heterostructure, simply considered into a fin-shaped gate, therefore it can be called, more precisely, Fin-HEMT.

In the following lines, the GaN FinFET device is presented. First, a geometrical description of the whole structure is reported paying attention to employed materials and contacts. Then, the operating principle of the transistor is analysed: the control of the gate contact is explained in order to underline the differences with respect to a conventional planar device. The role of the top gate is mainly related to the formation of the two-dimensional channel under and beyond the gate, while the side gates are responsible of the depletion regions, which affect the channel, mainly through the threshold voltage and output conductance.

4.1 Device structure

The device schematic is shown in figure 4.1. Starting from the bottom and going along the Z-direction, it is possible to appreciate the sequence of materials that consists of a 10 nm oxide barrier, a 1.8 μm GaN layer (including a 37 nm of GaN channel layer), a 11 nm $Al_{0.32}Ga_{0.68}N$ barrier layer and finally a 2 nm GaN cap. Moreover, on the cap between the source/drain and the gate, a 50 nm passivation layer of Si_3N_4 is deposited and along the gate length, an Au metal wraps around the body from three sides: on the GaN cap and the sidewalls as shown in figure. Paying attention to the YZ plane, the most useful values are the fin width w equal to 100 nm and the fin height h, whose value of 50 nm can be obtained by the sum of GaN channel, AlGaN barrier and GaN cap. Looking at the XZ plane, the main lengths are $L_G = 0.4\ \mu m$, $L_{GS} = 0.25\ \mu m$ and $L_{GD} = 1\ \mu m$. Instead, the structure is completely undoped, therefore the source and drain contacts on the opposite sides of the device are recessed.

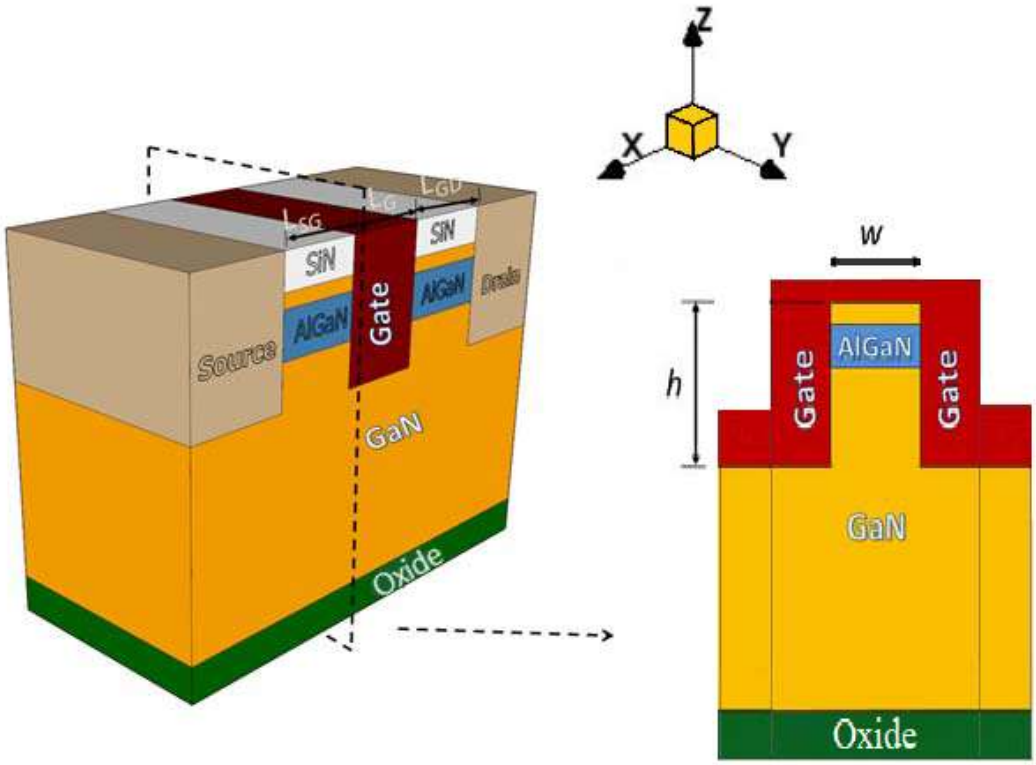

Figure 4.1: Device structure of the AlGaN/GaN FinFET

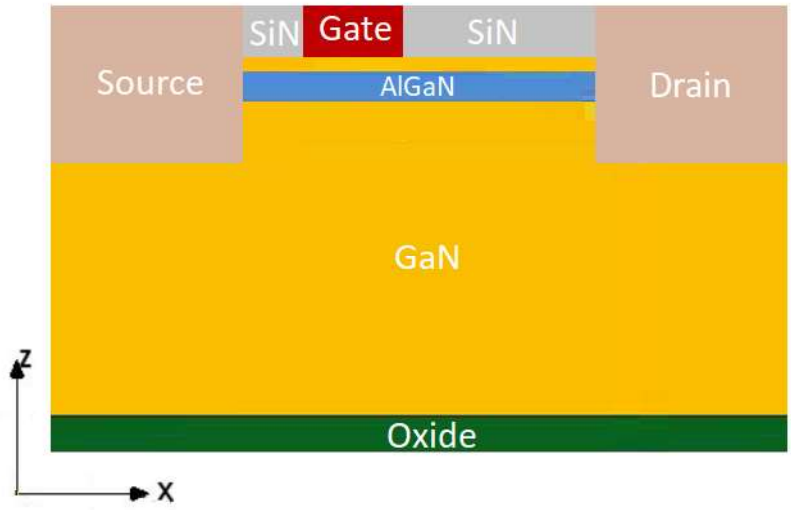

Figure 4.2: XZ representation of the AlGaN/GaN FinFET

4.2 Operating principle of the device

The Fin-HEMT structure can be analysed from two different point of views. Figure 4.2 shows the device on the XZ plane and, apart from the 2 nm GaN cap, the structure is equal to the conventional planar one of the previous chapter. In particular, the top gate and the passivation layers are deposited on the GaN/AlGaN/GaN heterostructure and are necessary for the operating principle of the device. On the other hand, the section of figure 4.1 shows the YZ plane of the same structure: again it can be noticed the top gate on the GaN/AlGaN/GaN heterostructure, but also two side gates whose effect was not present in the conventional device of the previous chapter and cannot be neglected.

4.2.1 Top gate control: formation of the 2DEG channel

The XZ plane of the structure is considered. At zero bias, the undoped GaN/AlGaN/-GaN heterostructure under the top gate is taken into account in order to analyse the polarization effect of each material. The polarization vectors are represented in figure 4.3a where they are considered along the C-direction with the Ga-face on the top.

The GaN cap and buffer are only characterized by the spontaneous component of the polarization which is shown in equation (3.1). On the other hand, the $Al_xGa_{1-x}N$ barrier with a mole fraction x equal to 0.32, is characterized by the spontaneous and the piezoelectric components. Substituting $x = 0.32$ into equations (3.2), (3.3), (3.4), (3.5), (3.6) and (3.7), it is possible to find the following results.

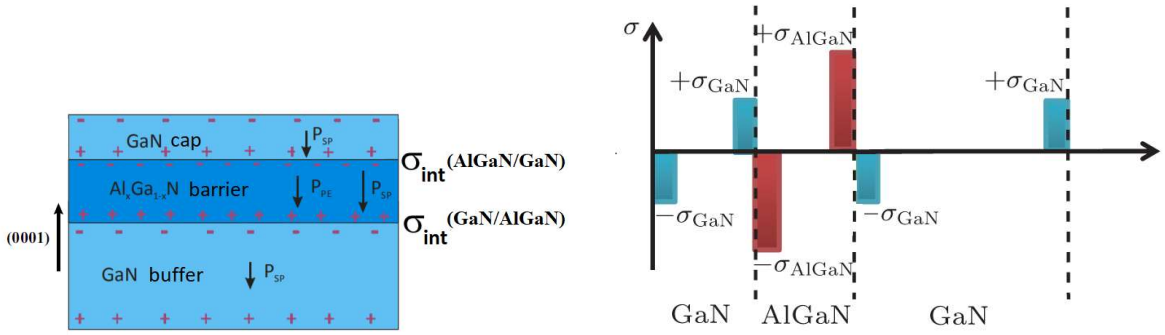

(a) Spontaneous and piezoelectric polarization (b) Charge density distribution

Figure 4.3: GaN/AlGaN/GaN heterostructure

$$P_{SP_z}(Al_{0.32}Ga_{0.68}N) = -0.04564 \quad C/m^2 \tag{4.1}$$

$$a_0(Al_{0.32}Ga_{0.68}N) = 3.164 \quad \mathring{A} \tag{4.2}$$

$$e_{31}(Al_{0.32}Ga_{0.68}N) = -0.3980 \quad C/m^2 \tag{4.3}$$

$$e_{33}(Al_{0.32}Ga_{0.68}N) = 1.4364 \quad C/m^2 \tag{4.4}$$

$$c_{13}(Al_{0.32}Ga_{0.68}N) = 1.0664 \cdot 10^{11} \quad Pa \tag{4.5}$$

$$c_{33}(Al_{0.32}Ga_{0.68}N) = 3.9 \cdot 10^{11} \quad Pa \tag{4.6}$$

The spontaneous contribution is just obtained through equation (4.1), while the piezoelectric one is calculated by substituting a_0, e_{31}, e_{33}, c_{13} and c_{33} into expression (2.13). Knowing that $relax = 0.1$, the result is shown as follows.

$$P_{PE_z}(Al_{0.32}Ga_{0.68}N) = -0.01124 \quad C/m^2 \tag{4.7}$$

In conclusion, the total polarization vector is given by the sum of the two contributions indicated in equation (4.8). Notice that all the polarization values have been expressed only along the z-direction because the x-and-y components are equal to zero, as already demonstrated in the theoretical section of the previous chapter.

$$P_z(Al_{0.32}Ga_{0.68}N) = (P_{SP_z} + P_{PE_z})(Al_{0.32}Ga_{0.68}N) = -0.05688 \quad C/m^2 \tag{4.8}$$

Once known all the polarization vectors, the sheet charge densities σ_{GaN} and $\sigma_{Al_{0.32}Ga_{0.68}N}$ can be calculated through equations (3.8) and (3.9). Moreover, it is interesting the calculation of the net polarization sheet charge densities $\sigma_{int}(AlGaN/GaN)$ and $\sigma_{int}(GaN/AlGaN)$, using $x = 0.32$ into the formula (3.11). The final values are shown in the following expressions.

$$\sigma_{GaN} = 0.029\ C/m^2 \qquad \sigma_{Al_{0.32}Ga_{0.68}N} = 0.05688\ C/m^2 \tag{4.9}$$

$$\sigma_{int}(AlGaN/GaN) = P_z(GaN) - P_z(Al_{0.32}Ga_{0.68}N) = 0.02788\ \ C/m^2 \tag{4.10}$$

$$\sigma_{int}(GaN/AlGaN) = P_z(Al_{0.32}Ga_{0.68}N) - P_z(GaN) = -0.02788\ \ C/m^2 \tag{4.11}$$

Notice that $\sigma_{int}(AlGaN/GaN)$ and $\sigma_{int}(GaN/AlGaN)$ have equal and opposite values, therefore in the following pictures they will be indicated respectively as $+\sigma_{int}$ and $-\sigma_{int}$.

Heterostructure under the top gate

The GaN/AlGaN/GaN heterostructure with an Au Schottky contact on the top is taken into account in order to understand how the polarization-induced charges imply the formation of the two-dimensional channel [16]. Figure 4.4 shows a graphical representation of the structure.

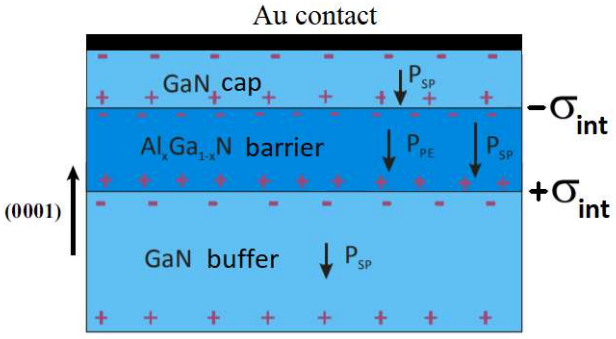

Figure 4.4: GaN/AlGaN/GaN heterostructure under the Au gate contact

The attention is firstly payed on the AlGaN layer: the charge sheet densities are distributed along the two opposite faces and produce an electric field responsible of the inclination of the semiconductors energy bands, as already indicated in figure 2.7. The electric field is strictly related to the thickness of the material d_{AlGaN}, whose variation

can produce different effects in the material. As already explained, a very small value of d does not imply any effect due to the polarization charges (figure 2.8a), while if the critical thickness is reached, electrons are stimulated into the conduction band and move thanks to the electric field(figure 2.8c). When electrons contact the GaN buffer layer, they accumulate in the conduction band and form the 2DEG channel.

Notice that the AlGaN/GaN heterostructure does not require the presence of donor states, as already explained, because it is characterized by a gate contact, therefore the Schottky barrier pushes down the energy bands of the structure and let more electrons to go into the GaN side.

In figure 4.5a the charge distribution is shown: it can be noticed not only the presence of the polarization-induced charges, but also of the charge density due to the 2DEG channel.

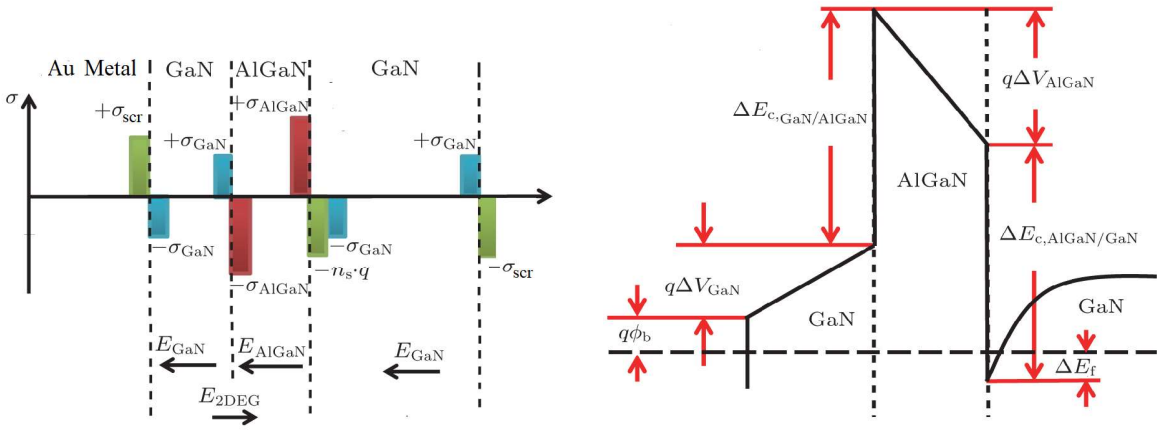

(a) Charge density distribution

(b) Conduction Band diagram

Figure 4.5: GaN/AlGaN/GaN heterostructure in presence of the 2DEG channel

It is interesting the calculation of the density n_s which is performed starting from the equations of GaN and AlGaN electric fields [16]. Equations (4.12) and (4.13) show their dependence on two parameters: the potential drops on the conduction band, called ΔV_{GaN} and ΔV_{AlGaN} and the thickness of the materials, d_{GaN} and d_{AlGaN}.

$$E_{GaN} = \frac{\Delta V_{GaN}}{d_{GaN}} \tag{4.12}$$

$$E_{AlGaN} = \frac{\Delta V_{Al_{0.32}Ga_{0.68}N}}{d_{Al_{0.32}Ga_{0.68}N}} \tag{4.13}$$

These expressions can be written as a functions of the charge sheet density n_s, as follows:

$$\frac{\Delta V_{Al_{0.32}Ga_{0.68}N}}{d_{Al_{0.32}Ga_{0.68}N}} = \frac{\sigma_{Al_{0.32}Ga_{0.68}N}}{\epsilon_{Al_{0.32}Ga_{0.68}N}} - \frac{qn_s}{\epsilon_{Al_{0.32}Ga_{0.68}N}} \tag{4.14}$$

$$\frac{\Delta V_{GaN}}{d_{GaN}} = \frac{\sigma_{GaN}}{\epsilon_{GaN}} - \frac{qn_s}{\epsilon_{GaN}} \tag{4.15}$$

where σ_{GaN} and $\sigma_{Al_{0.32}Ga_{0.68}N}$ are the polarization sheet charges found previously, while $\epsilon_{Al_{0.32}Ga_{0.68}N}$ and $\epsilon_{Al_{0.32}Ga_{0.68}N}$ the permittivities.

In figure 4.5b the conduction band diagram of the heterostructure is shown and it can be exploited to find a link between the potential drops ΔV_{GaN} and $\Delta V_{Al_{0.32}Ga_{0.68}N}$, which are shown in equation (4.16).

$$q\Delta V_{Al_{0.32}Ga_{0.68}N} = q\phi_B + \Delta E_f - q\Delta V_{GaN} \tag{4.16}$$

Notice that $q\phi_B$ is the Schottky barrier and ΔE_f is the distance between the Fermi level and the minimum edge of E_c. Substituting equation (4.15) into (4.16), it can be found the following result:

$$q\Delta V_{Al_{0.32}Ga_{0.68}N} = q\phi_B + \Delta E_f - q\left(\frac{\sigma_{GaN}}{\epsilon_{GaN}} - \frac{qn_s}{\epsilon_{GaN}}\right) \tag{4.17}$$

In conclusion, this expression is inserted into equation (4.14) and the final formula for n_s is calculated and shown as follows:

$$\begin{aligned} n_s = &\frac{1}{q(d_{GaN}\epsilon_{Al_{0.32}Ga_{0.68}N} + d_{Al_{0.32}Ga_{0.68}N}\epsilon_{GaN})} \cdot \Big[\epsilon_{GaN}\sigma_{Al_{0.32}Ga_{0.68}N}d_{Al_{0.32}Ga_{0.68}N} + \\ &+ \epsilon_{Al_{0.32}Ga_{0.68}N}\sigma_{GaN}d_{GaN} - \frac{q\phi_B + \Delta E_f}{q} \cdot \epsilon_{Al_{0.32}Ga_{0.68}N}\epsilon_{GaN}\Big] \end{aligned} \tag{4.18}$$

Heterostructure under the passivation layer

The GaN/AlGaN/GaN heterostructure is now analysed out of the gate with the passivation layer on the top and zero bias, in order to understand what are the differences in the formation of 2DEG channel with respect to the previous case. The representation of the structure is shown in figure 4.6 [17].

The behaviour is very similar to the one studied for the simple AlGaN/GaN heterostructure. Paying attention on the AlGaN layer, the polarization-induced charges produce an electric field and a consequent slope in the energy bands. Moreover, for a thickness of the material higher than the critical one, electrons go from the valence band to the conduction band and under the force of the electric field they move to the GaN side. The passivation layer does not act as the Schottky contact: it is not able to push

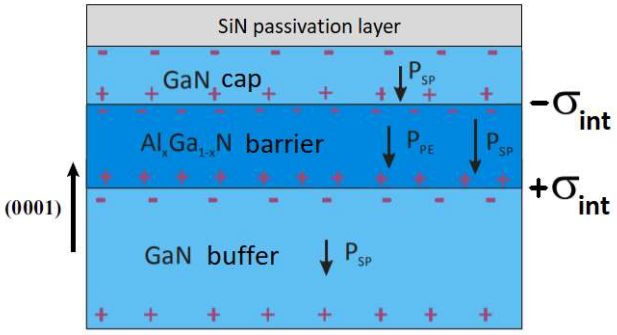

Figure 4.6: GaN/AlGaN/GaN heterostructure under the passivation layer

down the energy bands, therefore few electrons arrive in the GaN side and no 2DEG channel is formed. This result can be appreciated in the conduction band diagram of figure 4.8a. The solution is found through the addition of donor traps between the passivation layer and the GaN cap. As explained in chapter 3, when the donor state level reaches the Fermi level (figure 3.8b), ionized surface donors go into the conduction band and arrive in the GaN side, therefore the 2DEG channel is formed. The conduction band diagram changes as shown in figure 4.8b.

The charge distribution of the heterostructure can be appreciated in figure 4.7: the only difference with respect to the previous case (figure 4.5a) is the value $+\sigma_s$, which corresponds to the donor traps charge.

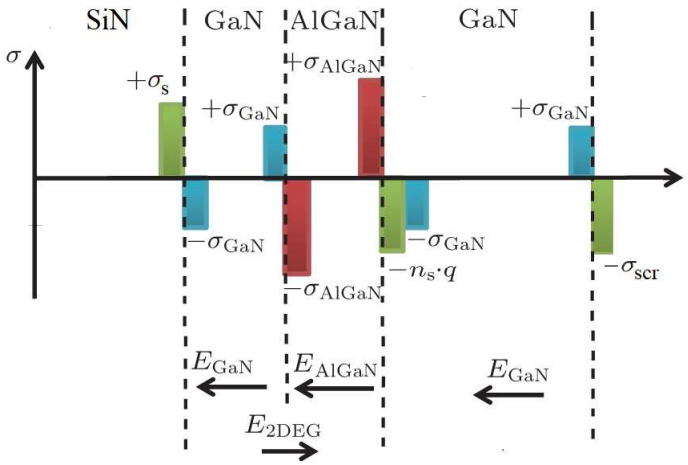

Figure 4.7: Charge distribution of a Sin/GaN/AlGaN/GaN heterostructure

Even in this case, it can be interesting the calculation of the 2DEG charge density n_s. The procedure is equal to the previous case and the final formula is the one shown

in equation (4.18) with the only difference that $q\phi_B$ is not the Schottky barrier, but the donor barrier height.

4.2.2 Side gates control

Now the structure can be analysed on the YZ plane. It can be noticed the presence of the top gate, whose role has been analysed in the previous section, and the side gates, which are laterally deposited on the heterostructure.

At zero bias, the lateral gates create with the GaN buffer layer a metal-semiconductor junction on the two sides of the fin-width. This implies the formation of two depletion regions: if the fin width is quite big, the effect of the depletion regions on the two-dimensional channel can be neglected and the behaviour of the device is very similar to a conventional planar one, while with a reduced fin width the 2DEG channel is laterally deplete by the metal-semiconductor junctions. It is possible to appreciated this behaviour on figure 4.9 where it can be noticed the bending of the conduction band due to the metal-semiconductor junctions.

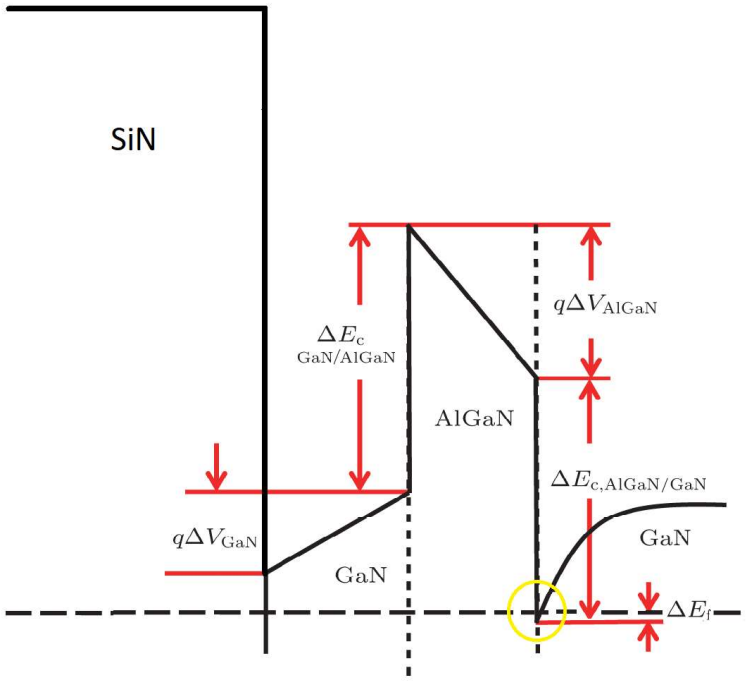

(a) Absence of donor traps

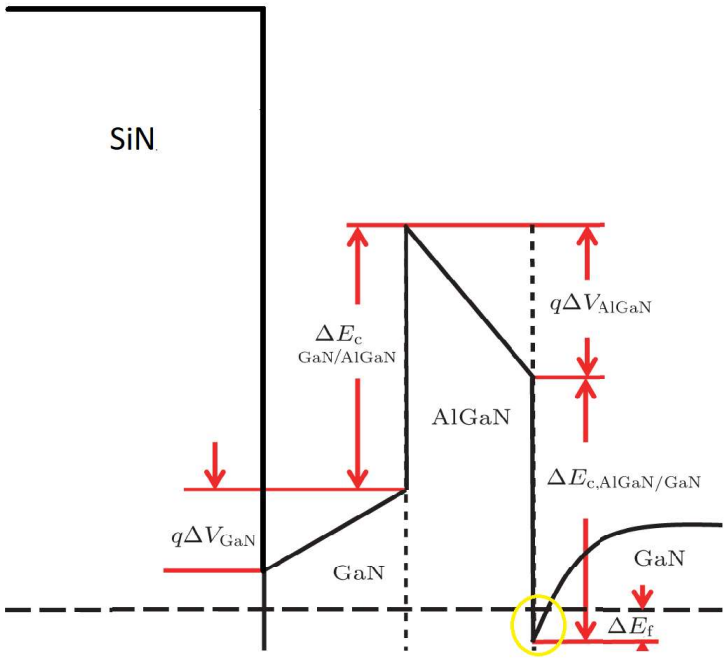

(b) Presence of traps

Figure 4.8: Conduction band diagram of a SiN/GaN/AlGaN/GaN heterostructure

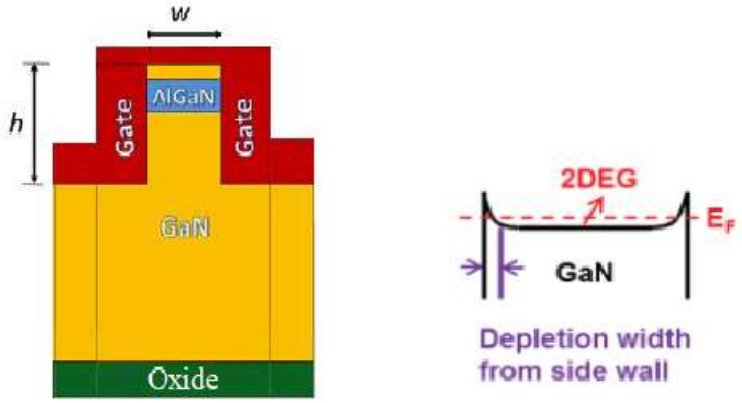

Figure 4.9: YZ representation of the Fin-HEMT device and conduction band diagram along the Y-axis

Chapter 5

Fin-HEMT simulations

Behaviour and performances of the Fin-HEMT have been verified through numerical simulations implemented on a TCAD (Technology Computer-Aided Design), called Synopsys Sentaurus. The simulation is based on two steps: the first one is focused on the structure generation and the second one on the device simulation.
The structure generation is performed through the Sentaurus Structure Editor tool, which is a two-dimensional and three-dimensional structure editor, but also a 3D process emulator. It allows the geometric realization of the Fin-HEMT structure, the definition of materials, electrical contacts, the generation of mesh and doping profiles. The device simulation is carried out using the Sentaurus Device tool, which allows the simulation of one-dimensional, two-dimensional and three-dimentional semiconductor devices. It is possible to define the type of contact (Ohmic, Schottky, etc) and the physical models necessary to verify a certain behaviour.

In this chapter the simulation codes are explained and the obtained results are presented. In the first part there are explanations about the structure generation code with details on materials, doping and mesh. In the second part the device simulation code is described and the obtained results are presented, paying attention on different aspects. First, the equilibrium condition of the device is investigated, then the DC simulations are performed in order to extract the drain current characteristics and transcharacteristics. Each result is compared with the three-dimensional structure that corresponds to a conventional planar HEMT, very similar to the one analysed in chapter 3.

5.1 Structure generation

The generation of the structure is performed through a code that starts from the definition of the geometric dimensions of the device, which have been listed at the beginning of the chapter 4. To follow, the materials to be used are introduced and the shape of gate, drain and source contacts is added. Then, the doping profiles are specified: the

device under analysis is not characterized by the presence of dopants, therefore this code section is only dedicated to the definition of the mole fraction. The last step consists in the generation of the mesh, which allows to decide the precision used in the simulation.

The simulated geometric device is shown in figure 5.1: it can be noticed the presence of a large substrate, necessary in 3D structures to avoid forcing the boundary conditions and confine the polarization charges at the bottom of the device. Cutting this structure along the X and Y axis, the accuracy of the mesh can be appreciated. Figure 5.2a shows the device on the XZ plane, where the mesh results more dense in the region between source and drain. In particular, a zoom under the gate region (figure 5.2c) demonstrates that the mesh precision is strongly increased. The same result can be obtained paying attention on the YZ plane, shown in figure 5.2b. The high accuracy of the mesh is concentrated around the fin width under the gate, as it can be easily appreciated in figure 5.2d.

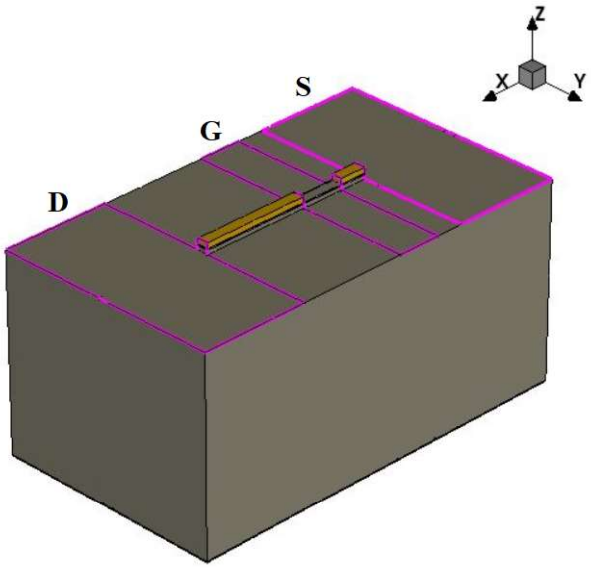

Figure 5.1: Structure of the Fin-HEMT device: in grey the GaN material, in violet the AlGaN material and in brown the Si_3N_4 material

Starting from this structure, the values of doping concentration and mole fraction can be easily verified. Figure 5.3 demonstrates the absence of dopants and the presence of a non-null mole fraction, equal to 0.32, in a very small area which corresponds to the AlGaN layer.

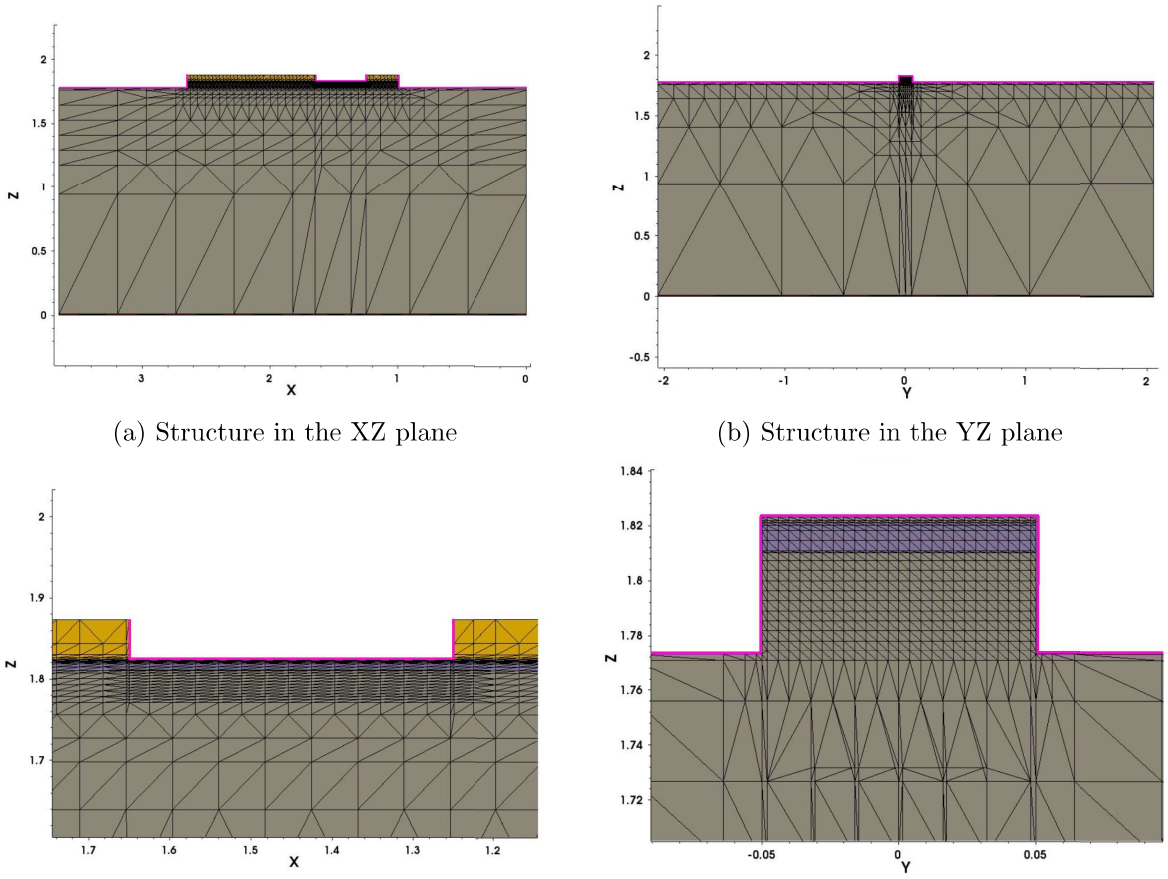

(a) Structure in the XZ plane

(b) Structure in the YZ plane

(c) Zoom on the gate region in the XZ plane

(d) Zoom on the gate region in the YZ plane

Figure 5.2: Mesh generation in the Fin-HEMT structure: in grey the GaN material, in violet the AlGaN material and in brown the Si_3N_4 material

5.2 Device simulation

The code used for the device simulation starts with the definition of the contacts: the gate is associated to a Schottky contact with the Au workfunction equal to 5 eV, while source and drain are simply ohmic contacts. Moreover, it is possible to define the initial bias voltage associated to each electrode, but in this case it is set to zero for all contacts. Then, the Sentaurus physical models are defined and explained starting from the *Mobility models*. The mobility of the carriers is expressed through three different models, the first one is related to phonon scattering which is only dependent on the lattice temperature. Equation (5.1) shows how the mobility varies with respect to the temperature T, the mobility due to bulk phonon scattering μ_L and a positive coefficient ζ dependent on the material [19].

$$\mu_{const} = \mu_L \left(\frac{T}{300K} \right)^{-\zeta} \tag{5.1}$$

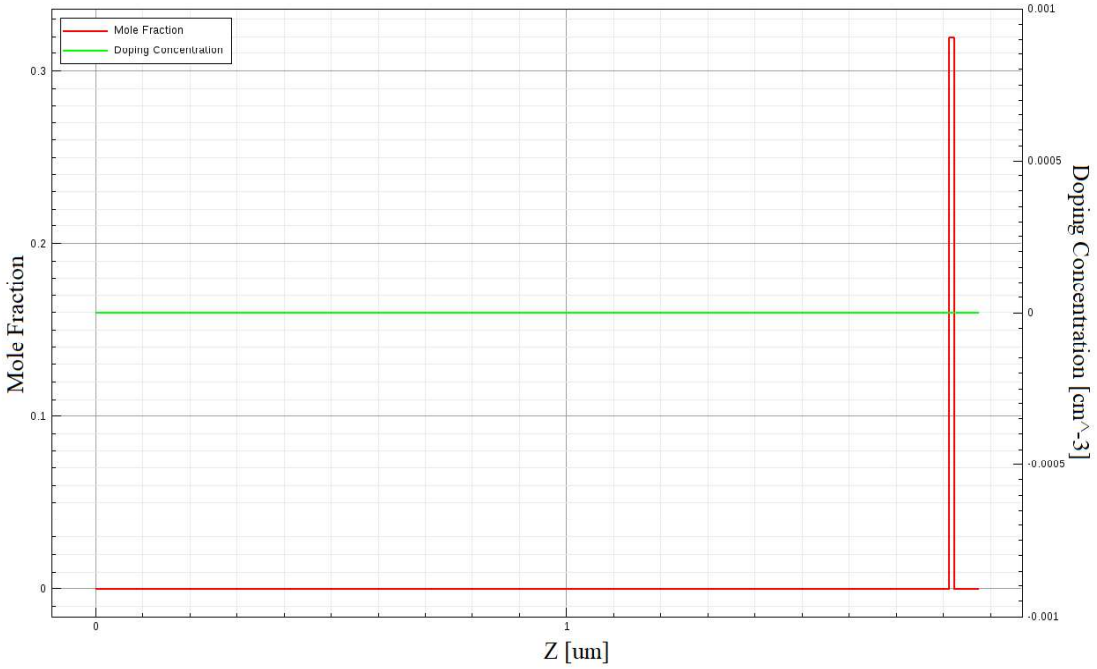

Figure 5.3: Mole fraction and doping concentration along the Z-direction

The second model used to describe the mobility takes into account the doping dependence and it has been proposed by Masetti through equation (5.2), where there is the doping concentration N, the reference mobilities μ_{min1}, μ_{min2} and μ_1, the reference doping concentrations P_c, C_r and C_s and finally, the exponents α and β. All there values can be found in the parameter file of each material [19].

$$\mu_{dop} = \mu_{min1} \cdot exp\left(-\frac{P_c}{N}\right) + \frac{\mu_{const} - \mu_{min2}}{1 + \left(\frac{N}{C_r}\right)^{\alpha}} - \frac{\mu_1}{(1 + \left(\frac{C_s}{N}\right)^{\beta}} \tag{5.2}$$

The third model for the mobility is the one dependent on the high field saturation: for high electric fields the the carrier drift velocity is not proportional to the electric field because the velocity saturates to a finite speed defined as v_{sat}. The high field saturation model exploits a submodel that depends on the actual mobility model, which has been proposed by Canali. Equation (5.3) shows the expression to calculate the new mobility, where μ_{low} denotes the low field mobility, F_{hfs} the driving field and β the temperature coefficient. All these values can be calculated though the formulas found in the parameter file of each material [19].

$$\mu(F) = \frac{(1+\alpha)\mu_{low}}{\alpha + \left[1 + \left(\frac{(1+\alpha)\mu_{low} \cdot F_{hfs}}{v_{sat}}\right)^{\beta}\right]^{1/\beta}} \tag{5.3}$$

Starting from the three mobility contributions, the final value can be obtained through

the Matthhiessen's rule, expressed in equation (5.4), where μ_1, μ_2,... are the different mobility components.

$$\mu = \frac{1}{\mu_1} + \frac{1}{\mu_2} + ... \tag{5.4}$$

Moreover, the *Sentaurus Device* supports different carrier transport models for semiconductors. The one used in this simulation is the *Drift-diffusion Model*, that calculates the current densities for electrons and holes through equations (5.5): ε is the electric field, n and p the electron and hole concentrations, μ_n and μ_p the electron and hole mobilities, D_n and D_p the electron and hole diffusivities, which can be found through Einstein's relations shown in (5.6).

$$\overline{J_n} = q\mu_n n\overline{\varepsilon} + qD_n\nabla n \tag{5.5}$$

$$\overline{J_p} = q\mu_p p\overline{\varepsilon} - qD_p\nabla p$$

$$D_n = k_B T\mu_n \tag{5.6}$$

$$D_p = k_B T\mu_p$$

Apart from the mobility and the carrier transport, the *Sentaurus Device* exploits other models: the heterointerface model that considers the presence of heterostructures in the simulation, the piezoelectric polarization model which includes the effect of spontaneous and piezoelectric polarizations according to the formulas of chapter 4, the traps model able to generate a certain concentration of donor traps (here equal to $3 \cdot 10^{13}$ cm^{-3}) between the passivation layer and the GaN cap.

The code also includes a 'Math' section where, for example, it is possible to insert a wanted precision or the kind of method to solve the problem, e.g. iterative, block interative, etc. The last part of the code is a 'Solve' section that changes with respect to the goal of the simulation and it will be explained for the equilibrium and out of equilibrium conditions.

5.2.1 Equilibrium condition analysis

In a physical system, the thermal equilibrium is the condition characterized by the absence of any energy exchange: the applied electric field should be zero and the total current should be null. In this conditions, it is possible to define the Poisson equation, shown in (5.7), where φ is the electrostatic potential, ρ the space charge density and ϵ the permittivity of the material. The value of ρ can be written as: $\rho = q(n - p + N_D - N_A + \frac{\rho_\pi}{q})$

where n and p are the concentrations of electrons and holes, N_D and N_A are the concentrations of donors and acceptors, ρ_π is the polarization-induced charge density found through the formula (2.16), as explained in chapter 2 [9].

$$\nabla \cdot \varphi = -\frac{\rho}{\epsilon} \tag{5.7}$$

In this case, the 'Solve' section includes the term *Poisson* in order to find a solution for the Poisson equation and achieve the equilibrium condition at zero initial bias. The simulation results provide different information about the device and the most important ones are analysed as follows.

Band gap and electron affinity

Band gap and electron affinity are shown in figure 5.4 where there is a zoom along the Z-direction of the device. Starting from the right hand side of the graph, it can be found the GaN cap, the AlGaN layer and, finally, the GaN buffer layer.

From the graph, the band gap of each semiconductor is extracted: it assumes a value equal to 3.435 eV for GaN and 4.147 eV for $Al_{0.32}Ga_{0.68}N$. The AlGaN band gap can be verified through the *Vegard's Law* as shown in equations (5.8).

$$\begin{aligned} &E_{gAlN} = 5.662\ eV \\ &E_{gGaN} = 3.435\ eV \\ &E_{gAl_{0.32}Ga_{0.68}N} = x \cdot E_{gAlN} + (1-x) \cdot E_{gGaN} = \\ &\qquad = 0.32 \cdot 5.662\ eV + 0.68 \cdot 3.435\ eV = 4.147\ eV \end{aligned} \tag{5.8}$$

This procedure is repeated for the electron affinity, which is equal to 3.958 eV for GaN and 3.422 eV for $Al_{0.32}Ga_{0.68}N$. As in the previous case, the AlGaN affinity can be verified using the *Vegard's Law*, as shown in equation (5.9).

$$\begin{aligned} &q\chi_{GaN} = 3.958\ eV \\ &q\chi_{AlN} = 2.283\ eV \\ &q\chi_{Al_{0.32}Ga_{0.68}N} = x \cdot q\chi_{AlN} + (1-x) \cdot q\chi_{GaN} = \\ &\qquad = 0.32 \cdot 2.283\ eV + 0.68 \cdot 3.958\ eV = 3.422\ eV \end{aligned} \tag{5.9}$$

Spontaneous and piezoelectric polarization

Spontaneous and piezoelectric polarization values are extracted from the simulation under the form of total polarization vectors, which are expressed in C/cm^2. Figure 5.5 shows their values along the X, Y and Z direction in the region under the gate. It can be noticed that the only component different from zero is the one along the Z direction,

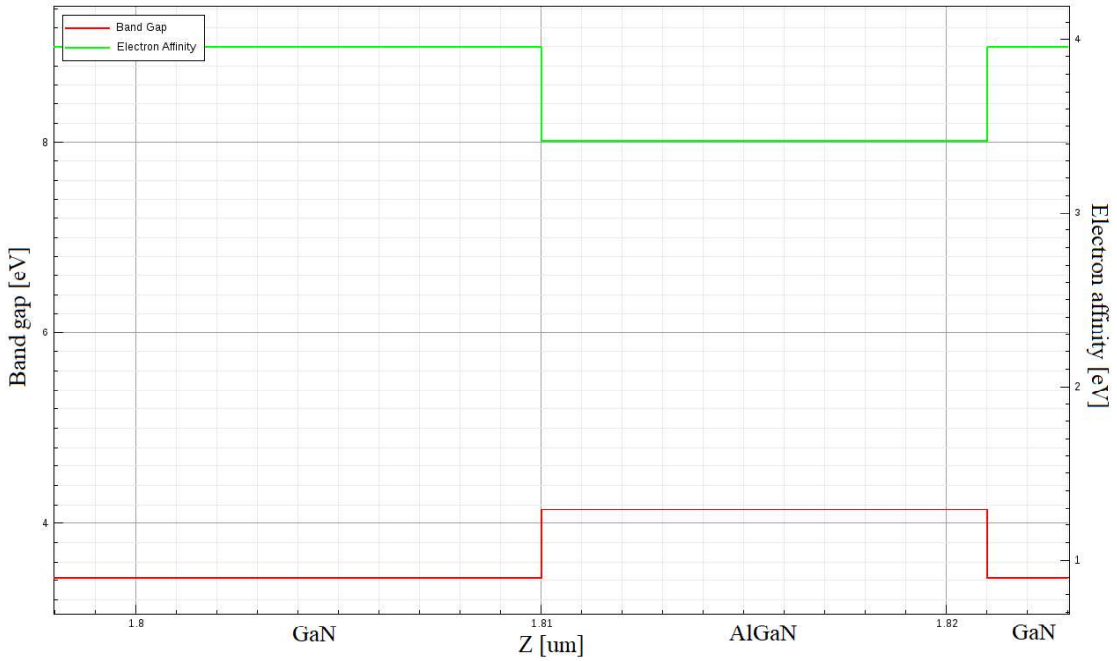

Figure 5.4: Band gap and electron affinity along the Z-direction

which assumes a value equal to $-2.9 \cdot 10^{-6}\ C/cm^2$ for the GaN and $-5.67 \cdot 10^{-6}\ C/cm^2$ for the $Al_{0.32}Ga_{0.68}N$, as expected. The simulated values can be verified by a comparison with equations (3.1) and (4.8).

Moreover, the simulation also provides the distribution of the polarization-induced charge concentration, expressed in cm^{-3} and shown in figure 5.6 in the region under the gate. In the picture there is a zoom on GaN/AlGaN/GaN heterostructure, where the GaN cap is on the right hand side. As expected, moving from the right to the left, it can be noticed that at the interface GaN/AlGaN a negative charge density is found, while at the interface AlGaN/GaN a positive one can be seen.

Traps

The GaN/AlGaN/GaN heterostructure under the passivation layer needs the presence of donor traps ($3 \cdot 10^{13}\ cm^{-3}$) at the interface between Si_3N_4 and GaN for the formation of the two-dimensional channel, as previously discussed. The concentration of ionized donors is shown in figure 5.7 where there is a zoom on the GaN/SiN interface.

Band diagram

One of the most important simulation results is the band diagram, the plot of the energy levels of the structure as a function of a spatial dimension. The band diagram can be very useful to understand the behaviour of a device at different bias conditions, in this

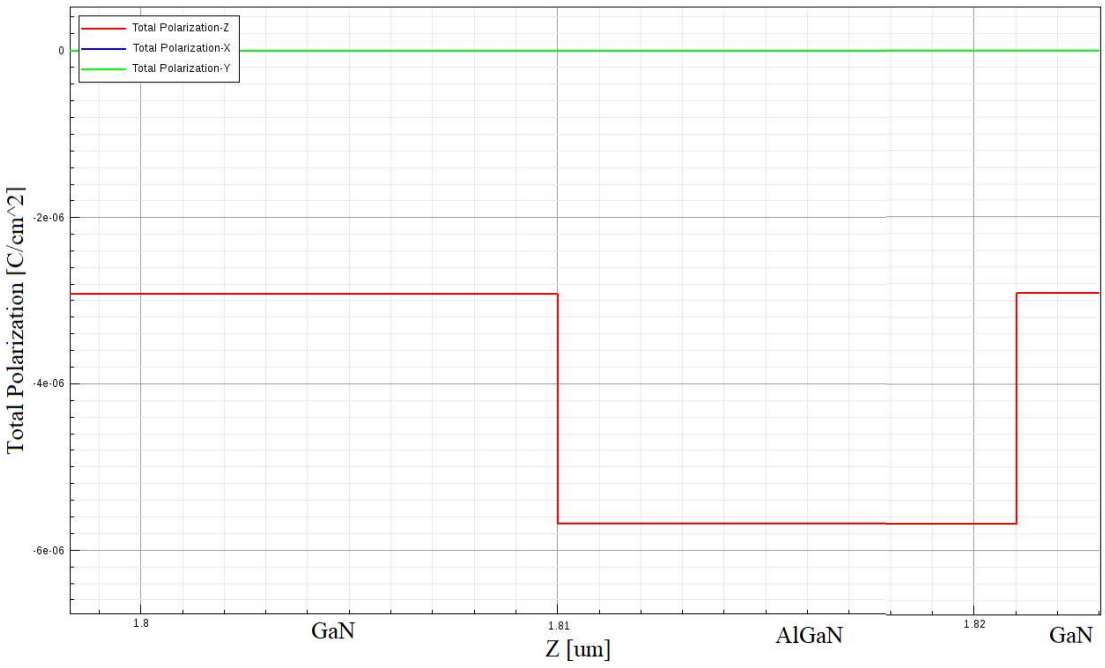

Figure 5.5: Total polarization vectors along the Z-direction in the region under the gate contact

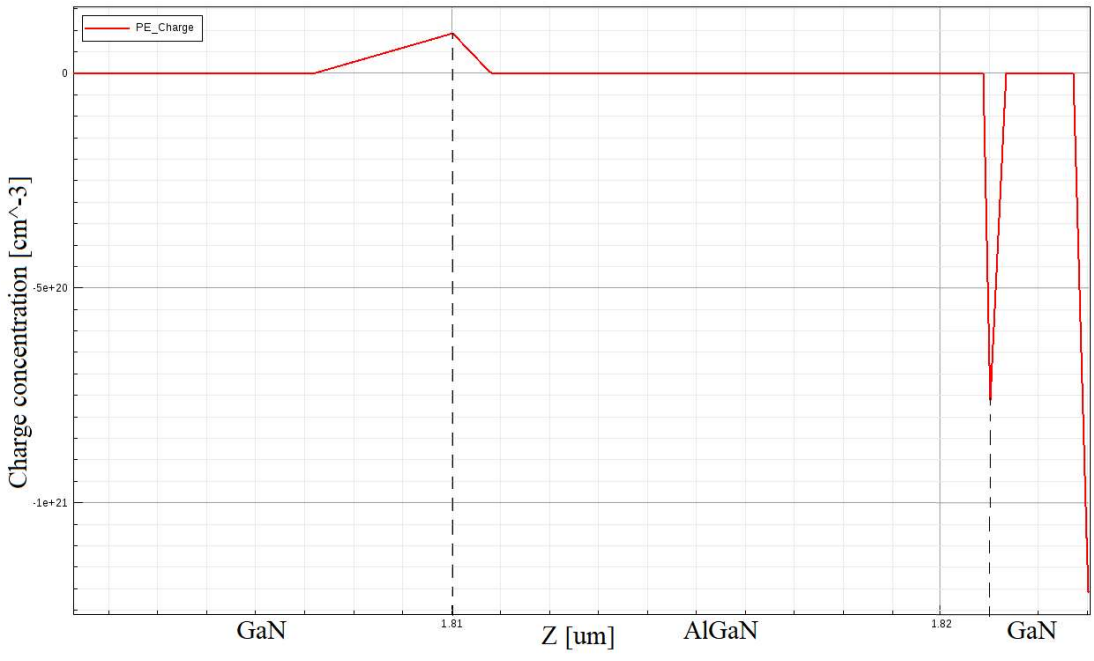

Figure 5.6: Polarization-induced charge density along the Z-direction in the region under the gate contact

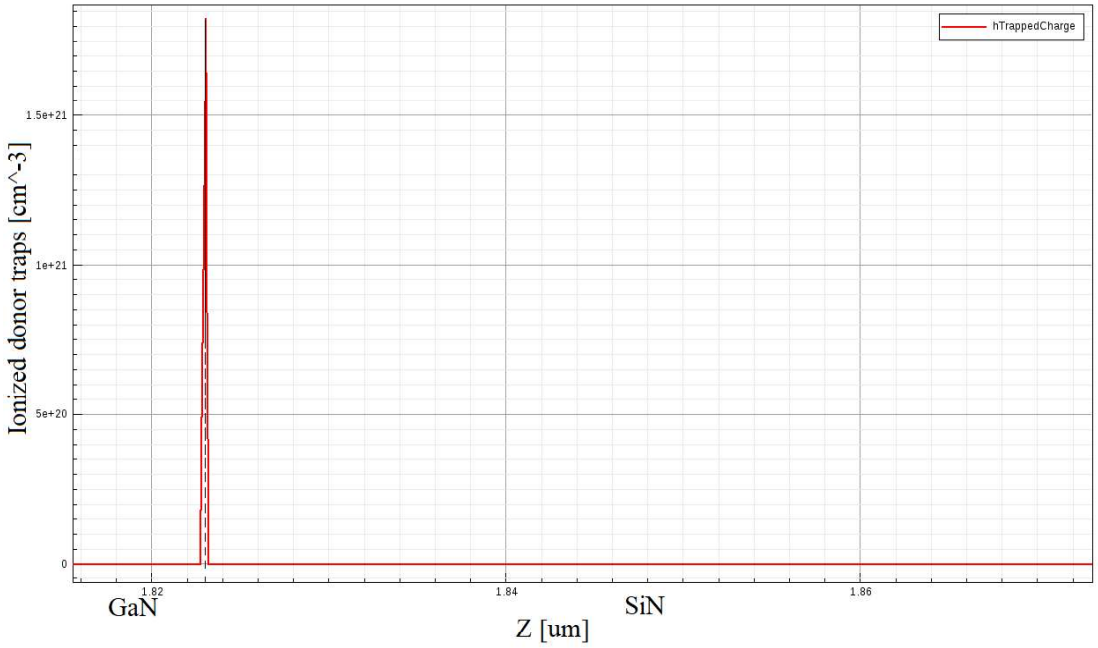

Figure 5.7: Ionized donor traps along the Z-direction at the interface GaN/SiN

case at the equilibrium condition. With this aim, two different structures are compared: the conventional HEMT (High electron mobility transistor), shown in figure 5.8, and the Fin-HEMT of figure 5.1.

First, the HEMT device is taken into account. On the XZ plane, it has the same geometrical characteristics of the Fin-HEMT device, as it can be seen in figures 5.9 a) and c). Differences can be appreciated on the YZ plane, because the structure is not fin-shaped and the gate contact does not wrap around the heterostructure. In fact, there is only a top gate deposited on the GaN cap, as it is shown in figures 5.9 b) and d).

The band diagrams are shown in figure 5.10. On the left (figure 5.10a) the energy bands of the GaN/AlGaN/GaN heterostructure under the gate contact are represented along the Z-axis. A zoom on the core of the heterostructure is shown: from the left to the right hand side it can be found the GaN cap, the AlGaN layer and the GaN buffer layer. The bending of the conduction band demonstrates the formation of the two-dimensional channel due to spontaneous and piezoelectric effect, as already explained in the previous chapter.
The second picture (figure 5.10b) is instead a representation of the band diagram of the GaN buffer layer considered along the Y-direction. The gate contact is only deposited on the GaN cap, therefore it cannot affect the energy bands which result completely flat.

Turning to the Fin-HEMT device: the gate contact wraps around the fin-shaped heterostructure (5.2d), therefore the effect of both the top gate and side gates is present.

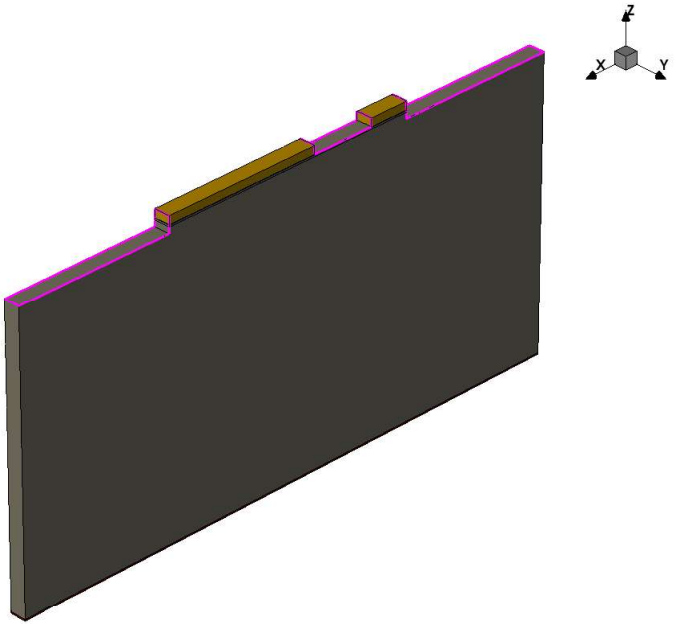

Figure 5.8: Structure of the HEMT device: in grey the GaN material, in violet the AlGaN material and in brown the Si_3N_4 material

Figure 5.11a represents the band diagram of the GaN/AlGaN/GaN heterostructure under the top gate along the Z-direction. The behaviour does not show differences with respect to the previous case, therefore the same considerations are valid. On the other hand, figure 5.11b shows the energy bands of the GaN buffer layer along the Y-axis: the top gate does not have any effect as for the HEMT, but the control of the side gates is responsible of the bands bending. In fact, the lateral contacts create a metal-semiconductor junction with the GaN buffer layer and at thermal equilibrium, there is an electron accumulation layer in the metal and an electron depleted region in the semiconductor that explains the behaviour of the energy bands. As a consequence, the 2DEG channel is not only dominated by the top gate, but also by the lateral gates that partially deplete it.

It can be interesting to dimension the energy quantities that characterize the band diagrams. They can be clearly seen in figure 5.12 a) and b) and calculated using equations (5.10), (5.11), (5.12), (5.13), (5.14) and (5.15).

$$q\Phi_B = q\Phi_M - q\chi_{GaN} = 5\ eV - 3.958\ eV = 1.042\ eV \tag{5.10}$$

$$\Delta E_{C_{AlGaN/GaN}} = q\chi_{GaN} - q\chi_{AlGaN} = 3.958\ eV - 3.422\ eV = 0.536\ eV \tag{5.11}$$

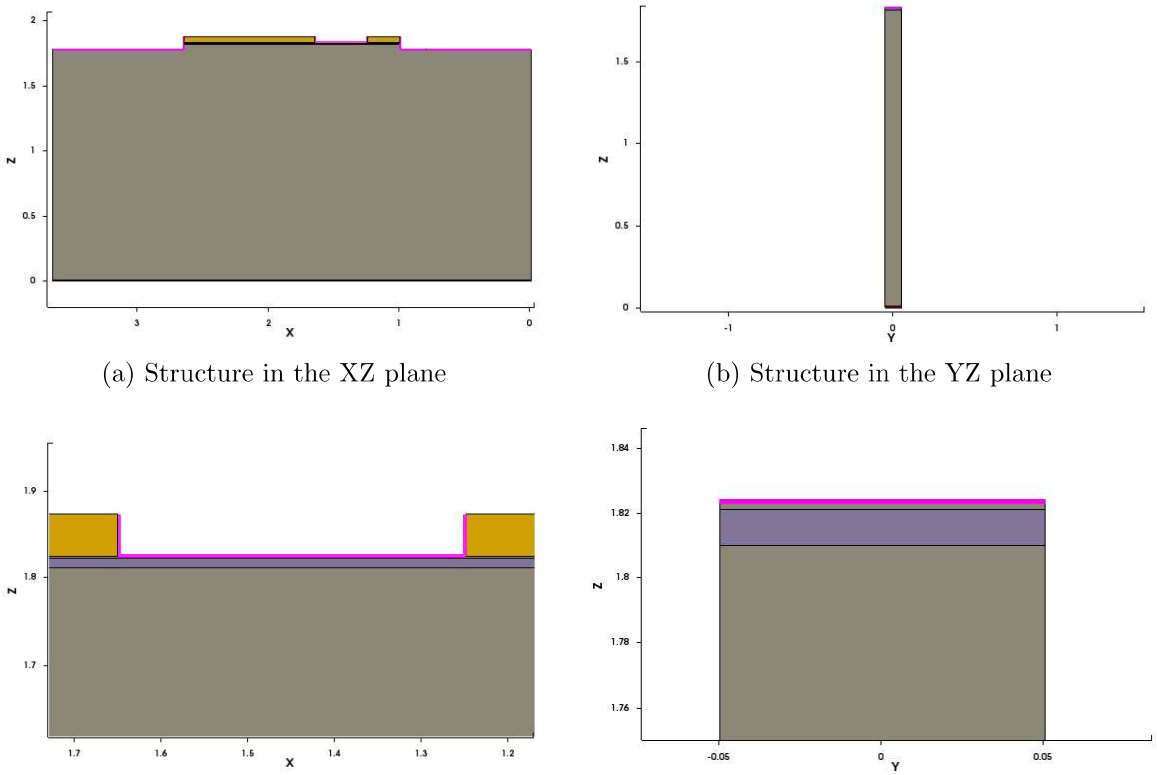

(a) Structure in the XZ plane

(b) Structure in the YZ plane

(c) Zoom on the gate region in the XZ plane

(d) Zoom on the gate region in the YZ plane

Figure 5.9: HEMT structure on XZ and YZ planes: in grey the GaN material, in violet the AlGaN material and in brown the Si_3N_4 material

$$\begin{aligned} \Delta E_g &= E_{g\,AlGaN} - E_{gGaN} = 4.147\ eV - 3.435\ eV = 0.7124.147\ eV - 3.435\ eV \\ \Delta E_{V_{AlGaN/GaN}} &= q\chi_{GaN} - q\chi_{AlGaN} - \Delta E_g = 0.536\ eV - 0.712\ eV = -0.176\ eV \end{aligned} \tag{5.12}$$

$$q\Delta V_{GaN} = E_{Cmin}(GaN\ cap) - E_{Cmax}(GaN\ cap) = -0.36\ eV \tag{5.13}$$

$$q\Delta V_{AlGaN} = E_{Cmax}(AlGaN\ layer) - E_{Cmin}(AlGaN\ layer) = 1.665\ eV \tag{5.14}$$

$$\Delta E_f = E_f - E_{Cmin} = 0 - (-0.257\ eV) = 0.257\ eV \tag{5.15}$$

The term $q\Phi_B$ is the Schottky barrier due to the metal-semiconductor junction: it can be seen between the top gate and the GaN cap and between the side gates and the GaN buffer layer. Moreover, it is expressed as the difference between the Au metal workfunction $q\Phi_M$ and the electron affinity of the GaN, χ_{GaN}. The values $\Delta E_{C_{AlGaN/GaN}}$ and $\Delta E_{V_{AlGaN/GaN}}$ are the conduction and valence band discontinuities: the first one

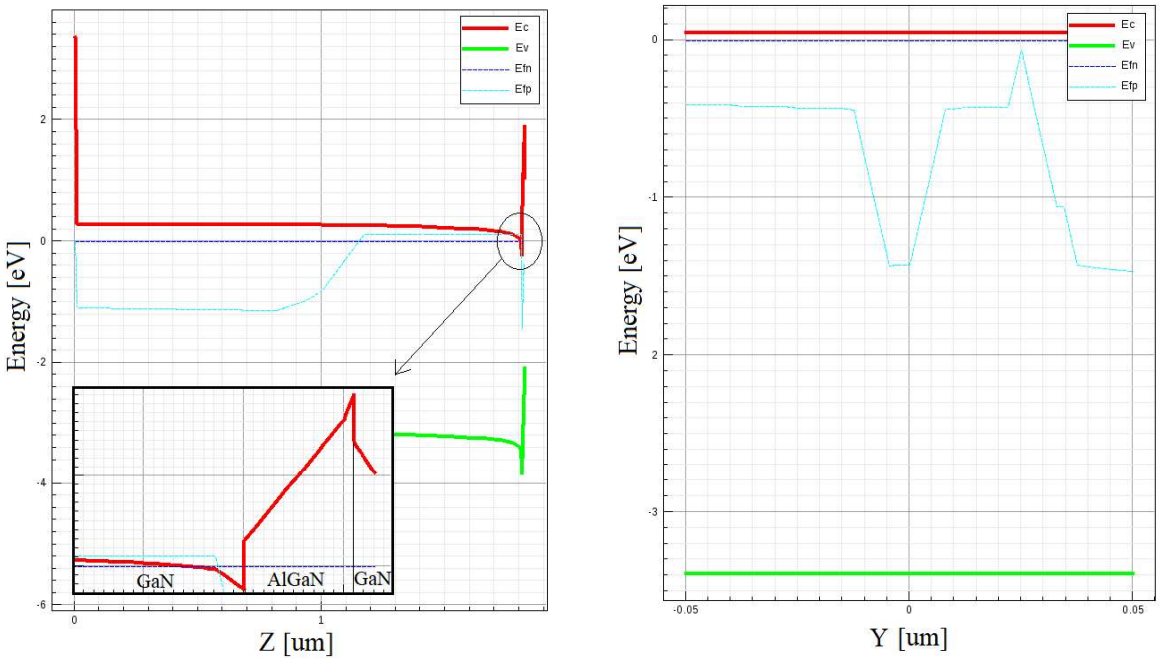

(a) Along the Z-direction (b) Along the Y-direction

Figure 5.10: Band diagram of the HEMT structure

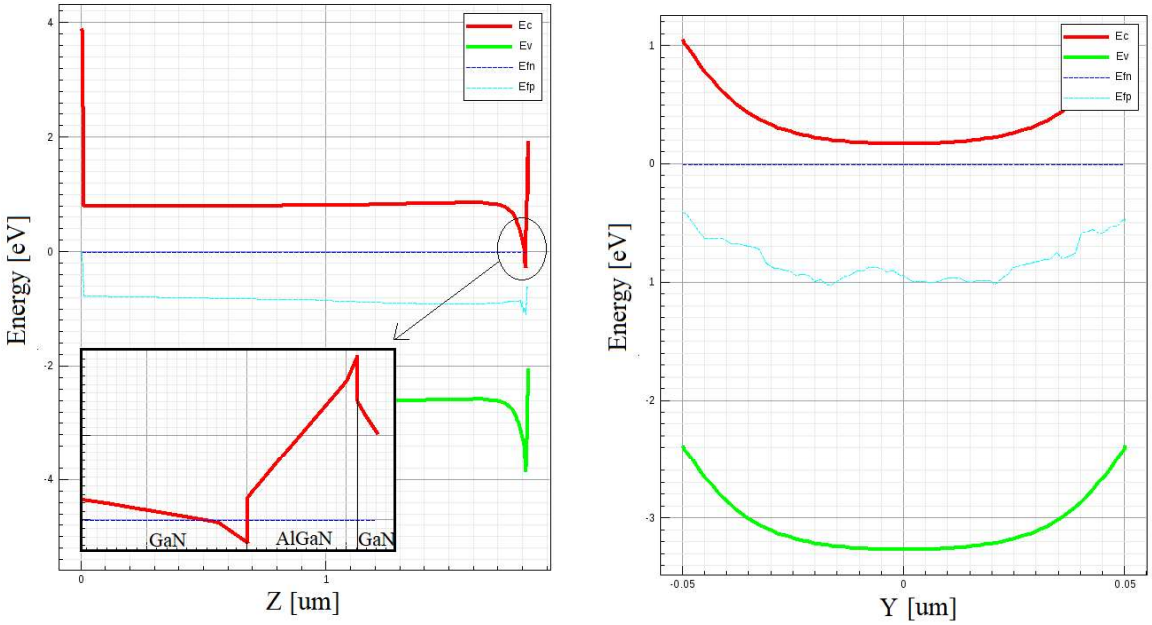

(a) Along the Z-direction (b) Along the Y-direction

Figure 5.11: Band diagram of the Fin-HEMT structure

depends on the electron affinity of GaN and AlGaN, while the second one also depends on the energy gap of the materials. Moreover, there are the potential drops $q\Delta V_{GaN}$ and $q\Delta V_{AlGaN}$, only dependent on the conduction band energy of, respectively, Gan cap and AlGaN layer. The last term is ΔE_f, defined as the distance between the Fermi level and the minimum of the conduction band.

Space charge

The space charge representation allows to understand how the charge is distributed at the equilibrium. The comparison between the HEMT and the FinFET can be useful to highlight the differences with respect to a conventional planar structure.

The HEMT device is taken into account. Figure 5.13a shows the YZ space charge distribution of the GaN/AlGaN/GaN heterostructure under the gate contact. It can be noticed a negative charge (in blue) at the interface AlGaN/GaN that represents the two-dimensional channel, only controlled by the top gate in this case. Moreover, in figure 5.13b there is the same distribution along the Z-direction: the peak of the curve, equal to $5.12 \cdot 10^{19}\ cm^{-3}$, is located at the interface between the AlGaN barrier and the GaN buffer layer, where the two-dimensional channel is formed.

To follow, the Fin-HEMT device is considered: figures 5.14 a) and b) represent the space charge distribution, respectively, on the YZ plane and along the Z-direction. On the left hand side figure, the negative charge (in blue) at the interface AlGaN/GaN corresponds to the 2DEG channel, whose distribution is quite different with respect to the previous case. This is due to the fact that it is dominated not only by the top gate, but also by the side gates that partially deplete it. As already explained, the lateral contacts create with the GaN buffer layer a metal-semiconductor junction and, as a consequence, a depletion region (in green). The right hand side figure is only useful to see the peak of the space charge at the interface AlGaN/GaN, equal to $5.34 \cdot 10^{19}\ cm^{-3}$.

5.2.2 Out of equilibrium analysis: DC simulations

Once the equilibrium condition is investigated, the out of equilibrium analysis can be performed in order to obtain a set of solutions at different bias points. The device simulation code remains the same and the only differences can be found in the 'Solve' section. In fact, it also includes a *Quasistationary* statement that specifies the quasistatic or steady state 'equilibrium' solutions to be obtained for a set of *Goals*, which can be defined for one or more electrodes .

The DC simulation is repeated, as in the previous case, for two devices: the conventional planar HEMT and the Fin-shaped HEMT. Purpose of this choice is to understand the differences between the two structures through the analysis of some output results

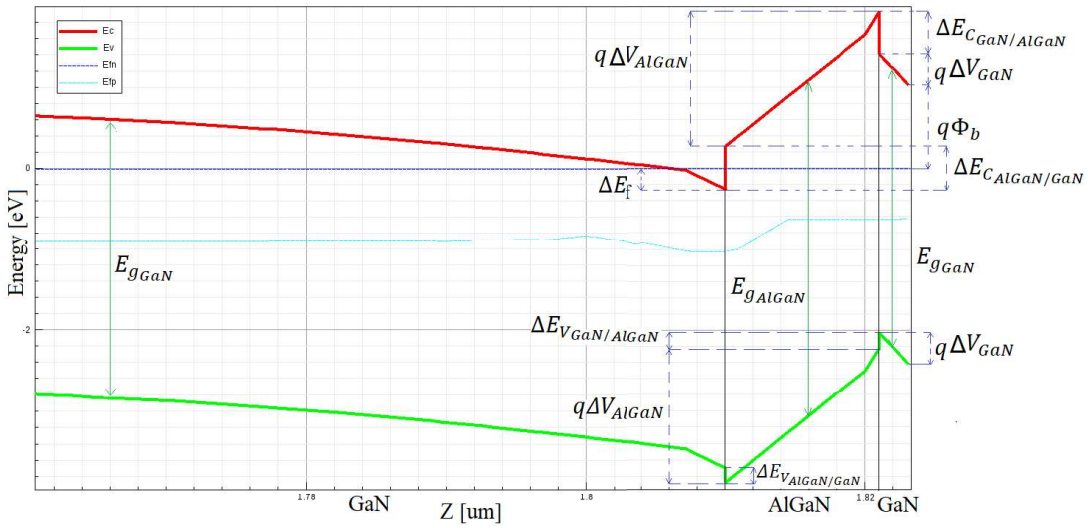

(a) Band diagram along the Z-direction of the heterostructure under the top gate

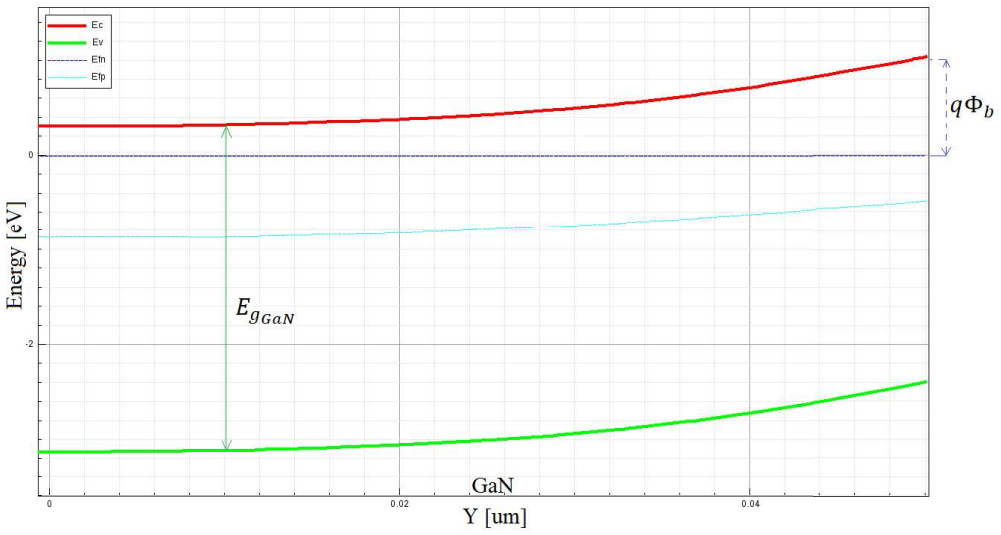

(b) Band diagram along the Y-direction of half of the GaN buffer layer

Figure 5.12: Zoom on the band diagrams of the Fin-HEMT

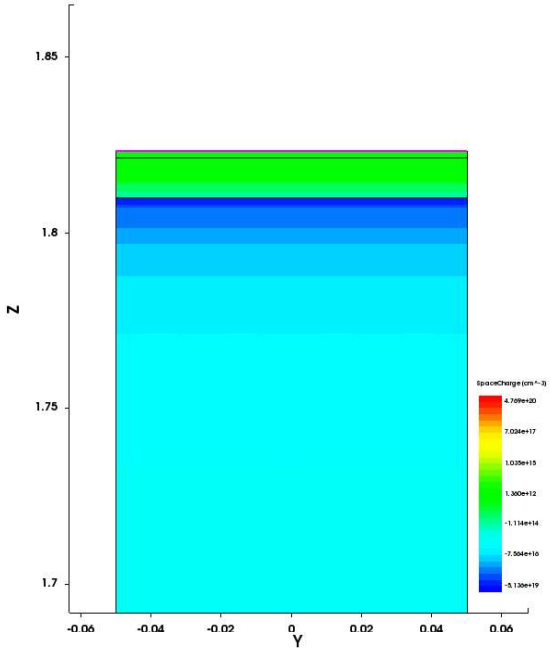

(a) Space charge distribution on the YZ plane

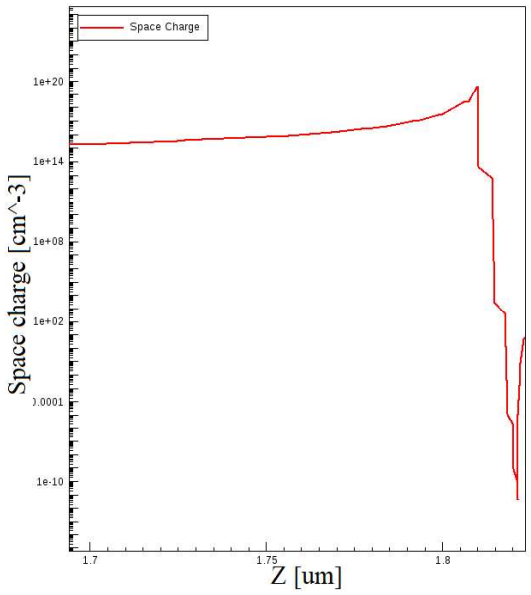

(b) Space charge distribution along the Z-direction at the center of the fin width

Figure 5.13: Space charge of a HEMT structure

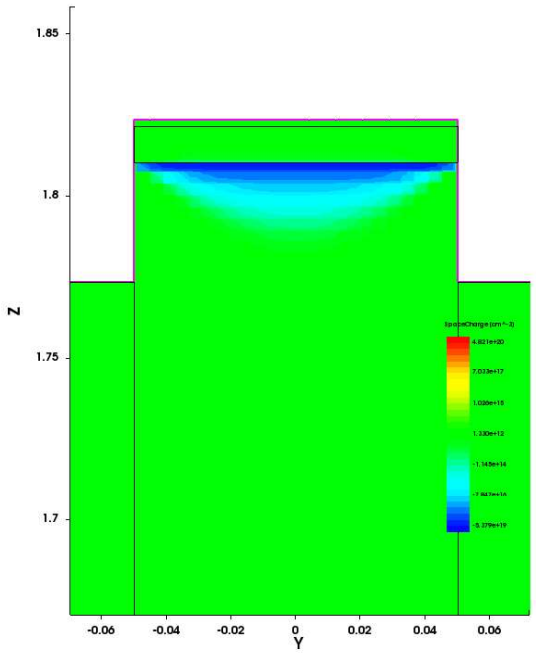

(a) Space charge distribution on the YZ plane

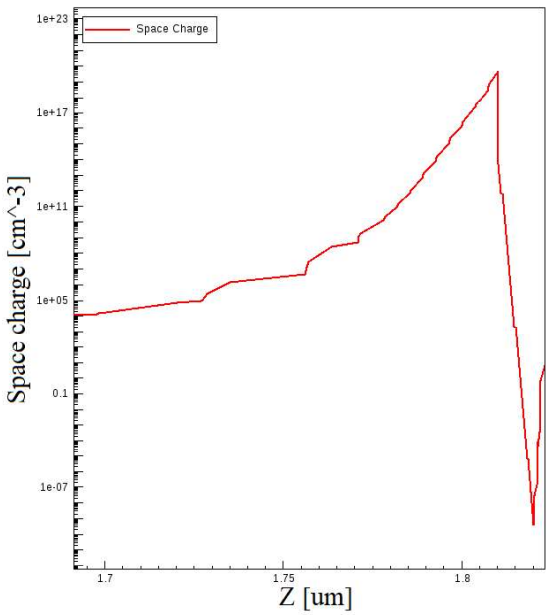

(b) Space charge distribution along the Z-direction at the center of the fin width

Figure 5.14: Space charge of a HEMT structure

that will be presented in the following.

The conventional HEMT is taken into account. The total drain current, expressed in A/μ m, is extracted from the simulation results and shown in figure 5.15. It is represented as a function of the gate voltage, whose values are included between -8 V and 2 V. Moreover, the curves are plotted for a set of drain voltages defined in the range between 1 V and 7 V with a step of 2 V. Taking into account these conditions, some interesting aspects can be appreciated. First, it can be noticed that above the threshold, increasing V_{ds} the current first grows (linear region) and then saturates, as expected. Instead, below the threshold the subthreshold slope depends on the drain voltage (see log graphs). Furthermore, there is a non-null current at $V_{gs} = 0$ V and $V_{ds} > 0$ V: at zero bias the polarization charges are responsible of the formation of the two-dimensional channel, as widely explained, therefore for each value of V_{ds} higher than zero, a current is created. In conclusion, a strongly negative threshold voltage can be seen: it assumes a value equal to -3.13 V for $V_{ds} = 7$ V.

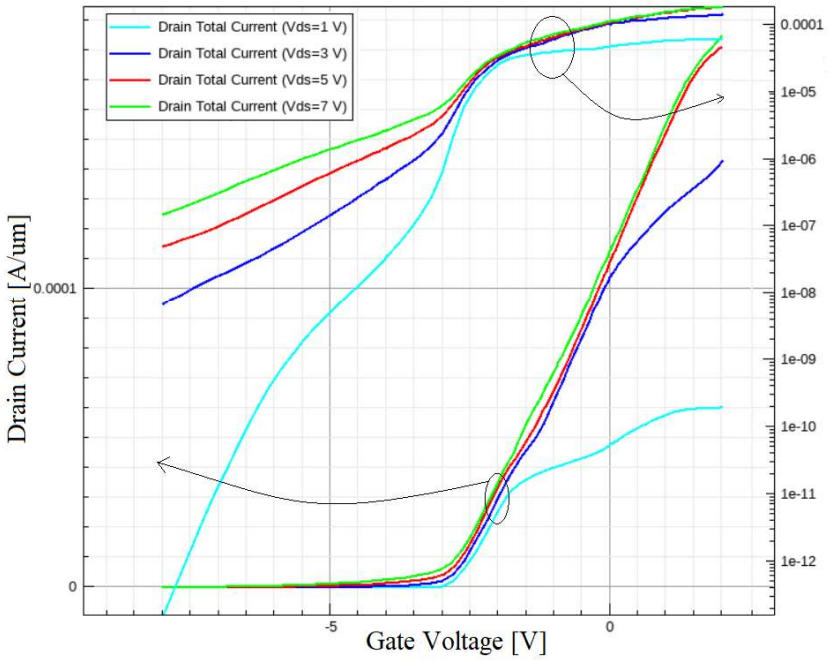

Figure 5.15: Drain current of the HEMT device as a function of the gate voltage: the left hand side axis represents the drain current and the right hand side the logarithm of the drain current

A second representation is shown in figure 5.16, where the drain current is expressed as a function of the drain voltage in a range included between 0 V and 7 V. The characteristics are computed for different gate voltages, whose values go from -4 V up to 1 V with a step of 1 V. The picture shows how, for a fixed drain voltage, the drain current decreases with lower values of V_{gs}, in particular it is near zero for a gate voltage under

threshold (red curve).

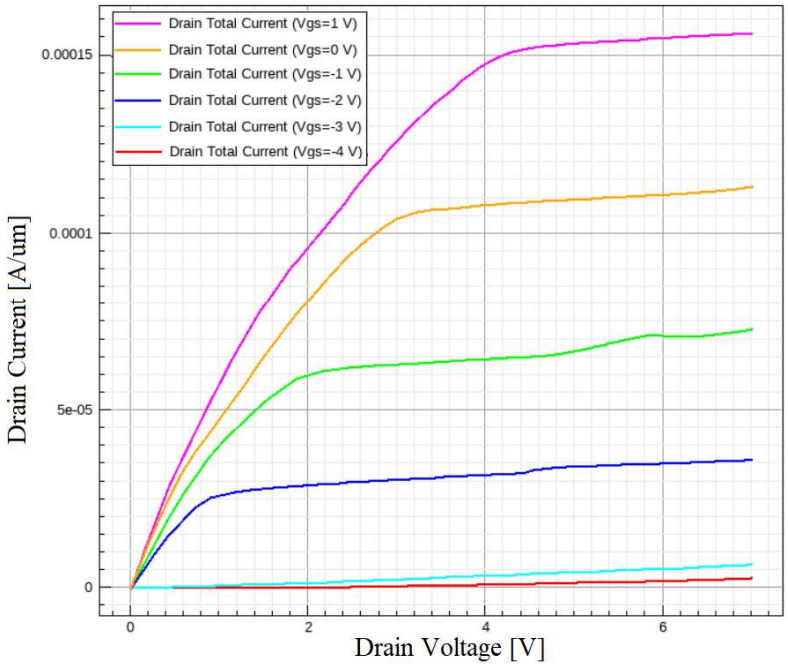

Figure 5.16: Drain current of the HEMT device as a function of the drain voltage

The same results are found for the Fin-HEMT device. Figure 5.17 shows the drain current as a function of a gate voltage that goes from - 3 V to 2 V and for values of V_{ds} between 1 V and 7 V with a step of 2 V. On the other hand, the drain current can be also plotted with respect to the drain voltage, as shown in figure 5.18 in a range between 0 V and 7 V. The characteristics are obtained for different gate voltage values included between -2 V and 1 V.

A comparison between the drain currents of the two devices can be interesting. Figures 5.19 a) and b) show a very similar behaviour of the structures, but some interesting differences have to be underlined. First, the threshold voltage is strongly increased and assumes a value equal to -1.40 V for $V_{ds} = 7$ V. Moreover, for fixed values of the gate voltage, the Fin-HEMT drain current is lower than the one of the planar structure.
It is possible to clarify these behaviours paying attention on the geometry of the devices: the conventional HEMT is only characterized by a top gate on the GaN/AlGaN/GaN heterostructure as shown in figure 5.9d, while in the FinFET the gate contact has a fin-shaped structure (figure 5.2d) and the formation of the 2DEG channel is controlled by top gate and side gates. As already explained, the lateral contacts are responsible of the formation of metal-semiconductor junctions with the GaN buffer layer that partially deplete and reduce the two-dimensional channel. The main consequence is an increase of the threshold voltage: the off-state in the Fin-HEMT is achieved more rapidly with

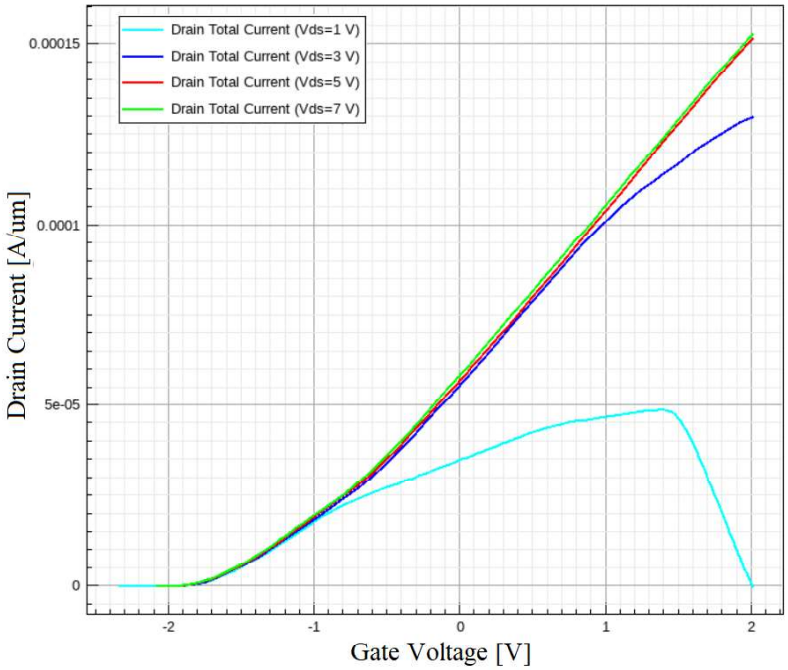

Figure 5.17: Drain current of the Fin-HEMT device as a function of the gate voltage: the left hand side axis represents the drain current and the right hand side the logarithm of the drain current

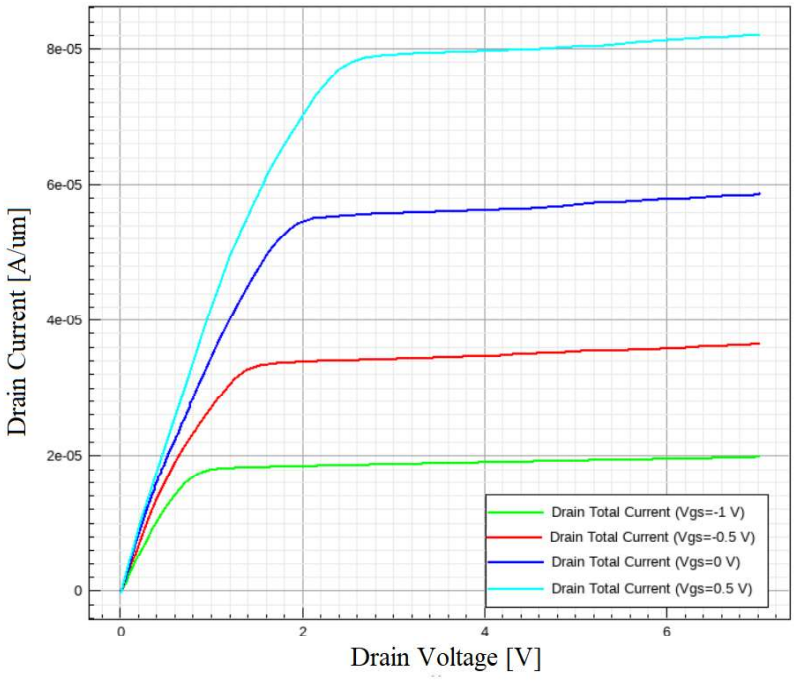

Figure 5.18: Drain current of the Fin-HEMT device as a function of the drain voltage

respect to the planar device, which is not affected by any depletion effect. The second consequence is related to the decreasing of the drain current due to the lowering of the 2DEG channel concentration.

Moreover, other important information need to be added. First, in figure 5.19a the better transconductance obtained in the Fin-HEMT structure can be seen through its steeper transcharacteristics with respect to the planar device. Second, figure 5.19b shows the better output conductance due to the flatter output characteristics of the FinFET with respect to the HEMT device. Higher transconductance and lower output conductance imply better performances of the device in analog applications.

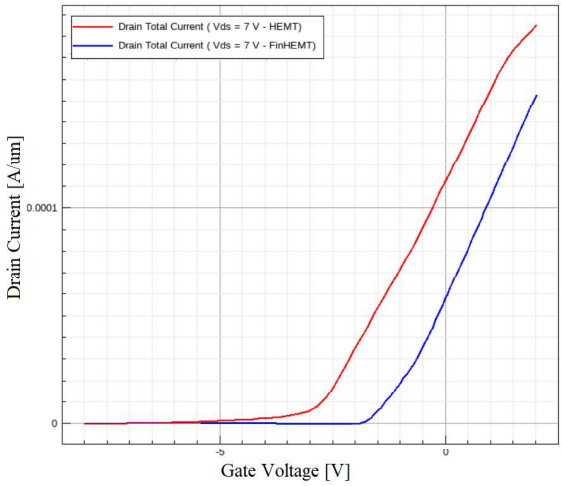

(a) Drain current as a function of the gate voltage for $V_{ds} = 7$ V

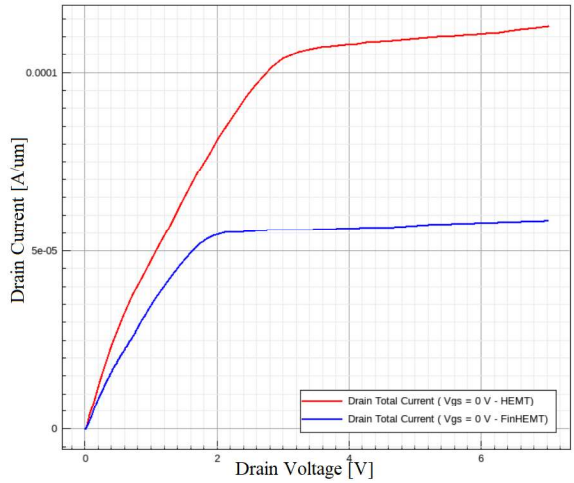

(b) Drain current as a function of the drain voltage for $V_{gs} = 0$ V

Figure 5.19: Comparison between HEMT and Fin-HEMT

Chapter 6

Fin-HEMT Parametric sensitivity

The equilibrium and out-of-equilibrium condition of the Fin-HEMT device have been analysed through a numerical simulation, implemented on the TCAD Synopsys Sentaurus. The simulation code has been divided in two parts: the structure generation on the Sentaurus Structure Editor tool and the device simulation on the Sentaurus Device tool. Each part has been described in the previous chapter in order to understand how to create the geometry and what are the main physical models to be applied. The simulation results for the equilibrium condition has been explained and some of them compared with a HEMT device. Moreover, the DC simulation results have been presented and, once again, compared with the conventional planar structure.

Since this analysis has shown potential benefits of the FinFET, new aspects can be investigated. In the following, the parametric sensitivity analysis is carried out: a specific parameter of the FinFET device, called from now on 'reference Fin-HEMT', is modified of a certain quantity, then the varied structure is simulated in order to compare the results with the reference ones. The aim is double: optimize the device performances by changing the geometrical or physical features and understand technology-dependent spread of the device. The parameters taken into account are the fin width and the fin height as geometrical quantities, while the polarization charges, the concentration of traps and the temperature are chosen as physical features.

6.1 Fin height

The fin height depends on three quantities shown in figure 6.1: the GaN cap height equal to 2 nm, the AlGaN layer height equal to 11 nm and a portion of the GaN buffer layer of 37 nm. The sum of these parameters gives the total value of the fin height, which is equal to 50 nm. In this case the sensitivity analysis is not focused on the total fin height, but on the 37 nm GaN buffer, which is modified in the simulation of $\pm 5\%$. This may

correspond to a variability of the mesa etching fin shaping.

The simulation on Synopsys Sentaurus does not show differences with respect to the previous case, apart from the GaN fin height h_{fin}, which is modified with the new values $h_{fin}(+5\%) = 38.85$ nm and $h_{fin}(-5\%) = 35.15$ nm. At this point, the simulations results can be analysed and a comparison can be done with respect to the reference structure.

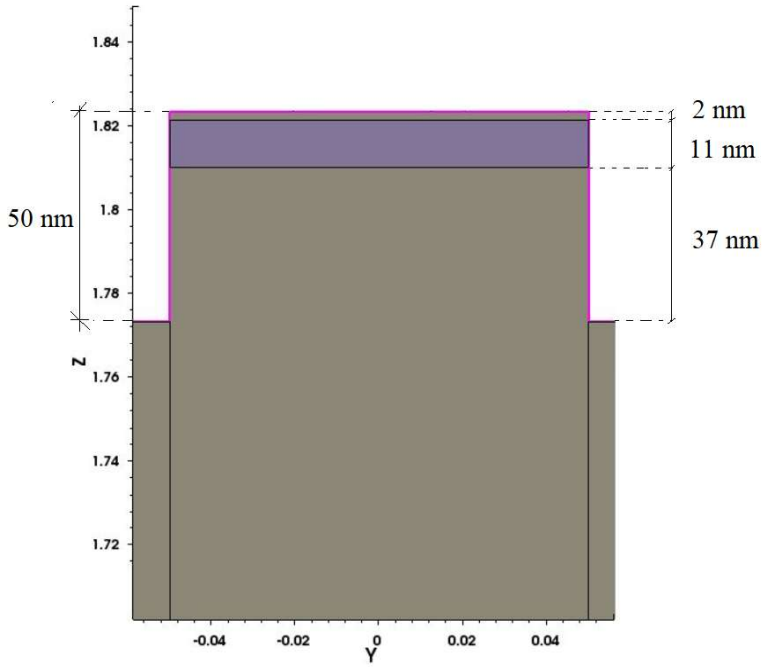

Figure 6.1: YZ plane of the Fin-HEMT structure: in grey the GaN material, in violet the AlGaN material and in brown the Si_3N_4 material

Figure 6.2 shows the behaviour of the drain current as a function of the gate voltage at $V_{ds} = 7$ V: the green and red curves correspond respectively to $h_{fin}(+5\%)$ nm and $h_{fin}(-5\%)$, while the blue curve is the one of the reference Fin-HEMT. The drain currents associated to the different structures do not show strong differences between them, therefore their behaviour is not strictly linked to the GaN layer height. In fact, the formation of the two-dimensional channel at the interface AlGaN/GaN and the consequent charge sheet concentration $-qn_s$ mainly depend on the heights of AlGaN layer and GaN cap, not of the GaN buffer layer. Nevertheless, it can be noticed that with an increasing of the gate voltage up to 2 V, the only red curve, obtained for $h_{fin}(-5\%)$, starts to assume lower values. Even if the formation of the 2DEG channel is not directly related to the GaN height, the fin-shaped gate gives a strong control on the channel through the top and lateral contacts. When the side contacts are reduced with the fin height, the control of the channel is slightly decreased, therefore lower values of the drain current are obtained.

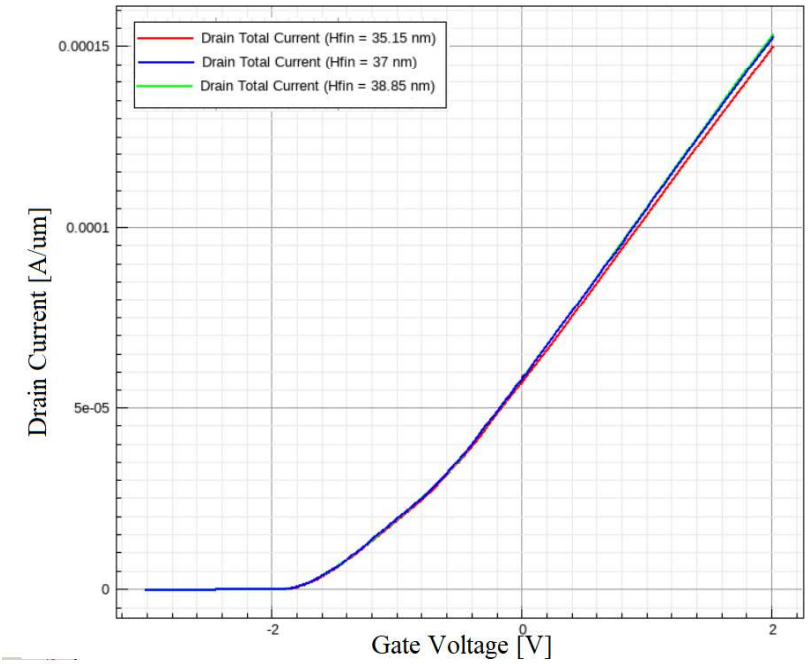

Figure 6.2: Transcharacteristics at $V_{ds} = 7$ V for different fin heights

For a better comprehension, figure 6.3 shows the electron density at $V_{ds} = 7$ V and $V_{gs} = 2$ V, where the difference between the structures is more evident. Figures a) and b) are 2D representations on the YZ plane in the region under the gate, while figure c) is a more intuitive graph with the behaviour of the electron concentration in the same conditions along the Y-axis at the interface AlGaN/GaN (in the GaN side). The picture gives a comparison between the reference structure and the modified ones, in order to highlight the variation of density and, therefore, of current. The maximum value of electron density is reached at the center of the fin and assumes the following values: $1.6 \cdot 10^{19}$ cm^{-3} at 35.15 nm, $1.65 \cdot 10^{19}$ cm^{-3} at 37 nm and $1.72 \cdot 10^{19}$ cm^{-3} at 38.85 nm.

Starting from the transcharacteristics of figure 6.2, the sensitivity with respect to the fin height variations can be calculated using the formula (6.1): $I_d(\pm 5\%)$ and $h_{fin}(\pm 5\%)$ are, respectively, the total drain current and the fin height of the modified device, while I_d and h_{fin} are, respectively, the total drain current and the fin height the reference structure. The gate voltages and the correspondent drain currents are chosen in a specific range included between 1 V and 2 V. In fact, this interval shows a more evident current variation between the modified structures and the reference one. The results are shown in figure 6.4: both the curves have a linear behaviour, but a different slope. The derivative of the sensitivity with respect to the gate voltage or, in other words, the slope of the curve corresponds to the trasconductance, indicated in equation (6.2), which results positive in both cases and slightly higher for the blue curve.

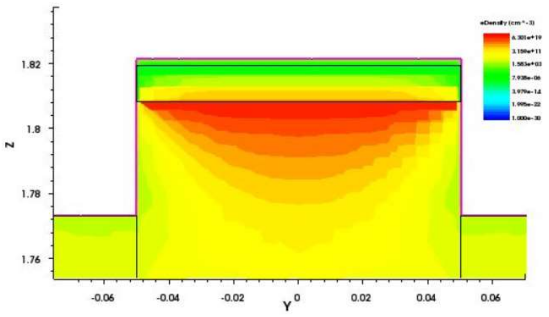

(a) YZ representation for $h_{fin} = 35.15$ nm

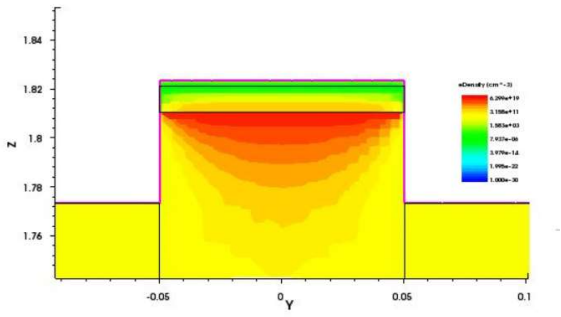

(b) YZ representation for $h_{fin} = 37$ nm

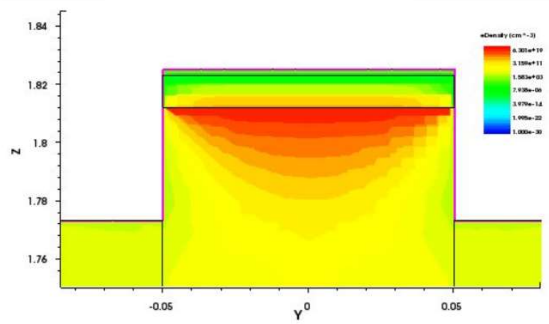

(c) YZ representation for $h_{fin} = 38.85$ nm

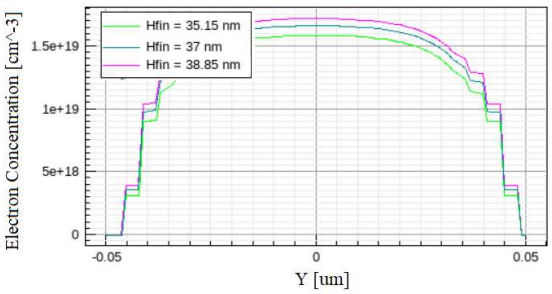

(d) Electron density: comparison along the Y direction

Figure 6.3: Electron density representations at $V_{gs} = 2$ V and $V_{ds} = 7$ V

$$S\Big|_{V_{gs}}^{h_{fin}} = \frac{\Delta I_d}{\Delta h_{fin}} = \frac{I_d(\pm 5\%) - I_d}{h_{fin}(\pm 5\%) - h_{fin}} \tag{6.1}$$

$$S_{gm}\Big|_{V_{gs}}^{h_{fin}} = \frac{\dfrac{dI_d(\pm 5\%)}{dV_{gs}} - \dfrac{dI_d}{dV_{gs}}}{h_{fin}(\pm 5\%) - h_{fin}} \tag{6.2}$$

6.2 Fin width

The second parameter taken into account is the fin width W_{fin}, whose value in the reference structure is equal to 100 nm. A variation of $\pm 10\%$ is considered and the modified values $W_{fin}(+10\%) = 110$ nm and $W_{fin}(-10\%) = 90$ nm are inserted in the simulation in order to analyse the results.

Figures 6.5 a) and b) show the total drain current for the different fin widths. On the left hand side there are the transcharacteristics at $V_{ds} = 7$ V, where the blue curve represents the drain current of the reference structure, while the green and red curves are obtained for, respectively, $W_{fin}(+10\%)$ and $W_{fin}(-10\%)$, which are symmetrical with

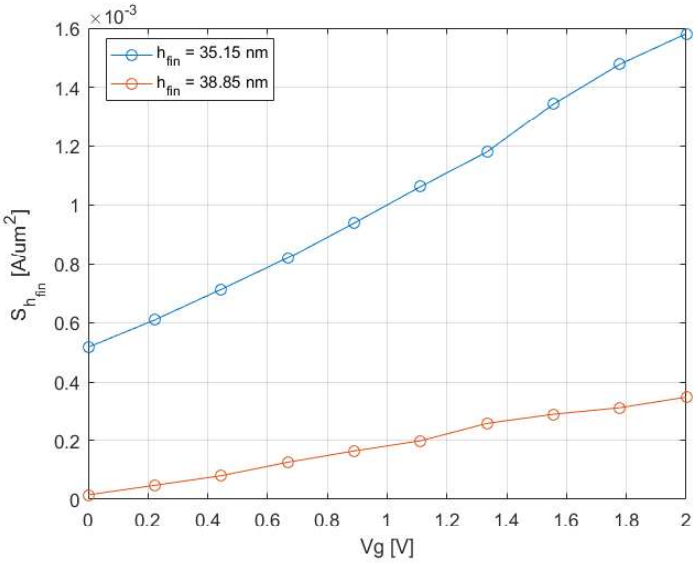

Figure 6.4: Sensitivity as a function of the gate voltage at $V_{ds} = 7$ V

respect to the blue one. On right hand side, the drain current is expressed as a function of the drain voltage for $V_{gs} = 0$ V: the magenta curve is the one of the reference structure, while the green and red ones correspond, respectively, to a fin width of 110 nm and 90 nm. Important observations can be underlined and explained in the following lines.
First, for a fixed V_{gs}, the drain current characteristics assumes very different values with respect to the reference ones: in figure 6.5a, the green curve shows a higher drain current, while the red one a lower drain current. This effect is strongly evident with an increasing of the gate voltage, as expected. Moreover, a variation of the threshold voltage can be seen, in particular with 90 nm fin width, the threshold increases to a value equal to -1.27 V, while for $W_{fin}(+10\%) = 110$ nm, the value assumed by V_{th} is equal to -1.52V.
As regards figure 6.5b, it demonstrates that for a fixed drain voltage, there is an increasing of the current with W_{fin}, as expected. Moreover, the better control of the SCEs can be appreciated through to the better output conductance.

Once again, this behaviour can be connected to the formation of the two-dimensional channel. The device under analysis is characterized by a fin-shaped gate contact, therefore it is controlled by both the top gate and the side gates. The top gate is responsible of the formation of the 2DEG channel, while the side gates create the metal-semiconductor junctions with the GaN layer, which partially deplete the channel. The more the fin width is reduced, the more the depletion of the channel is rapid and effective. This phenomenon has two consequences, that are analysed starting from the device with 90 nm fin width. First, with a reduced fin width, there is a decreasing of the channel charge density and a consequent lower drain current with respect to the reference one; second, the threshold voltage is shifted towards positive values with respect to the one of the

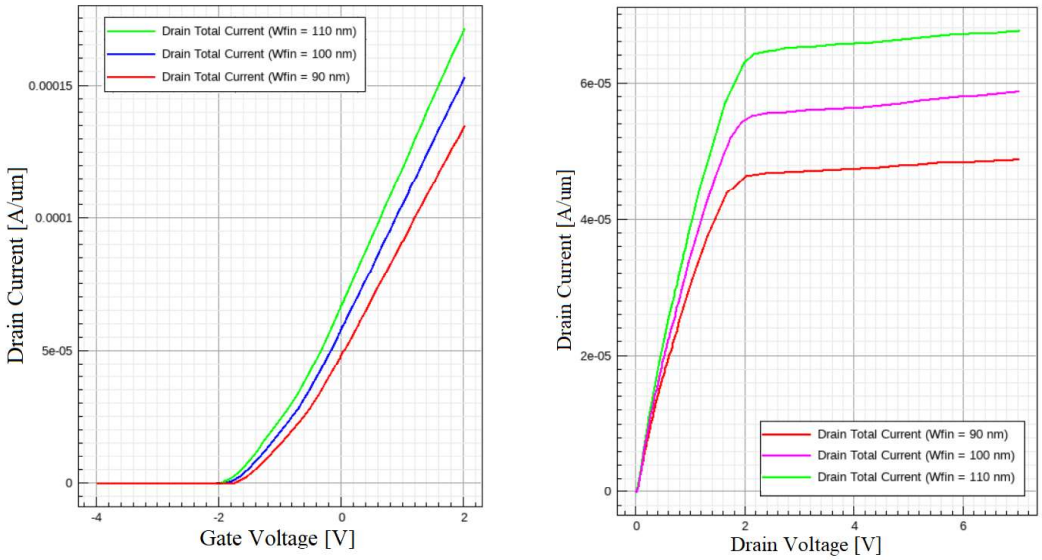

(a) Drain current as a function of the gate voltage at $V_{ds} = 7$ V

(b) Drain current as a function of the drain voltage at $V_{gs} = 0$ V

Figure 6.5: Drain current behaviour for different fin widths

reference device (figure 6.5a). The same reasoning is valid for $W_{fin}(+10\%) = 110$ nm, where there are opposite consequences: the increasing of the drain current and the reduction of the threshold voltage.

In order to verify the observations explained above, a 2D representation of the electron density in the region under the gate is given in figures 6.6 a), b) and c): the region coloured in red corresponds to a strong electron concentration at the interface AlGaN/-GaN. Taking into account these figures, it is not possible to measure the maximum value of the electron density for each fin width, therefore a new graph is analysed. Figure 6.6 d) shows the electron concentration along the Y-axis at the interface AlGaN/GaN (in the GaN side). The electron density peak is reached in the middle of the fin and it increases with W_{fin}, assuming the following values: $3.41 \cdot 10^{18}$ cm^{-3} at 90 nm, $3.47 \cdot 10^{18}$ cm^{-3} at 100 nm and $3.56 \cdot 10^{18}$ cm^{-3} at 110 nm.

The sensitivity with respect to the W_{fin} parameter can be obtained through equation (6.7): $Id(\pm 10\%)$ and $W_{fin}(\pm 10\%)$ are, respectively, the total drain current and the fin height of the modified device, while I_d and W_{fin} are, respectively, the total drain current and the fin height the reference structure. First, it has been calculated at $V_{ds} = 7$ V as a function of the gate voltage in the interval between -1 V and 2 V, where the variation is more clear. Figure 6.7 shows the results, which verify, more or less, a linear behaviour of the sensitivity in both cases. The slopes of the curves are very similar, therefore the fin width variation does not change the transconductance, shown in equation (6.4).

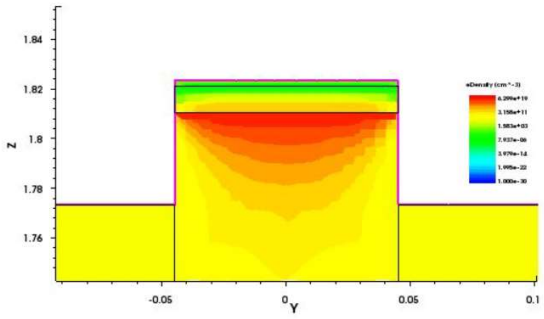

(a) YZ representation for $W_{fin} = 90$ nm

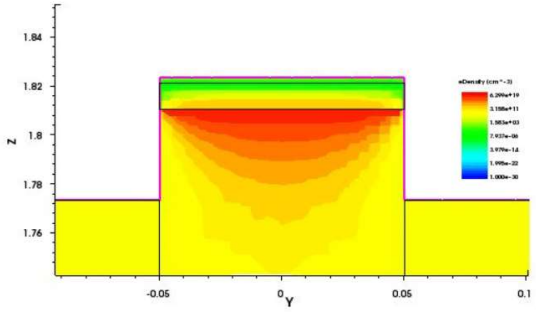

(b) YZ representation for $W_{fin} = 100$ nm

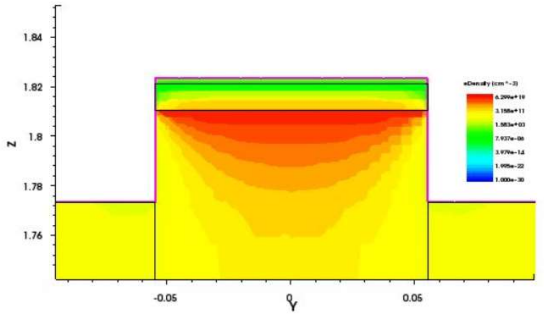

(c) YZ representation for $W_{fin} = 110$ nm

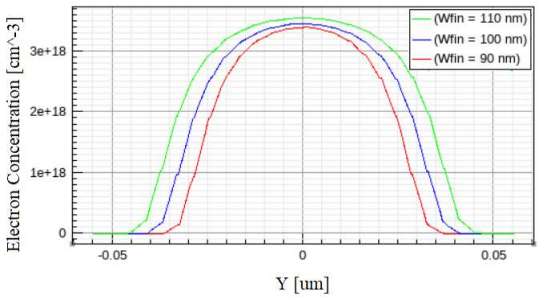

(d) Electron density: comparison along the Y direction

Figure 6.6: Electron density representations at $V_{gs} = 2$ V and $V_{ds} = 7$ V

Then, the same parameter is obtained for $V_{gs} = 0$ V as a function of the drain voltage in the range between 3 V and 7 V. The result in figure 6.8 shows an increasing sensitivity for 90 nm fin width and a decreasing behaviour of the same parameter for 110 nm fin width. An accurate analysis allows to obtain information about the output conductance, calculated through (6.5). In fact, in the first half of the graph (up to 5 V), the curves have the same slightly positive slope, while in the second half the behaviour is completely different. The blue curve has a strongly positive slope, therefore a higher output conductance, while the red curve has a negative slope and a smaller output conductance, which represents a good result for analog/RF applications.

$$S\Big|_{V_{gs},V_{ds}}^{W_{fin}} = \frac{\Delta I_d}{\Delta W_{fin}} = \frac{I_d(\pm 10\%) - I_d}{W_{fin}(\pm 10\%) - W_{fin}} \tag{6.3}$$

$$S_{gm}\Big|_{V_{gs}}^{W_{fin}} = \frac{\dfrac{dI'_d}{dV_{gs}} - \dfrac{dI_d}{dV_{gs}}}{W'_{fin} - W_{fin}} \tag{6.4}$$

$$S_{Cds}\Big|_{V_{ds}}^{W_{fin}} = \frac{\dfrac{dI'_d}{dV_{ds}} - \dfrac{dI_d}{dV_{ds}}}{W'_{fin} - W_{fin}} \tag{6.5}$$

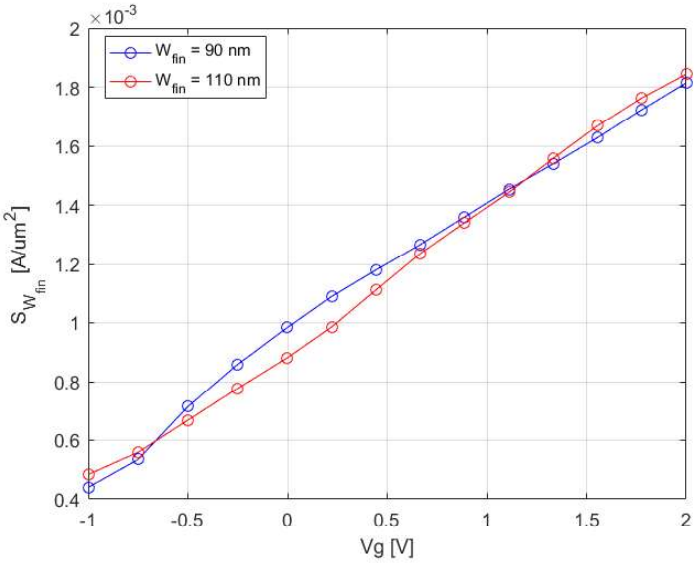

Figure 6.7: Sensitivity as a function of the gate voltage at $V_{ds} = 7$ V

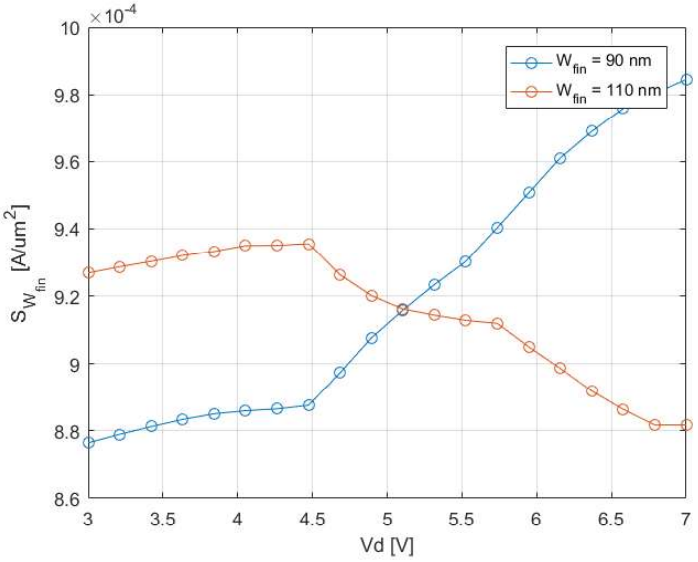

Figure 6.8: Sensitivity as a function of the drain voltage at $V_{gs} = 0$ V

Wide Fin-HEMT

To investigate even more the effect of the most critical parameter of the FinFET, a comparison can be done between the reference Fin-HEMT, called in this case *narrow*, and a wide Fin-HEMT, obtained increasing the fin width up to 200 nm. The variation is really important with respect to the previous case, therefore the results are analysed separately.

Figures 6.9 shows a drain current of the device: on the left hand side it is expressed as a function of the gate voltage at $V_{ds} = 1, 3, 5, 7$ V, while on the right hand side the same current is represented as a function of the drain voltage at $V_{gs} = -1, -0.5, 0, 0.5$ V. The transcharacteristics (figure a) shows that, for a fixed value of V_{gs}, the drain current of the wide structure is strongly increased with respect to the one of the narrow device. Moreover, the threshold is equal to -2.12 V for $V_{ds} = 7$ V, therefore is shifted towards negative values. This aspect can also be appreciated in the characteristics (figure b) where the drain current is still non-null for a gate voltage equal to -1 V. Moreover, the characteristics show a much worse output conductance due to the increasing of the fin width that leads to a weaker control of the channel.

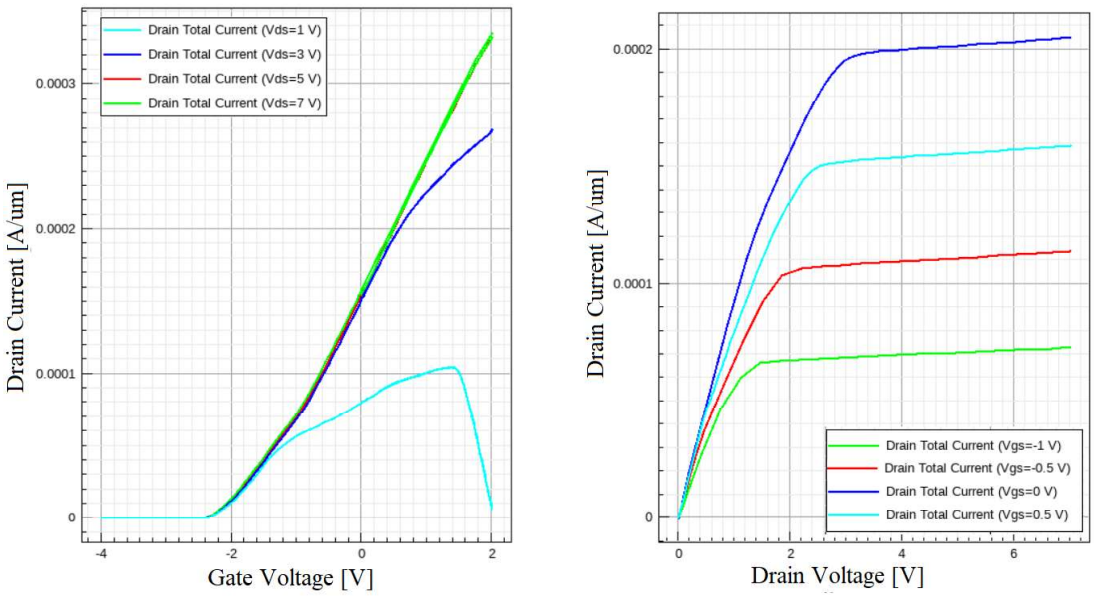

(a) Drain current as a function of the gate voltage

(b) Drain current as a function of the drain voltage

Figure 6.9: Drain current behaviour for $W_{fin} = 200$ nm

The reasons of this behaviour are exactly the ones previously explained: the lateral sides of the fin-shaped gate contacts create, through a metal-semiconductor junction with the GaN layer, two depletion regions, whose effect is really weak on the 2DEG channel due to the high value of the fin width. This implies not only a higher current, but also a lower threshold due to the difficulties to turn off the channel in this case. In order to clarify these aspects, the electron density in the region under the gate contact is shown in figure 6.10: figures a) and b) are 2D representations of the electron density on the YZ plane, while in figure c) there is the electron concentration along the Y axis. It can be noticed that in the wide FinFET the electron density is higher than the narrow one and its maximum value is $3.53 \cdot 10^{18}$ cm^{-3} at 100 nm and $3.81 \cdot 10^{18}$ cm^{-3} at 200 nm.

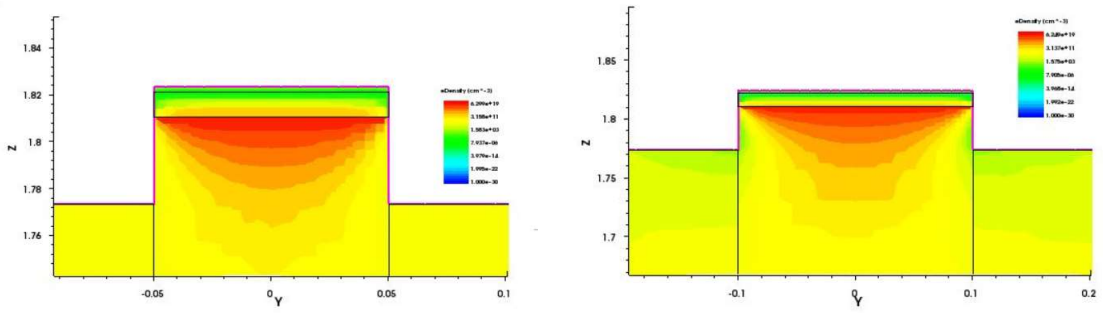

(a) YZ representation for $W_{fin} = 100$ nm

(b) YZ representation for $W_{fin} = 200$ nm

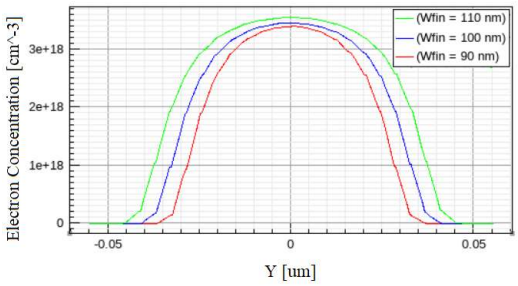

(c) Electron density: comparison along the Y direction

Figure 6.10: Electron density representations at $V_{gs} = 2$ V and $V_{ds} = 7$ V

As in the previous case the sensitivity can be calculated: figure 6.11 shows the linear behaviour of the sensitivity with respect to the gate voltage. The derivative of this parameter with respect to V_{gs} is a positive and quite big quantity, not very different with respect to the ones found previously. Moreover, figure 6.12 is a representation of the sensitivity as a function of the drain voltage, characterized by an evident positive slope and, as a consequence, an increasing output conductance.

6.3 Polarization charge

The polarization-induced charge density is the third parameter that has been modified. As already explained in chapter 2, it can be obtained through the formula (2.16), where $\overline{P}$ is the polarization vector, characterized by a non-null z-component.

The Sentaurus simulator gives the possibility to change the polarization-induced charge density through a slightly modified formula, shown in equation (6.6): the only difference with respect to the previous one is due to the 'activation' coefficient called a, a floating number included between 0 and 1 (used by default). In this case, the selected values are 0.85, 0.9 and 0.95 and the results are compared to the ones of the reference structure, characterized by an activation equal to 1.

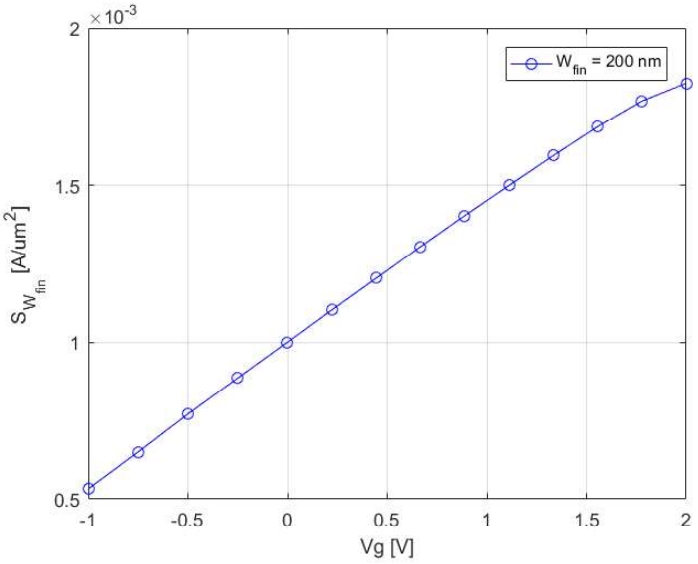

Figure 6.11: Sensitivity as a function of the gate voltage at $V_{ds} = 7$ V

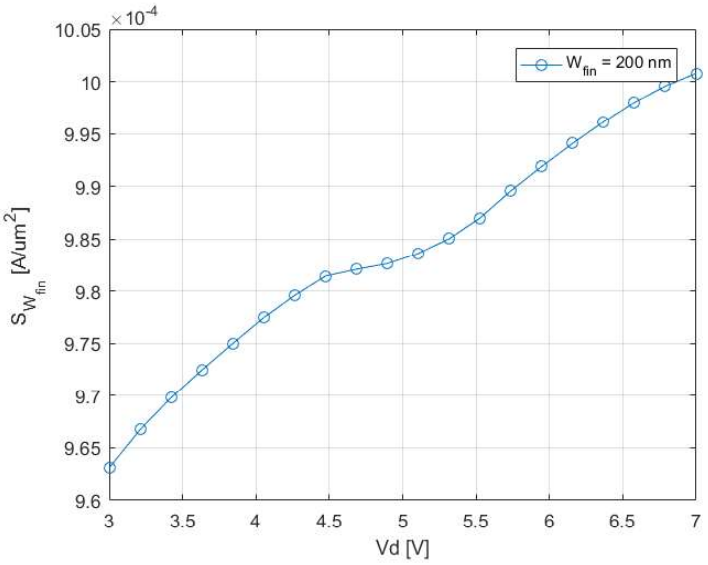

Figure 6.12: Sensitivity as a function of the drain voltage at $V_{gs} = 0$ V

$$\rho_\pi = -a \cdot \nabla \overline{P} \tag{6.6}$$

Figures 6.13 a) and b) show the total drain current for the different activation coefficients. On the left hand side there are the transcharacteristics at $V_{ds} = 7$ V: it can be noticed that for a fixed value of the gate voltage, the drain current increases with the activation coefficient. Moreover, on the right hand side, the behaviour of the drain current with respect to the gate voltage at $V_{gs} = 0$ V is shown: for a fixed drain voltage, the current increases with the activation coefficient. To understand this phenomenon, the

formation of the two-dimensional channel is considered. As widely explained, an undoped GaN/AlGaN/GaN heterostructure under the gate contact is characterized by the formation of the 2DEG channel thanks to the presence of the polarization-induced charges. The electron charge density of the channel is strongly dependent on the polarization-induced concentration, therefore if the activation coefficient increases, the concentration of electrons in the channel becomes higher. Figures 6.14 a) and b) show, respectively, the polarization-induced charges and the electron density in the channel at the equilibrium along the Z-direction and how they increase with higher activation coefficients. Moreover, figure 6.15 shows the band diagram at the equilibrium condition of the GaN/AlGaN/-GaN heterostructure under the gate contact: an increasing of the activation coefficient produces a deeper bending of the conduction band.

Apart from the equilibrium condition, the behaviour of the electron density in the channel, explained above, can be verified with an applied voltage. Figures 6.16 a), b) and c) show the 2D distribution of electrons at $V_{gs} = 2$ V and $V_{ds} = 7$ V for the three different activation coefficients. Moreover, in figure 6.16d there is the electron concentration along the Y-direction at the interface AlGAN/GaN (in the GaN side), whose values increase with the activation coefficient. In the middle of the fin they achieve a maximum equal to $2.46 \cdot 10^{18}$ for $a = 0.85$, $2.77 \cdot 10^{18}$ for $a = 0.9$, $3.03 \cdot 10^{18}$ for $a = 0.95$ and $3.24 \cdot 10^{18}$ for $a = 1$.

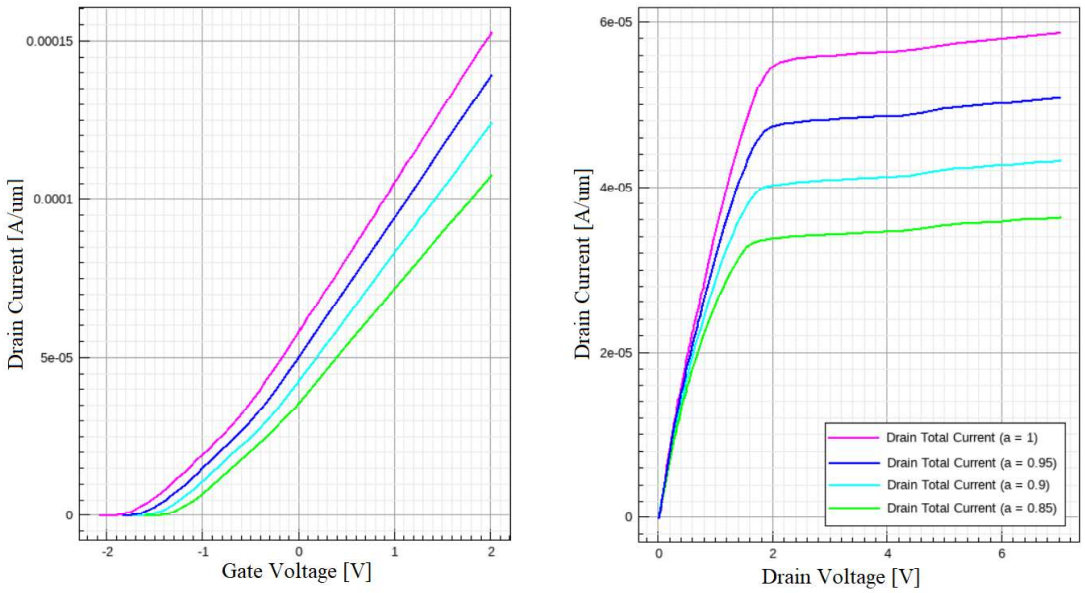

(a) Drain current as a function of the gate voltage at $V_{ds} = 7$ V

(b) Drain current as a function of the drain voltage at $V_{gs} = 0$ V

Figure 6.13: Drain current behaviour for different activation coefficients

This explanation is useful to understand the behaviour of the drain current and in particular, the variation of the threshold voltage for different values of a. In fact, the

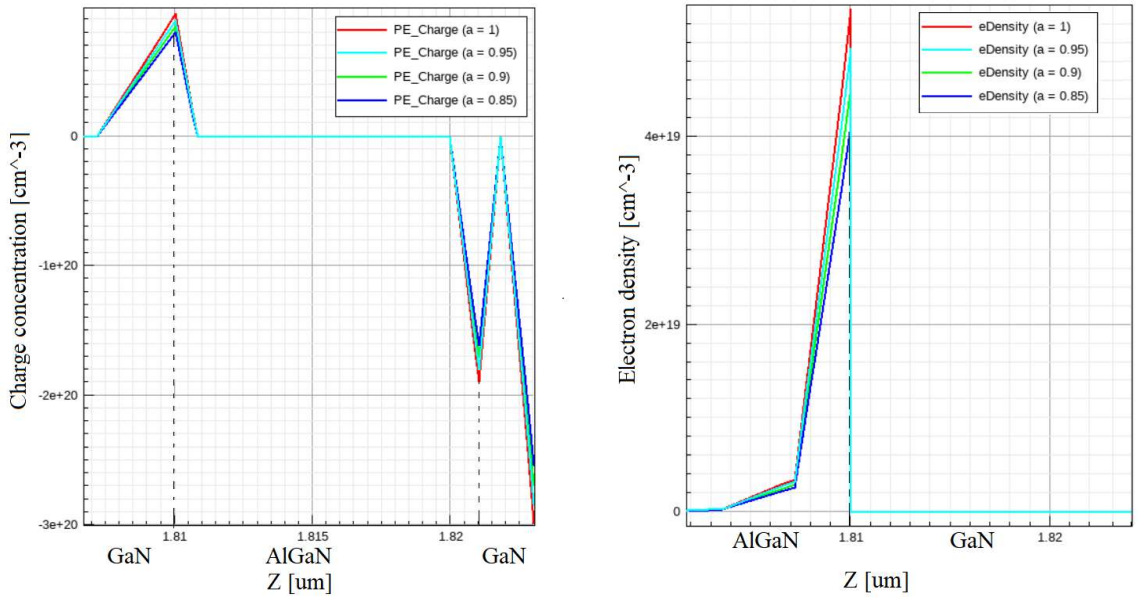

(a) Polarization-induced charge concentration in the GaN/AlGaN/GaN heterostructure

(b) Electron density of the 2DEG channel at the interface AlGaN/GaN

Figure 6.14: Comparison between HEMT and Fin-HEMT at the equilibrium

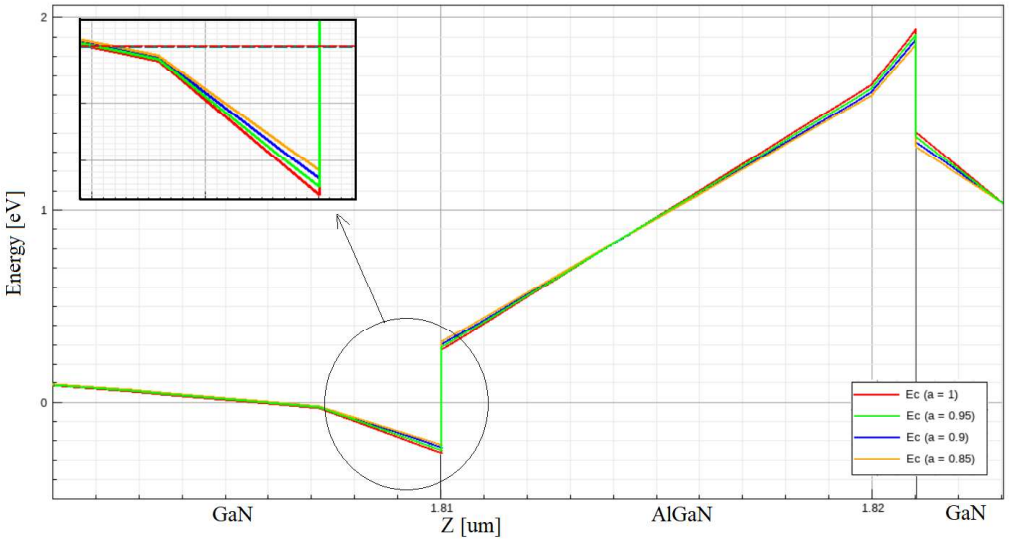

Figure 6.15: Conduction band diagram of the Fin-HEMT in the heterostructure region for different activation coefficients: zoom on the bending of the conduction band under the Fermi level

higher is the activation, the more are the polarization induced charge and the electron density of the channel, therefore a more negative voltage is necessary to turn off the device. In conclusion, an increasing of the activation coefficient implies a shift of the threshold towards negative values, which are listed as follows: -1.40 V for $a = 1$, -1.30

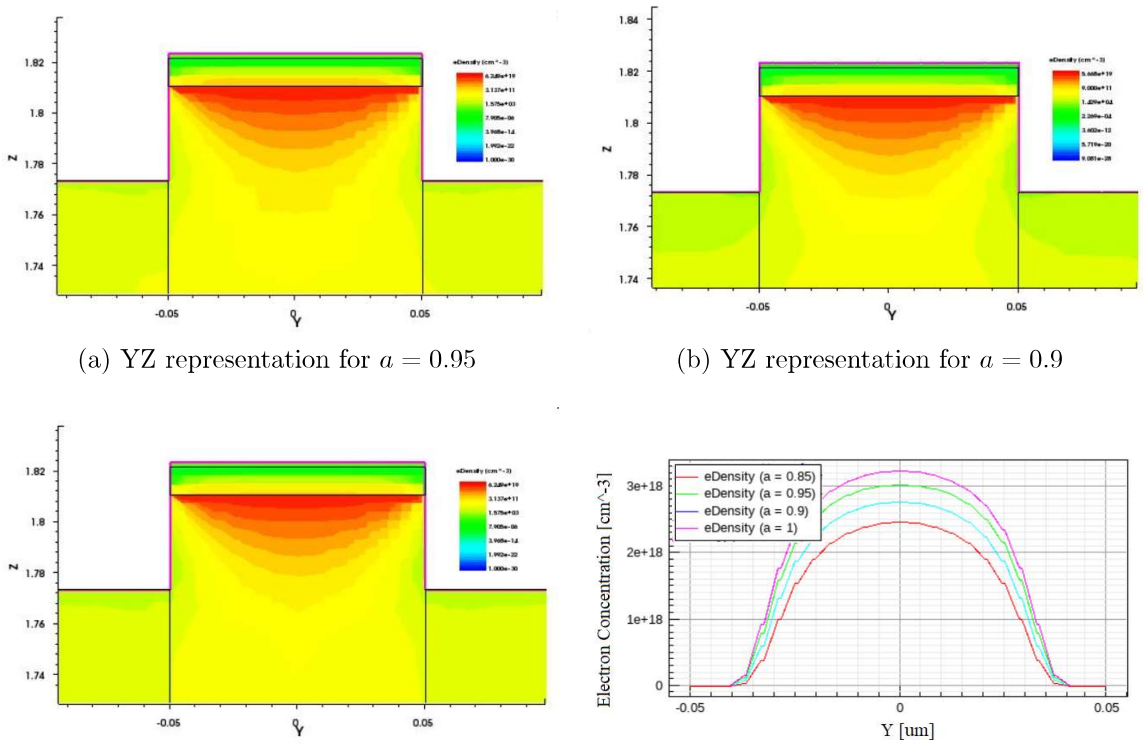

(a) YZ representation for $a = 0.95$

(b) YZ representation for $a = 0.9$

(c) YZ representation for $a = 0.85$

(d) Electron density: comparison along the Y direction

Figure 6.16: Electron density representations at $V_{gs} = 2$ V and $V_{ds} = 7$ V

V for $a = 0.95$, -1.26 V for $a = 0.90$ and -1.22 V for $a = 0.85$.

As in the previous cases, the sensitivity can be calculated in this case using the following formula:

$$S\Big|_{V_{gs},V_{ds}}^{a} = \frac{\Delta I_d}{\Delta a} = \frac{I'_d - I_d}{a' - a} \tag{6.7}$$

where I'_d and a' are respectively, the drain current and the activation coefficient for the modified structure, while I_d and a are respectively, the drain current and the activation coefficient of the reference Fin-HEMT. Figure 6.17 shows the behaviour of the sensitivity at $V_{ds} = 7$ V as a function of the gate voltage, which is chosen into a range between 0 V and 2 V. The variation of S_a is linear for all the activation coefficients and its derivative with respect to the gate voltage corresponds to a transconductance, indicated in equation (6.8), that increases with a decreasing of a. Moreover, it is possible to represent the sensitivity for $V_{gs} = 0$ V as a function of the drain voltage, included into an interval between 5 V and 7 V. Even in this case, the behaviour is linear and the slope gives a not so high output conductance, shown in formula (6.9).

$$S_{gm}\Big|_{V_{gs}}^{a} = \frac{\frac{dI'_d}{dV_{gs}} - \frac{dI_d}{dV_{gs}}}{a' - a} \tag{6.8}$$

$$S_{Cds}\Big|_{V_{ds}}^{a} = \frac{\frac{dI'_d}{dV_{ds}} - \frac{dI_d}{dV_{ds}}}{a' - a} \tag{6.9}$$

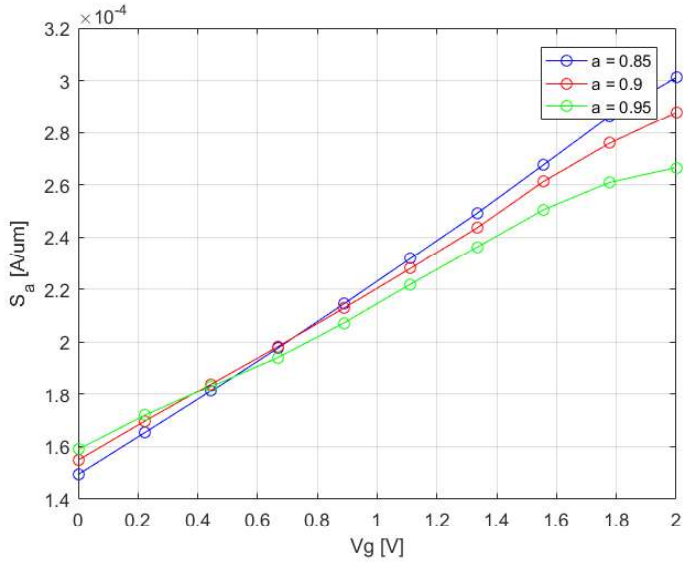

Figure 6.17: Sensitivity as a function of the gate voltage at $V_{ds} = 7$ V

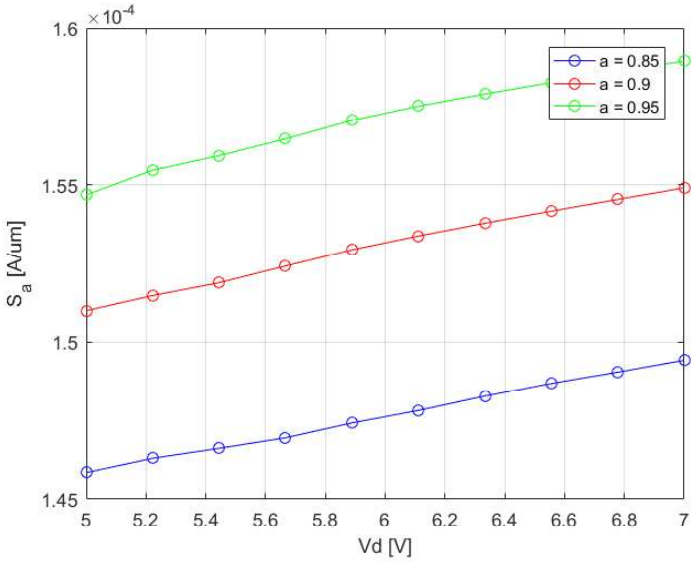

Figure 6.18: Sensitivity as a function of the drain voltage at $V_{gs} = 0$ V

6.4 Temperature

The temperature is another focus parameter of the parametric sensitivity analysis, especially for the typical applications of GaN devices which include power stages. The reference value in the simulations is equal to 300 K and it has been varied in the range between 280 K and 380K. The quantities exploited in the simulation are 280 K, 330 K, 350 K and 380 K and the obtained results are compared with the reference ones, as always.

The behaviour of the drain current as a function of the gate voltage at $V_{ds} = 7$ V is shown in figure 6.19, where it can be noticed that the temperature dependence changes with respect to V_{gs}. In particular above the threshold, a higher temperature implies a lower drain current, while in the subthreshold region the drain current increases with the temperature. The behaviour of the device above the threshold is explained by the presence of the two-dimensional channel, which can be expressed by the mobility model of equation (5.1). This equation demonstrates how the mobility decreases with an increasing temperature, therefore the drain current due to the 2DEG channel is reduced. The subthreshold region shows the opposite behaviour: the two-dimensional channel is not present anymore due to the fact that the device is turning off, therefore the mobility model, previously explained, does not dominates in this case. There are other conditions that influence the device, for example the temperature dependence on both, band gap and electron density of states (DOS). The band gap is related to temperature through equation (6.10), where $E_g(0)$ is the band gap at 0 K, α and β are material parameters. On the other hand, the DOS can be expressed as shown in equation (6.11), where $N_c(300K)$ is the density of states at 300 K and T is the temperature. Looking at both equations, it can be noticed that for an increasing temperature, the band gap is reduced and the DOS is increased. As a consequence, the number of carrier and the related drain current become higher.

$$E_g(T) = E_g(0) - \alpha \frac{T^2}{T + \beta} \tag{6.10}$$

$$N_c(T) = N_c(300K) \left(\frac{T}{300K} \right)^{\frac{3}{2}} \tag{6.11}$$

The variation of electron mobility, energy gap and effective density of states with the temperature can be seen along the Z-axis in figures 6.20 a), b) and c), respectively. It can be clearly appreciated the reduction of the mobility with the temperature and at the same time the increasing of the other two quantities.

Moreover, it is interesting to verify the behaviour of the current, explained above. Figure 6.21 shows the electron density along the Y direction in the region under the gate

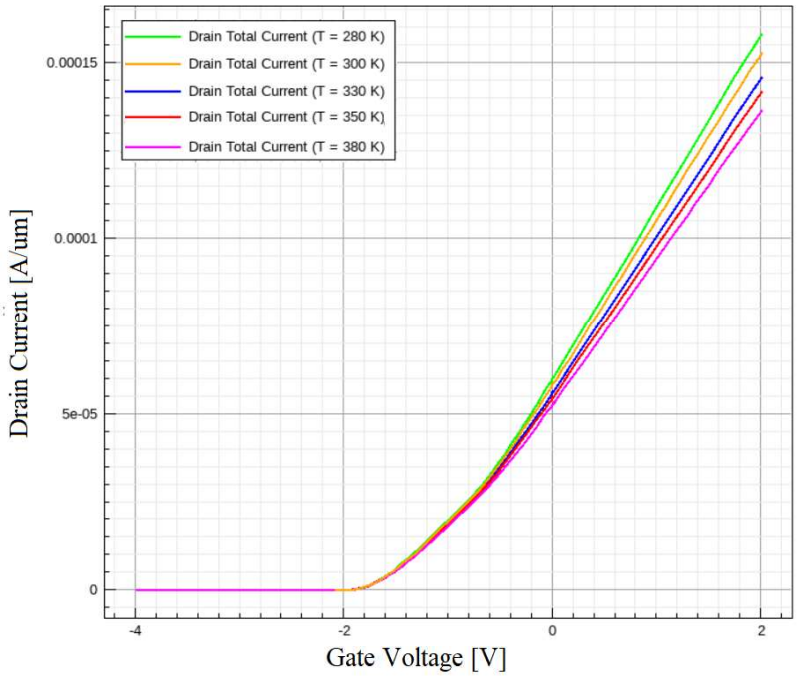

Figure 6.19: Drain current as a function of the gate voltage at $V_{ds} = 7$ V

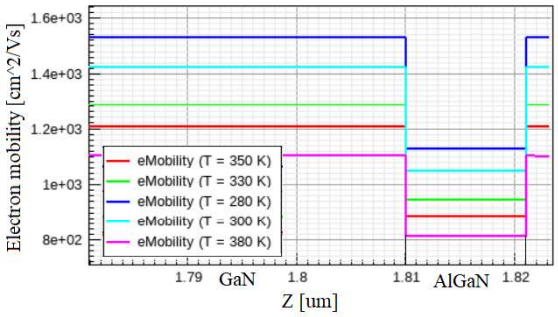

(a) Electron mobility

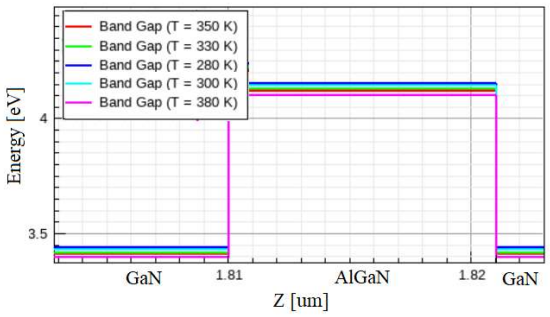

(b) Energy gap

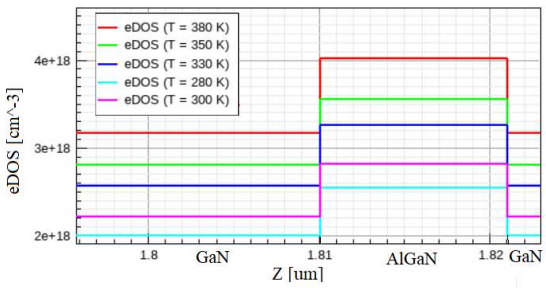

(c) Effective density of states

Figure 6.20: Behaviour of different quantities along the Z-axis for T=280 K, 300 K, 330 K, 350 K, 380 K

and at the interface AlGaN/GaN (in the GaN side). On the left hand side, the bias point is chosen above the threshold in order to verify that the current decreases with an increasing temperature. In fact, the electron density demonstrates this behaviour. On the right hand side, the bias point is under the threshold, where a lower temperature gives a reduction of the current. In fact, the electron density increases with the temperature and verifies this aspect.

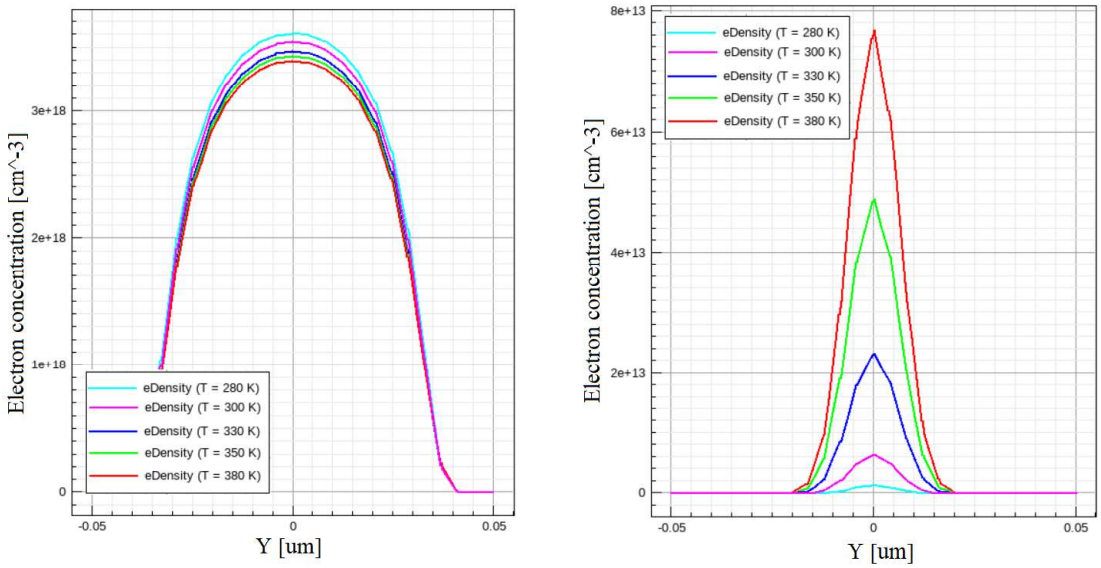

(a) Electron concentration at $V_{ds} = 7$ V and $V_{gs} = 2$ V

(b) Electron concentration at $V_{ds} = 7$ V and $V_{gs} = -1.9$ V

Figure 6.21: Electron concentration along the Y-direction

In conclusion, information about the sensitivity can be interesting. The sensitivity parameter for $V_{ds} = 7$ as a function the gate voltage is obtained as shown in equation (6.12): I'_d and T' are respectively, the drain current and the temperature for the modified structure, I_d is the drain current of the reference Fin-HEMT and T is its temperature equal to 300 K. The range chosen for the gate voltage is included between -0.5 V and 2 V, where the variation of temperature is evident. The results are shown in figure 6.22: the curves have a linear and decreasing behaviour, unless for the blue one at $T = 280$ K that has a slightly modified behaviour with an increasing of V_g. Moreover, the slope, which corresponds to the transconductance found through formula (6.13), is negative and more accentuated in the blue curve.

$$S\Big|_{V_{gs}}^{T} = \frac{\Delta I_d}{\Delta T} = \frac{I'_d - I_d}{T' - T} \tag{6.12}$$

$$S_{gm}\Big|_{V_{gs}}^{T} = \frac{\frac{dI_d'}{dV_{gs}} - \frac{dI_d}{dV_{gs}}}{T' - T} \tag{6.13}$$

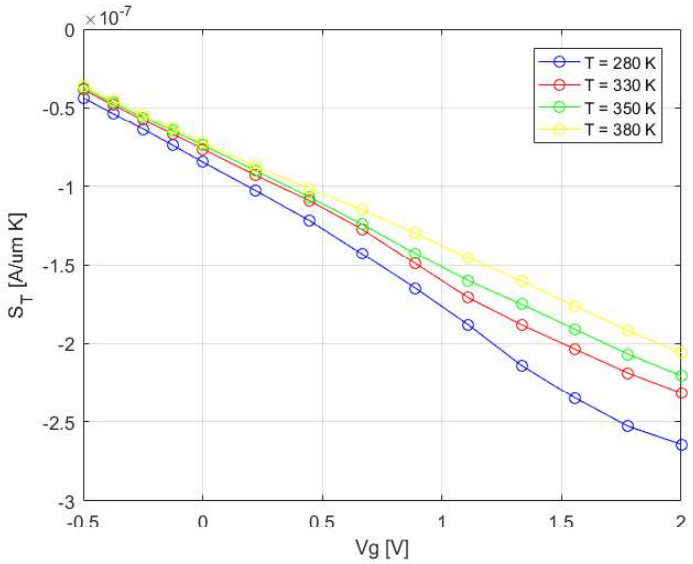

Figure 6.22: Sensitivity as a function of the gate voltage at $V_{ds} = 7$ V

6.5 Trap concentration

The trap concentration is the last quantity under analysis. The presence of traps has been necessary for the formation of the two-dimensional channel under the passivation layers that connect the gate to the source/drain contact. The reference concentration is $3 \cdot 10^{13}\ cm^{-3}$ and in this section it is modified of different quantities: $\pm 2\%$, $\pm 5\%$ and $\pm 10\%$.

Figure 6.23 shows the total drain current for different traps concentrations. In particular figure a) describes the behaviour of the current as a function of the gate voltage at $V_{ds} = 7$ V and shows that, for a fixed gate voltage, the value of I_d decreases with a lower concentration of traps. This aspect is more evident for positive values of V_{gs} and for strong reduction of traps: the orange and the red curves correspond to a variation of -5% and -10%, respectively, and they produce a larger decreasing of current with respect to the other curves. The same considerations are valid for figure b), where the current is shown as a function of the drain voltage at $V_{gs} = 0$ V.

The behaviour of the device in this specific case can be explained as follows. The traps have been inserted at the interface between the passivation layer and the GaN cap

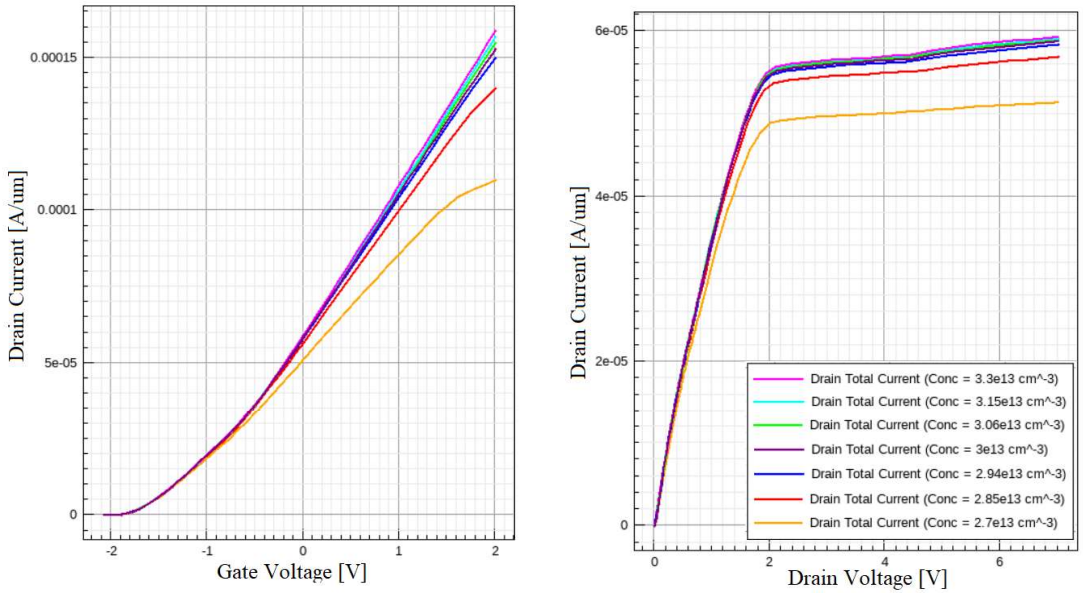

(a) Drain current as a function of the gate voltage at $V_{ds} = 7$ V

(b) Drain current as a function of the drain voltage at $V_{gs} = 0$ V

Figure 6.23: Drain current behaviour for different traps concentrations

in order to allow the formation of the channel in the regions out of the gate. As already explained in the previous chapter, when they are ionized, they are able to push down the conduction band and form the two-dimensional channel. In this way, they create a link between the 2DEG channel under the gate and the source/drain contact. This mechanism works if the concentration of traps is quite high to produce a sufficient number of ionized trapped donors, which are responsible of the 2DEG channel formation. Therefore, a strong reduction of the traps (for example -5% and -10%) can lead to a very low number of ionized donors, which are not not able anymore to guarantee the same electron density in the channel. The main consequence is the decreasing in the drain current, which is more evident if the voltage is increased. Figures 6.24 a) and b) show how different is the concentration of ionized donor traps and electron density with a variation of $\pm 10\%$ at $V_{ds} = 7$ V and different gate voltages. It can be noticed the strong difference between the curves obtained with the lowest traps concentration (2.7e13 cm^{-3}) and the ones obtained with the highest one (3.3e13 cm^{-3}). Moreover, it can be seen that, in each case, with a higher gate voltage, the ionized traps are reduced for some reasons and, as a consequence, the electron density and the drain current are decreased.

Finally, the sensitivity can be calculated through formula (6.14): I_d' and $Conc'$ are respectively, the drain current and the concentration for the modified structure, I_d is the drain current of the reference Fin-HEMT and $Conc$ is its traps concentration equal to 3e13 cm^{-3}. Figure 6.25 shows the sensitivity at $V_{ds} = 7$ V as a function of the gate

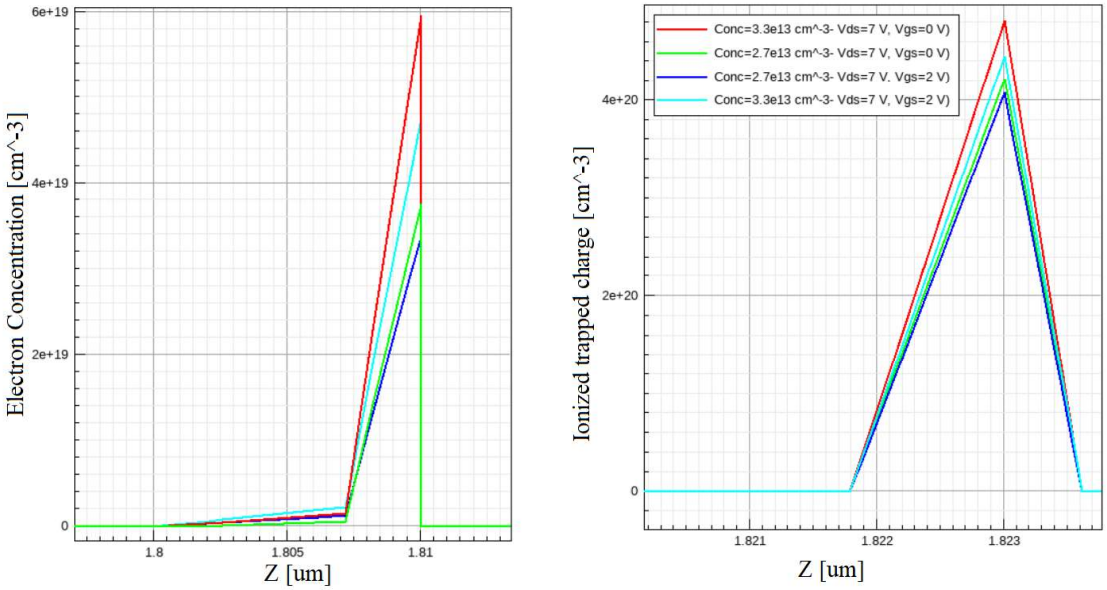

(a) Electron concentration along the Z-axis

(b) Ionized trapped charge along the Z-axis

Figure 6.24: Behaviour for a ±10% variation of traps

voltage, chosen in the range between 0 V and 2 V. The behaviour of the curves seems linear until 1.4 V, moreover the positive slope increases with the concentration of traps and can be calculated through equation (6.15). This means that if the concentration increases, there is a higher transconductance. On the other hand, figure 6.26 shows the same parameter at $V_{gs} = 0$ V as a function of the drain voltage, which is included between 4 V and 7 V. The curves are more or less flat and their slope implies a low output conductance, calculated through formula (6.16), which does not change with the different variations.

$$S\Big|_{V_{gs},V_{ds}}^{Conc} = \frac{\Delta I_d}{\Delta T} = \frac{I'_d - I_d}{Conc' - Conc} \tag{6.14}$$

$$S_{gm}\Big|_{V_{gs}}^{Conc} = \frac{\frac{dI'_d}{dV_{gs}} - \frac{dI_d}{dV_{gs}}}{Conc' - Conc} \tag{6.15}$$

$$S_{Cds}\Big|_{V_{ds}}^{Conc} = \frac{\frac{dI'_d}{dV_{ds}} - \frac{dI_d}{dV_{ds}}}{Conc' - Conc} \tag{6.16}$$

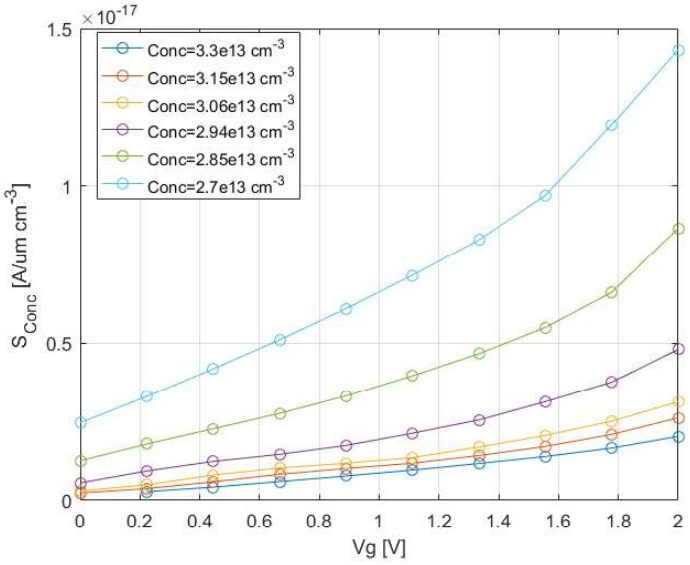

Figure 6.25: Sensitivity as a function of the gate voltage at $V_{ds} = 7$ V

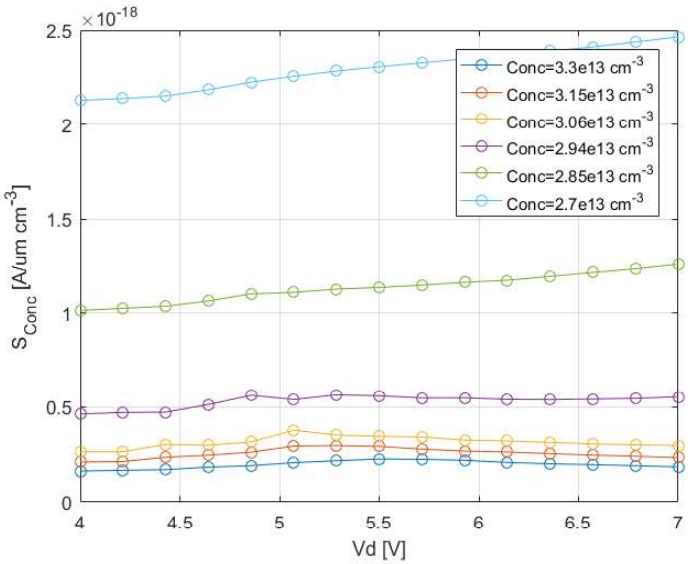

Figure 6.26: Sensitivity as a function of the gate voltage at $V_{ds} = 7$ V

Chapter 7

Summary and conclusions

The GaN FinFET structure is one of the most recent and unconventional proposals in the wide panorama of electronic devices, which has been analysed in different steps.

The electronic properties of nitride-based semiconductors have been widely discussed in order to highlight their superior characteristics with respect to conventional materials: wide band gap, high electron mobility, low intrinsic carrier density, high electron mobility, high breakdown field, high thermal stability and high saturation velocity. In the past years, they have only been exploited into conventional 2D devices: many technological solutions have been studied in order to improve their performances in both analog and digital applications. Unfortunately, the two dimensional structure of these devices limits their output performances and reduces the possibility to find advantages in employing them.

In this scenario, a new three-dimensional structure has been exploited thanks to the improvements provided with respect to a conventional planar one: strong gate electrostatic control of the channel, reduction of SCEs, shallower threshold voltage, better OFF performances, higher ON/OFF current ratio. The proposed FinFET structures found in literature are different and they show positive aspects suitable for both analog and digital applications. In this thesis, the analysis is only focused on an GaN/AlGaN/GaN FinFET device and this choice is mainly due to two reasons. First, there are not many implementations of this kind of structure, therefore it is interesting study its behaviour. Moreover, this configuration gives the possibility to investigate more the analog/RF field, than the digital one.

The TCAD Synopsys Sentaurus has been used to implement the numerical simulation of the device. Both the conventional HEMT and Fin-HEMT have been simulated in order to verify their differences. The simulation results have been confirmed the presence in the FinFET of a higher threshold voltage and a lower output drain current with respect to a planar device. Moreover, better performances in analog/RF applications have

been verified thanks to the higher transconductance and the lower output conductance.

Since the analysis has shown potential benefits of the FinFET, the parametric sensitivity analysis has been carried out with the aim of optimize the device performances by changing the geometrical and physical features. The fin height variation of $\pm 5\%$ does not produces strong differences in the drain current: the sensitivity behaviour with respect to the gate voltage results linear and the transconductance slightly increases with a reduction of the height. The fin width variation of $\pm 10\%$ shows evident differences in the output drain current and threshold voltage. The sensitivity is obtained with respect to gate and drain voltages: in the first case it shows similar transconductance with different fin widths, while an improvement in the output conductance is obtained for a positive variation of W_{fin}.
The other variations concern not the geometrical structure of the device, but a physical feature. In particular, the activation coefficient of the polarization charges is varied: the output drain current is modified together with the threshold. The sensitivity with respect to the gate voltage shows, as in the previous cases, a linear behaviour with an improvement of the transconductance for lower values of the activation coefficient. Then, a variation of temperature is performed and demonstrates only slight variations of the drain current. The sensitivity is, in this case, linear with respect to gate voltages, for temperatures higher than 330 K, and produces a lower transconductance with a decreasing of the temperature. The last variation is applied to the concentration of traps and shows strong differences in the drain current, but not in the threshold voltage. Here, the sensitivity with respect to the gate voltage is not linear anymore and shows an increasing transconductance with a higher traps concentration. On the other hand the sensitivity with respect to the drain voltages results flat and does not show differences in the output conductance values.

Bibliography

[1] Alessio Pantellini, *Sviluppo di un dispositivo Switch in Nitruro di Gallio (GaN) ad alta potenza per applicazioni nei front-end dei moduli T/R*, 2010/2011

[2] http://www.ioffe.ru/SVA/NSM/Semicond

[3] Politecnico di Milano, *Dispositivi attivi a microonde e tecnologie di fabbricazione di circuiti planari*

[4] Federico Lombardo, *Impiego dell'Arseniuro di Gallio nelle moderne tecnologie ULSI*, 2009/2010

[5] Jack Browne, *Whats the Difference Between GaN and GaAs?*, July 2016

[6] Jose L.Jimenez, *Comparing GaAs and GaN technologies for RF*, 2017

[7] Mirko Bellesini, *Caratterizzazione mediante misure dinamiche e di elettroluminescenza di dispositivi AlGaN/GaN HEMT con elettrodo di gate trasparente*, 2009/2010

[8] Power Electronics Europe, *Can Gallium Nitride Replace silicon?*, 2010

[9] Fabrizio Bonani, *Semiconductor alloys and heterostructures*, High speed electron devices, 2017

[10] Umesh Mishra, Jasprit Singh, *Semiconductors Device Physics and Design*, 2008 Springer

[11] $https://en.wikipedia.org/wiki/Crystal_system$

[12] $https://en.wikipedia.org/wiki/Hexagonal_crystal_family$

[13] https://en.wikipedia.org/wiki/Epitaxy

[14] https://en.wikipedia.org/wiki/Centrosymmetry

[15] E. T. Yu, X. Z. Dang, P. M. Asbeck, S. S. Lau, *Spontaneous and piezoelectric polarization effects in IIIV nitride heterostructures*, May 1999

[16] He Xiao-Guang, Zhao De-Gang, Jiang De-Sheng, *Formation of two-dimensional electron gas at AlGaN/GaN heterostructure and the derivation of its sheet density expression* . Chinese Physics B, 2015

[17] Peter Moens, *General overview on GaN power devices*, 2017

[18] $https://wiki.materialsproject.org/Piezoelectricity_calculations$

[19] $http://www.sentaurus.dsod.pl/manuals/data/sdevice_ug.pdf$

[20] *Characteristics of GaN and AlGaN/GaN FinFETs*, Ki-Sik Im a, Hee-Sung Kang a, Jae-Hoon Lee b, Sung-Jae Chang c, Sorin Cristoloveanu c, Maryline Bawedin d, Jung-Hee Lee, May 2014

[21] *Performance Improvement and Sub−60 mV/Decade Swing in AlGaN/GaN FinFETs by Simultaneous Activation of 2DEG and Sidewall MOS Channels*, Yue Xu , Sorin Cristoloveanu, Maryline Bawedin, Ki-Sik Im and Jung-Hee Lee, March 2018

[22] *Dependence of Device Performances on Fin Dimensions in AlGaN/GaN Recessed-Gate Nanoscale FinFET*, Gwan Min Yoo, Jae Hwa Seo, Young Jun Yoon, Young Jae Kim, Sung Yoon Kim, Hye Su Kang, Hye Rim Eun, Ra Hee Kwon, Young In Jang, and In Man Kang, Seong Min Lee, Seongjae Cho, 2014

[23] *Investigation of GaN Fin-HEMTs with micron-scale fin width*, Li-Cheng Chang, Ming Yang, Yi-Hong Jiang, Chao-Hsin Wu, 2017

[24] *Enhancement-Mode AlGaN/GaN FinFETs With High On/Off Performance in 100 nm Gate Length*, E. Ture, P. Brckner, R. Quay, O. Ambacher, M. Alsharef, R. Granzner, F. Schwierz

[25] *RF Performance of Trigate GaN HEMTs*, Mohamed Alsharef, Max Christiansen, Ralf Granzner, Erdin Ture, Rdiger Quay, Oliver Ambacher, Frank Schwierz, November 2016

[26] *GaN-based FinFET with double-channel AlGaN/GaN heterostructure*, Chong Wang, Xin Wang, Xuefeng Zheng, Qing He, Ji Wu, Ye Tian, Wei Mao, Xiaohua Ma and Yue Hao, March 2018

[27] *Current Stability in Multi-Mesa-Channel AlGaN/GaN HEMTs*, Kota Ohi, Joel Tacla Asubar, Kenya Nishiguchi, and Tamotsu Hashizume, October 2013

Appendix A

Sentaurus input files

**********sde_dvs.cmd**********

```
(define SUBDOPGaN 0) ; [um] uniform concentration of Layer 1e14
(define SUBDOPAlGaN 0)          ; [um] uniform concentration of Layer 1e14
(define WGaN -@Wfin_Half@); [um] Thickness of the substrate (Fin width)
(define HalfSpacing -1); [um] Half of the spacing between two fins -2
(define LG 0.4); [um] Gate length;
(define LS 1); [um] Source/Drain length
(define Lgs 0.25); [um] Gate to Source
(define Lgd 1); [um] Gate to Drain
(define GaNa LS); [um]
(define GaNb (+ LS Lgs)); [um]
(define GaNc (+ GaNb LG)); [um]
(define GaNd (+ GaNc Lgd)); [um]
(define W (+ GaNd LS)); [um] Length Substrate
(define XS LS); [um] source position
(define XD (- W LS)); [um] drain position
(define Wtot (+ WGaN HalfSpacing));[um] Total width
(define HAlGaN 0.011); [um] AlGaN layer height
(define HGaN @Hfin@); [um] GaN height
(define HGaNbody 1.763); [um] GaN bulk height
(define HFIN (+ HGaN HAlGaN)); [um] fin height
(define HtopGate 0.036); [um] Metal top-gate height
(define Hsub 0.010); [um] Substrate height
(define Hcap 0.002); [um] Cap height
```

; CREATE THE STRUCTURE

(define A1 (sdegeo:create-cuboid (position GaNa (* WGaN -1) (+ Hsub HGaNbody HFIN Hcap)) (position GaNb WGaN (+ Hsub HGaNbody HFIN Hcap 0.05)) "Si3N4" "pass1"))

(define A2 (sdegeo:create-cuboid (position GaNc (* WGaN -1) (+ Hsub HGaNbody HFIN Hcap)) (position GaNd WGaN (+ Hsub HGaNbody HFIN Hcap 0.05)) "Si3N4" "pass2"))

(define B (sdegeo:create-cuboid (position 0 (* WGaN -1) (+ Hsub HGaNbody HFIN)) (position W WGaN (+ Hsub HGaNbody HFIN Hcap)) "GaN" "Cap"))

(define C (sdegeo:create-cuboid (position 0 (* WGaN -1) (+ Hsub HGaNbody HGaN)) (position W WGaN (+ Hsub HGaNbody HFIN)) "AlGaN" "Layer"))

(define D (sdegeo:create-cuboid (position 0 (* WGaN -1) Hsub) (position W WGaN (+ Hsub HGaNbody HGaN)) "GaN" "Bulk"))

(define E (sdegeo:create-cuboid (position 0 (* WGaN -1) 0) (position W WGaN Hsub) "Oxide" "Base"))

(define L (sdegeo:create-cuboid (position GaNb WGaN Hsub) (position GaNc Wtot (+ Hsub HGaNbody)) "GaN" "Lat1"))

(define M (sdegeo:create-cuboid (position GaNb WGaN 0) (position GaNc Wtot Hsub) "Oxide" "Baselat1"))

(define N (sdegeo:create-cuboid (position GaNb (* WGaN -1) Hsub) (position GaNc (* Wtot -1) (+ Hsub HGaNbody)) "GaN" "Lat2"))

(define O (sdegeo:create-cuboid (position GaNb (* WGaN -1) 0) (position GaNc (* Wtot -1) Hsub) "Oxide" "Baselat2"))

(define LS1 (sdegeo:create-cuboid (position 0 WGaN Hsub) (position GaNa Wtot (+ Hsub HGaNbody)) "GaN" "Lat1S1"))

(define MS1 (sdegeo:create-cuboid (position 0 WGaN 0) (position GaNa Wtot Hsub) "Oxide" "Baselat1S1"))

(define NS1 (sdegeo:create-cuboid (position 0 (* WGaN -1) Hsub) (position GaNa (* Wtot -1) (+ Hsub HGaNbody)) "GaN" "Lat2S1"))

(define OS1 (sdegeo:create-cuboid (position 0 (* WGaN -1) 0) (position GaNa (* Wtot -1) Hsub) "Oxide" "Baselat2S1"))

(define LS2 (sdegeo:create-cuboid (position GaNd WGaN Hsub) (position W Wtot (+ Hsub HGaNbody)) "GaN" "Lat1S2"))

(define MS2 (sdegeo:create-cuboid (position GaNd WGaN 0) (position W Wtot Hsub) "Oxide" "Baselat1S2"))

(define NS2 (sdegeo:create-cuboid (position GaNd (* WGaN -1) Hsub) (position W (* Wtot -1) (+ Hsub HGaNbody)) "GaN" "Lat2S2"))

(define OS2 (sdegeo:create-cuboid (position GaNd (* WGaN -1) 0) (position W (* Wtot -1) Hsub) "Oxide" "Baselat2S2"))

(define LL (sdegeo:create-cuboid (position GaNa WGaN Hsub) (position GaNb Wtot (+ Hsub HGaNbody)) "GaN" "Lat1_agg1"))

```
(define MM (sdegeo:create-cuboid (position GaNa WGaN 0) (position GaNb Wtot Hsub) "Oxide" "Baselat1_agg1"))

(define NN (sdegeo:create-cuboid (position GaNa (* WGaN -1) Hsub) (position GaNb (* Wtot -1) (+ Hsub HGaNbody)) "GaN" "Lat2_agg1"))

(define OO (sdegeo:create-cuboid (position GaNa (* WGaN -1) 0) (position GaNb (* Wtot -1) Hsub) "Oxide" "Baselat2_agg1"))

(define LLL (sdegeo:create-cuboid (position GaNc WGaN Hsub) (position GaNd Wtot (+ Hsub HGaNbody)) "GaN" "Lat1_agg2"))

(define MMM (sdegeo:create-cuboid (position GaNc WGaN 0) (position GaNd Wtot Hsub) "Oxide" "Baselat1_agg2"))


(define NNN (sdegeo:create-cuboid (position GaNc (* WGaN -1) Hsub) (position GaNd (* Wtot -1) (+ Hsub HGaNbody)) "GaN" "Lat2_agg2"))

(define OOO (sdegeo:create-cuboid (position GaNc (* WGaN -1) 0) (position GaNd (* Wtot -1) Hsub) "Oxide" "Baselat2_agg2"))

; ADD CONTACTS

; Gate contact

(sdegeo:define-contact-set "Gate"      4.0  (color:rgb 1.0 0.0 0.0 ) "##" )

(sdegeo:set-current-contact-set "Gate")

(define Q2 (sdegeo:create-cuboid (position GaNb (* WGaN -1) (+ HFIN Hsub HGaNbody Hcap)) (position GaNc WGaN (+ Hcap HFIN Hsub HGaNbody 2)) "Metal" "Gate"))

(sdegeo:set-contact-boundary-faces Q2)

(sdegeo:delete-region Q2)

(define M (sdegeo:create-cuboid (position GaNb WGaN (+ Hsub HGaNbody)) (position GaNc (- WGaN HtopGate) (+ Hsub HGaNbody HFIN Hcap)) "Metal" "Gate"))

(sdegeo:set-contact-boundary-faces M)

(sdegeo:delete-region M)

(define N (sdegeo:create-cuboid (position GaNb WGaN (+ Hsub HGaNbody)) (position GaNc Wtot (+ Hsub HGaNbody HtopGate)) "Metal" "Gate"))

(sdegeo:set-contact-boundary-faces N)

(sdegeo:delete-region N)

(define O (sdegeo:create-cuboid (position GaNb (* WGaN -1) (+ Hsub HGaNbody)) (position GaNc (* (- WGaN HtopGate) -1) (+ Hsub HGaNbody HFIN Hcap)) "Metal" "Gate"))

(sdegeo:set-contact-boundary-faces O)

(sdegeo:delete-region O)
```

```
(define P (sdegeo:create-cuboid (position GaNb (* WGaN -1) (+ Hsub HGaNbody)) (position GaNc (* Wtot -1) (+ Hsub HGaNbody HtopGate)) "Metal" "Gate"))

(sdegeo:set-contact-boundary-faces P)

(sdegeo:delete-region P)


(sdegeo:define-contact-set "Source"      4.0  (color:rgb 1.0 0.0 0.0 ) "##" )

(sdegeo:set-current-contact-set "Source")

(define Q (sdegeo:create-cuboid (position 0 (* Wtot -1) (+  Hsub HGaNbody )) (position GaNa Wtot (+ Hcap HFIN Hsub HGaNbody 2)) "Metal" "Gate"))

(sdegeo:set-contact-boundary-faces Q)

(sdegeo:delete-region Q)


(sdegeo:define-contact-set "Drain"      4.0  (color:rgb 1.0 0.0 0.0 ) "##" )

(sdegeo:set-current-contact-set "Drain")

(define Q1 (sdegeo:create-cuboid (position GaNd (* Wtot -1) (+ Hsub HGaNbody )) (position W Wtot (+ Hcap HFIN Hsub HGaNbody 2)) "Metal" "Gate"))

(sdegeo:set-contact-boundary-faces Q1)

(sdegeo:delete-region Q1)



; ADD DOPING

; Define regions (windows) where we want to put doping

; Define the kind of doping

(sdedr:define-constant-profile "ConstantProfileDefinition_1"  "ArsenicActiveConcentration" SUBDOPGaN)

(sdedr:define-constant-profile "ConstantProfileDefinition_2"  "ArsenicActiveConcentration" SUBDOPAlGaN)

(sdedr:define-constant-profile "xmole_AlGaN_const" "xMoleFraction" 0.32)


; Place the doping in the correct window

(sdedr:define-constant-profile-region "ConstantProfilePlacement_1" "ConstantProfileDefinition_2" "Layer")

(sdedr:define-constant-profile-region "ConstantProfilePlacement_2" "xmole_AlGaN_const" "Layer")



; Left gate contact edge
```

(sdedr:define-refinement-window "pezzo" "Cuboid" (position 0 (* WGaN -1) 1.3) (position W WGaN (+ Hsub HGaNbody)))

(sdedr:define-refinement-window "centro" "Cuboid" (position 0 (* WGaN -1) Hsub) (position W WGaN 1.3))

(sdedr:define-refinement-window "channel" "Cuboid" (position GaNb (* WGaN -1) (+ Hsub HGaNbody 0.01)) (position GaNc WGaN (+ Hsub HGaNbody HFIN)))

(sdedr:define-refinement-window "channelGS" "Cuboid" (position GaNa (* WGaN -1) (+ Hsub HGaNbody 0.01)) (position GaNb WGaN (+ Hsub HGaNbody HFIN)))

(sdedr:define-refinement-window "channelGD" "Cuboid" (position GaNc (* WGaN -1) (+ Hsub HGaNbody 0.01)) (position GaNd WGaN (+ Hsub HGaNbody HFIN)))

(sdedr:define-refinement-window "pezzolat1" "Cuboid" (position 0 WGaN 1.85) (position W Wtot (+ Hsub HGaNbody)))

(sdedr:define-refinement-window "pezzolat2" "Cuboid" (position 0 (* WGaN -1) 1.85) (position W (* Wtot -1) (+ Hsub HGaNbody)))

(sdedr:define-refinement-size "Ref.size.cap" 0.05 0.02 0.05 0.05 0.02 0.05)

(sdedr:define-refinement-size "Ref.size.channel" 0.05 0.02 0.01 0.05 0.02 0.01)

(sdedr:define-refinement-size "Ref.size.channelGATE" 0.05 0.005 0.005 0.05 0.005 0.005)

(sdedr:define-refinement-size "Ref.size.fitto" 0.05 0.02 0.002 0.05 0.02 0.002)

(sdedr:define-refinement-size "Ref.size.pezzo" 0.5 0.2 0.2 0.5 0.2 0.2)

(sdedr:define-refinement-placement "Ref.bulk1" "Ref.size.pezzo" "pezzo")

(sdedr:define-refinement-placement "Ref.bulk2" "Ref.size.channelGATE" "channel")

(sdedr:define-refinement-placement "Ref.bulk3" "Ref.size.channel" "channelGS")

(sdedr:define-refinement-placement "Ref.bulk4" "Ref.size.channel" "channelGD")

(sdedr:define-refinement-placement "Ref.lat1" "Ref.size.pezzo" "pezzolat1")

(sdedr:define-refinement-placement "Ref.lat2" "Ref.size.pezzo" "pezzolat2")

(sdedr:define-refinement-region "Ref.cap" "Ref.size.fitto" "Cap")

; GENERATE MESH (CHANGE THE NAME IN " " FOR DIFFERENT STRUCTURES)

(sde:build-mesh "snmesh" "" "n@node@_msh")

**********sdevice_des.cmd**********

```
File {* input files:
        Grid    = "@tdr@"
        Current = "@plot@"
        Plot    = "@tdrdat@"
        Parameter = "@parameter@"
}

# Please do not change this Section
Electrode{
 { Name="Gate"   Voltage= 0.0 Schottky Workfunction = 5}
  { Name="Drain"   Voltage= 0.0 EqOhmic}
 { Name="Source"   Voltage= 0.0 EqOhmic}
 }

Physics {
  Mobility(DopingDependence eHighFieldSaturation)
  EffectiveIntrinsicDensity( NoBandGapNarrowing )
  Fermi
  Recombination(SRH Auger Radiative eAvalanche(Eparallel))
  Piezoelectric_Polarization (strain activation = @act@)
  Aniso(Poisson direction = zAxis)
  Heterointerface
  Temperature = @T@
}

Physics( RegionInterface="pass1/Cap" ){
        Traps(
                (Donor Level Conc= @Conc@ EnergyMid= 0.7 FromMidBandGap)
        )
}

Physics( RegionInterface="pass2/Cap" ){
```

```
        Traps(
                (Donor Level Conc= @Conc@ EnergyMid= 0.7 FromMidBandGap)
        )
}

Physics( RegionInterface="Bulk/Base" ){
Piezoelectric_Polarization(activation = 0)}

Physics( RegionInterface="Lat1/Baselat1" ){
Piezoelectric_Polarization(activation = 0)}

Physics( RegionInterface="Lat2/Baselat2" ){
Piezoelectric_Polarization(activation = 0)}

Physics( RegionInterface="Lat1S1/Baselat1S1" ){
Piezoelectric_Polarization(activation = 0)}

Physics( RegionInterface="Lat2S1/Baselat2S1" ){
Piezoelectric_Polarization(activation = 0)}

Physics( RegionInterface="Lat1S2/Baselat1S2" ){
Piezoelectric_Polarization(activation = 0)}

Physics( RegionInterface="Lat2S2/Baselat2S2" ){
Piezoelectric_Polarization(activation = 0)}

Physics( RegionInterface="Lat1_agg1/Baselat1_agg1" ){
Piezoelectric_Polarization(activation = 0)}

Physics( RegionInterface="Lat2_agg1/Baselat2_agg1" ){
Piezoelectric_Polarization(activation = 0)}
```

```
Physics( RegionInterface="Lat1_agg2/Baselat1_agg2" ){
Piezoelectric_Polarization(activation = 0)}

Physics( RegionInterface="Lat2_agg2/Baselat2_agg2" ){
Piezoelectric_Polarization(activation = 0)}

Physics( RegionInterface="Bulk/Lat1" ){
Piezoelectric_Polarization(activation = 0)}

Physics( RegionInterface="Bulk/Lat2" ){
Piezoelectric_Polarization(activation = 0)}


Physics( RegionInterface="Bulk/Lat1_agg1" ){
Piezoelectric_Polarization(activation = 0)}

Physics( RegionInterface="Bulk/Lat2_agg1" ){
Piezoelectric_Polarization(activation = 0)}

Physics( RegionInterface="Bulk/Lat1_agg2" ){
Piezoelectric_Polarization(activation = 0)}

Physics( RegionInterface="Bulk/Lat2_agg2" ){
Piezoelectric_Polarization(activation = 0)}

Physics( RegionInterface="Bulk/Lat1S1" ){
Piezoelectric_Polarization(activation = 0)}

Physics( RegionInterface="Bulk/Lat1S2" ){
Piezoelectric_Polarization(activation = 0)}

Physics( RegionInterface="Bulk/Lat2S1" ){
```

```
Piezoelectric_Polarization(activation = 0)}

Physics( RegionInterface="Bulk/Lat2S2" ){
Piezoelectric_Polarization(activation = 0)}

Physics( Region="Lat1_agg1" ){
Piezoelectric_Polarization(activation = 0)}

Physics( Region="Lat2_agg1" ){
Piezoelectric_Polarization(activation = 0)}

Physics( Region="Lat1_agg2" ){
Piezoelectric_Polarization(activation = 0)}
Physics( Region="Lat2_agg2" ){
Piezoelectric_Polarization(activation = 0)}

Physics( RegionInterface="Lat1S1/Lat1_agg1" ){
Piezoelectric_Polarization(activation = 0)}

Physics( RegionInterface="Lat1_agg1/Lat1" ){
Piezoelectric_Polarization(activation = 0)}

Physics( RegionInterface="Lat1/Lat1_agg2" ){
Piezoelectric_Polarization(activation = 0)}

Physics( RegionInterface="Lat1_agg2/Lat1S2" ){
Piezoelectric_Polarization(activation = 0)}

Physics( RegionInterface="Lat2S1/Lat2_agg1" ){
Piezoelectric_Polarization(activation = 0)}

Physics( RegionInterface="Lat2_agg1/Lat2" ){
```

```
Piezoelectric_Polarization(activation = 0)}

Physics( RegionInterface="Lat2/Lat2_agg2" ){
Piezoelectric_Polarization(activation = 0)}

Physics( RegionInterface="Lat2_agg2/Lat2S2" ){
Piezoelectric_Polarization(activation = 0)}

Plot{
*--Fields, charges, energies (Chapter 7)
  ElectricField/Vector Potential SpaceCharge
  eQuasiFermiEnergy hQuasiFermiEnergy
  eEffectiveStateDensity hEffectiveStateDensity
*--Densities and Currents, etc (Chapter 8)
  eDensity hDensity DonorConcentration AcceptorConcentration
  TotalCurrent/Vector eCurrent/Vector hCurrent/Vector
  eMobility hMobility
  eVelocity hVelocity
  CurrentPotential

*--Temperature (Chapter 9)
  eTemperature
  * hTemperature Temperature

*--Heat generation
  * TotalHeat eJouleHeat hJouleHeat RecombinationHeat

*--Driving forces
  eGradQuasiFermi/Vector hGradQuasiFermi/Vector
  eEparallel hEparallel
  eEnormal hEnormal
```

```
*--Band structure/Composition
  BandGap
  Affinity
  ConductionBand ValenceBand
  xMoleFraction
  ConductionBandEnergy ValenceBandEneergy

*--Traps
  eTrappedCharge  hTrappedCharge
  eGapStatesRecombination hGapStatesRecombination

*--Piezoelectric effect
  PE_Polarization/vector
PE_Charge
  PiezoCharge
}

Math {
        Iterations= 100
        EquilibriumSolution(Iterations= 500)
        ExtendedPrecision
        Digits= 8
        Method=Blocked
         SubMethod=ILS
        NumberOfThreads=10
        eDrForceRefDens= 1e8
        hDrForceRefDens= 1e8
}

################################################
# COMPUTE EQUILIBRIUM SOLUTION
################################################
```

```
Solve {
        # initial solution
        Coupled(Iterations= 500){Poisson}
        Coupled(Iterations= 500){ Poisson Electron Hole  }
        Plot(FilePrefix="equil@node@")

Quasistationary (
                InitialStep= 0.000001 Minstep= 1e-12 MaxStep= 0.05
                Goal{Name="Drain" Voltage=1}
        ) {
                Coupled {Poisson Electron Hole}
                Plot(FilePrefix="n@node@_Vd1" Time=(1)}
NewCurrentPrefix="IdVg_Vd1_pos"
Quasistationary (
                InitialStep= 0.0001 Minstep= 1e-12 MaxStep= 0.05
                Goal{Name="Gate" Voltage=2}
        ) {
                Coupled {Poisson Electron Hole}
                Plot(FilePrefix="n@node@_Vd1Vg2" Time=(1))
}

Load(FilePrefix="n@node@_Vd1")
NewCurrentPrefix="IdVg_Vd1_neg"
Quasistationary (
                InitialStep= 0.0001 Minstep= 1e-12 MaxStep= 0.05
                Goal{Name="Gate" Voltage=-4}
        ) {
                Coupled {Poisson Electron Hole}
                Plot(FilePrefix="n@node@_Vd1Vg-4" Time=(1))}
}
```

```
************************************sdevice.par*************************************
Material = "GaN" {
#include "GaN.par"}

Material = "AlGaN" {
#include "AlGaN.par"}

Material = "AlN" {
#include "AlN.par"}

Material = "Si3N4" {
#include "Si3N4.par"}
Piezoelectric_Polarization{
Formula = 2}
```